CHANNEL ESTIMATION FOR OFDM SYSTEMS

A THESIS SUBMITTED TO
THE GRADUATE SCHOOL OF NATURAL AND APPLIED SCIENCES
OF
MIDDLE EAST TECHNICAL UNIVERSITY

BY

İLKER GÜREL

IN PARTIAL FULFILLMENT OF THE REQUIREMENTS
FOR
THE DEGREE OF MASTER OF SCIENCE
IN
ELECTRICAL AND ELECTRONICS
ENGINEERING

NOVEMBER 2005

Approval of the Graduate School of Natural and Applied Sciences

Prof. Dr. Canan ÖZGEN
Director

I certify that this thesis satisfies all the requirements as a thesis for the degree of Master of Science.

Prof. Dr. İsmet ERKMEN
Head of Department

This is to certify that we have read this thesis and that in our opinion it is fully adequate, in scope and quality, as a thesis for the degree of Master of Science.

Prof. Dr. Yalçın TANIK
Co-Supervisor

Asst. Prof. Dr. Arzu TUNCAY KOÇ
Supervisor

Examining Committee Members

Prof. Dr. Mete SEVERCAN	(METU, EE)	
Asst. Prof. Dr. Arzu TUNCAY KOÇ	(METU, EE)	
Prof. Dr. Yalçın TANIK	(METU, EE)	
Asst. Prof. Dr. Ali Özgür YILMAZ	(METU, EE)	
Dr. Faik EKEN	(ASELSAN)	

I hereby declare that all information in this document has been obtained and presented in accordance with academic rules and ethical conduct. I also declare that, as required by these rules and conduct, I have fully cited and referenced all material and results that are not original to this work.

Name, Last name : İLKER GÜREL

Signature :

ABSTRACT

CHANNEL ESTIMATION FOR OFDM SYSTEMS

Gürel, İlker

M. S., Department of Electrical and Electronics Engineering

Supervisor : Asst. Prof. Dr. Arzu TUNCAY KOÇ

Co-Supervisor : Prof. Dr. Yalçın TANIK

November 2005, 135 pages

In this thesis, various pilot symbol aided channel estimation and tracking methods are investigated and their performances are compared for an OFDM system with packet based communication on HF channel. For the HF channel, Watterson HF channel model is used. The compared methods are least squares (LS) channel estimation, linear minimum mean square error (LMMSE) channel estimation, least mean squares (LMS) channel tracking, recursive least squares (RLS) channel tracking, constant position model based Kalman filter channel tracking, and constant velocity model based Kalman filter channel tracking. For LMS and RLS methods some adaptive approaches are also investigated.

Keywords: Orthogonal Frequency Division Multiplexing (OFDM), Ionospheric High Frequency (HF) Channel, Linear Channel Modelling, Channel Estimation, Channel Tracking

ÖZ

DİKGEN SIKLIK BÖLÜMLÜ ÇOĞULLAMA SİSTEMLERİ
İÇİN KANAL KESTİRİMİ

Gürel, İlker

Yüksek Lisans, Elektrik Elektronik Mühendisliği Bölümü

Tez Yöneticisi : Yrd. Doç. Dr. Arzu TUNCAY KOÇ

Ortak Tez Yöneticisi: Prof. Dr. Yalçın TANIK

Kasım 2005, 135 sayfa

Bu tezde, HF kanalında çeşitli pilot sembol temelli kanal kestirim ve takip algoritmaları incelenmiş ve paket veri yapısı temelli OFDM sistemleri için performansları karşılaştırılmıştır. HF kanalı için Watterson HF kanal modeli kullanılmıştır. LS kanal kestirim yöntemi, LMMSE kanal kestirim yöntemi, LMS kanal takibi yöntemi, RLS kanal takibi yöntemi, sabit pozisyon modeline dayanan Kalman filtresi kanal takip yöntemi ve sabit hız modeline dayanan Kalman filtresi kanal takip yöntemi performansları karşılaştırılmıştır. LMS ve RLS yöntemleri için adaptif yaklaşımlar da incelenmiştir.

Anahtar Kelimeler: Dikgen Sıklık Bölümlü Çoğullama (OFDM), İyonosferik Yüksek Frekans (HF) Kanalı, Doğrusal Kanal Modelleme, Kanal Kestirimi, Kanal Takibi

To My Parents

ACKNOWLEDGMENTS

I wish to express my deepest gratitude to my supervisor Asst. Prof. Dr. Arzu TUNCAY KOÇ and co-supervisor Prof. Dr. Yalçın TANIK for their guidance, advice, criticism, encouragements, and insight throughout the research.

I would like to thank Ertuğrul KOLAĞASIOĞLU, Dr. Faik EKEN, and Çağdaş Enis DOYURAN for their suggestions and comments. I would also like to thank ASELSAN, Inc. for the facilities provided for me to complete this thesis.

Special thanks are to my parents who provided me with the necessary motivation to complete this study.

TABLE OF CONTENTS

LIST OF TABLES

LIST OF FIGURES

LIST OF ABBREVIATIONS

OFDM: Orthogonal Frequency Division Multiplexing

DAB: Digital Audio Broadcasting

DVB: Digital Video Broadcasting

HF: High Freqeuncy

LS: Least Squares

LMMSE: Linear Minimum Mean Square Error

LMS: Least Mean Squares

RLS: Recursive Least Squares

CHAPTER 1

INTRODUCTION

Orthogonal Frequency Division Multiplexing (OFDM) is a promising multicarrier modulation technique for high data rate for wireless communications. The subchannels of OFDM are overlapping due to the orthogonality of the subcarriers. The overlapping of subchannels makes efficient use of the spectrum. Since the channel is divided into narrowband flat fading channels, OFDM is more resistant to frequency selective fading than single carrier systems are. Inter symbol interference (ISI), overlap of consequent symbols, and inter carrier interference (ICI), loss of orthogonality between subcarriers, can be eliminated through the use of a guard interval. Using adequate channel coding and interleaving, symbols lost due to the frequency selectivity of the channel can be recovered. Channel equalization becomes simpler than using adaptive equalization techniques with single carrier systems. OFDM is computationally efficient by using fast Fourier transform (FFT) techniques to implement modulation and demodulation functions. It is less sensitive to sample timing offsets than single carrier systems are. It provides good protection against co-channel interference and impulsive parasitic noise. These are the considerable advanges of OFDM [1].

Besides the advantages of the OFDM systems, there are two disadvantages [1]. The first one is that the OFDM signals have a noise like amplitude with very large dynamic range. Therefore it requires radio frequency (RF) power amplifiers with a high peak to average power ratio. The second one is that OFDM systems are more sensitive to carrier frequency offset and drift than single carrier systems are, due to leakage of the discrete Fourier transform (DFT).

In recent years, as a wideband communication method, OFDM has gained considerable popularity. For example, OFDM has started to be used for Digital Audio Broadcasting (DAB) and Digital Video Broadcasting (DVB). Besides commercial applications, there are also some military applications of OFDM such as Wireless Local Area Network (WLAN) [2].

Considering the features of the OFDM system, it is a suitable choice for time varying multipath fading channels because OFDM can combat ISI caused by the dispersive fading of wireless channels. Due to the nature of the time varying multipath fading channels, channel estimation and/or tracking should be used for coherent detection in order to reduce the channel impairments and detect the transmitted symbols properly. Besides, in order to exploit the channel further for a better communication, the communication system should be adapted to the channel conditions. This can be done by using channel estimation and/or tracking [2].

In the literature, there are numerous channel estimation and tracking methods. Channel tracking methods are used together with channel estimation methods for packet based communications. Also, for OFDM systems there are various methods. Although these methods are used to combat with all kinds of wireless channels, HF channels are not so investigated especially for OFDM systems.

The aim of this thesis is to investigate some promising channel estimation and tracking methods for HF channels in an OFDM system with packet based communication. These methods are least squares (LS) channel estimation method, linear minimum mean square error (LMMSE) channel estimation method, least mean square (LMS) channel tracking method, recursive least squares (RLS) channel tracking method, constant position model based Kalman filter channel tracking method, and constant velocity model based Kalman filter channel tracking method. Among all, constant velocity model based Kalman filter can be seen as a promising channel tracking method because the tracking ability of Kalman filter is increased with the employed kinematic model.

In order to investigate these methods, a packet based communication system is constructed and various simulations were performed. In these simulations, for the HF channel, Watterson HF channel model is used.

In chapter 2, OFDM is investigated in detail. In chapter 3, time varying multipath fading channels and HF channels are explained in detail. In chapter 4, the derivations of the selected channel estimation and tracking methods are given. These methods are investigated by performing some simulations. In chapter 5, the results of these simulations are given. Finally, the work is concluded in chapter 6.

CHAPTER 2

ORTHOGONAL FREQUENCY DIVISION MULTIPLEXING (OFDM)

OFDM is a multicarrier communication technique. Multicarrier modulation (MCM) is a communication approach where the available channel bandwidth is subdivided into a number of parallel subchannels so that data is transmitted over these subchannels. The multicarrier modulated signal is usually of the following form [3]:

$$s(t) = \sum_{j} g(t - jT) \sum_{i=1}^{N} \left[a_{ij} \cos(2\pi f_i t) + b_{ij} \sin(2\pi f_i t) \right] \tag{2.1}$$

where N is the number of subchannels and also the number of carriers, f_i (i=1,2,...,N) are the carrier frequencies, a_{ij} and b_{ij} are modulating symbols of an M_i-ary symbol set, g(t) is the modulating pulse shape, and T is the symbol duration.

In the presence of channel distortions, such as multipath effect and Doppler shift, the channel is subdivided into a number of subchannels such that in each subchannel the distortions are reduced or totally removed. Moreover, MCM systems use a symbol duration that is N times that of an equivalent single carrier transmission system. This long symbol time produces much greater immunity to intersymbol interference (ISI) than single carrier systems.

The earliest MCM modems borrowed from conventional frequency division multiplexing (FDM) technology, using filters to completely separate the subbands. The second generation modems increased bandwidth efficiency to 100% using staggered QAM. Orthogonality of subcarriers is achieved by staggering the data and this results in overlapping of the subchannels. The third generation modems benefit from DSP technology where both transmitter and receiver can be implemented using fast and cheap fast Fourier transform (FFT) processors. The modulation and demodulation of the data can be performed with these FFT processors.

In this chapter, first OFDM will be introduced. Then, OFDM will be investigated over time varying multipath fading channels. In order to reduce the channel impairments caused by the multipath fading, the use of guard interval will be explained. Finally, the description of the OFDM system structure will be given.

2.1 Introduction to OFDM

OFDM is actually a special type of MCM. In general for MCM, the subcarrier spacing is selected sufficiently high such that the individual spectra of subcarriers do not overlap. In OFDM, however, the subcarrier spacing is kept at the minimum level, which preserves the orthogonality between subcarriers in time, even though the individual subcarrier spectra may overlap.

In general, an OFDM signal is defined as follows [4]:

$$x(t) = \sum_{i=0}^{N-1} a_i e^{j\frac{2\pi it}{T}} s(t), \;\; 0 \le t \le T \qquad (2.2)$$

where a_i denotes the complex valued symbol modulating the i^{th} carrier, s(t) is the time window function defined in the interval [0,T], N is the number of subcarriers, and T denotes the OFDM symbol duration. As seen from equation (2.2) the individual subcarriers are spaced $\Delta f=1/T$ apart.

The correlation coefficient between the subcarriers may be expressed as follows:

$$\rho_{km} = \frac{1}{T}\int_0^T e^{j\frac{2\pi kt}{T}} e^{-j\frac{2\pi mt}{T}} dt = \begin{cases} 1, m = k \\ 0, m \neq k \end{cases} \quad (2.3)$$

Therefore, subcarriers are mutually orthogonal in the symbol interval. This property is used for demodulating the OFDM signal. Assuming that s(t) is a rectangular function with magnitude 1 for the sake of simplicity, the demodulation is performed as follows [4]:

$$\begin{aligned} \frac{1}{T}\int_0^T e^{-j\frac{2\pi kt}{T}} \left[\sum_{i=0}^{N-1} a_i e^{j\frac{2\pi it}{T}}\right] dt &= \sum_{i=0}^{N-1} a_i \frac{1}{T}\int_0^T e^{j\frac{2\pi(i-k)t}{T}} dt \\ &= \begin{cases} a_k, i = k \\ 0 \quad , i \neq k \end{cases} \end{aligned} \quad (2.4)$$

When s(t) is not a rectangular pulse shape, it must be selected so that there is no intercarrier interference (ICI), loss of orthogonality between subcarriers in demodulation.

The spectrum of the OFDM symbol is expressed as follows [4]:

$$X(f) = FT\{x(t)\} = \sum_{i=0}^{N-1} a_i \int_{-\infty}^{\infty} e^{-j2\pi ft} e^{j\frac{2\pi it}{T}} s(t) dt = \sum_{i=0}^{N-1} a_i S(f - i/T) \quad (2.5)$$

Here, S(f) is the Fourier transform of s(t). In order to demodulate the k^{th} subcarrier, the OFDM receiver essentially samples the frequency spectrum at subcarrier frequency k/T. So, for the elimination of ICI, S(f) should satisfy the following equation:

$$S(\frac{k-i}{T}) = \begin{cases} 1, k = i \\ 0, k \neq i \end{cases} \quad (2.6)$$

Hence,

$$\frac{1}{T}\int_0^T x(t)e^{-j\frac{2\pi kt}{T}}dt = \frac{1}{T}X(\frac{k}{T}) = \frac{1}{T}\sum_{i=0}^{N-1}a_i S(\frac{k-i}{T}) = \begin{cases} a_k / T, & i = k \\ 0, & i \neq k \end{cases} \quad (2.7)$$

For S(f), sinc(fT) is the simplest choice, and this yields a rectangular time window. The practical problem of this is the high out of band radiation, because the tails of S(f) decrease only inversely proportional with f. In order to reduce the out of band radiation, a raised cosine time window can be employed, which is given as follows [4]:

$$s(t) = \begin{cases} \frac{1}{2}\left(1+\cos(\pi + \frac{\pi t}{\beta T})\right), & 0 \le t \le \beta T \\ 1, & \beta T \le t \le T \\ \frac{1}{2}\left(1+\cos(\frac{\pi(t-T)}{\beta T})\right), & T \le t \le (1+\beta)T \end{cases} \quad (2.8)$$

Here, $0 \le \beta \le 1$ is the roll off factor. The corresponding spectrum can be expressed as given below:

$$S(f) = \text{sinc}(fT)\frac{\cos(\pi\beta fT)}{1-4\beta^2 f^2 T^2} \quad (2.9)$$

which satisfies no ICI condition. The advantage of the raised cosine window is that the tails of the spectrum decay as $1/f^3$, which considerably reduces the out of band radiation. However, depending on the parameter β, there is an overlap region between consecutive OFDM frames, which increases the multipath delay sensitivity as will be discussed in the following paragraphs [4].

If x(t) is sampled with a period of T/N,

$$x(k\frac{T}{N}) = x_k = \sum_{i=0}^{N-1} a_i e^{j2\pi\frac{k}{N}i} s_k = N.IDFT_N(a_i).s_k\ , \qquad k = 0,1,...,N-1 \qquad (2.10)$$

where s_k=s(kT/N). This inverse discrete Fourier transform (IDFT) operation is performed in the transmitter for modulation. In the receiver, for the demodulation the DFT operation is performed. Assuming that s_k are equal to 1 for all k=0,1,2,...,N-1, using equation (2.10) the following equation can be written for demodulation:

$$\begin{aligned}
\frac{1}{N}DFT_N(x_k) &= \frac{1}{N}\sum_{k=0}^{N-1} x_k e^{-j2\pi\frac{n}{N}k} \\
&= \frac{1}{N}DFT_N(N.IDFT_N(a_i)) \\
&= \frac{1}{N}\sum_{k=0}^{N-1}\left[\sum_{i=0}^{N-1} a_i e^{j2\pi\frac{k}{N}i}\right] e^{-j2\pi\frac{n}{N}k} \\
&= \begin{cases} a_n, & n = i \\ 0, & n \neq i \end{cases}, \qquad i = 0,1,...,N-1
\end{aligned} \qquad (2.11)$$

In equation (2.10), the IDFT can be seen as a linear transformation mapping the complex data symbols [a_0, a_1, ..., a_{N-1}] to OFDM symbols [x_0, x_1, ..., x_{N-1}]. Assuming s_k are equal to 1 for all k=0,1,2,...,N-1, this linear transformation can be represented in matrix form as follows:

$$\overline{x} = \overline{W}\,\overline{a} \qquad (2.12)$$

where

$$\overline{W} = \begin{bmatrix} 1 & 1 & 1 & \cdots & 1 \\ 1 & W_1 & W_1^2 & \cdots & W_1^{N-1} \\ 1 & W_2 & W_2^2 & \cdots & W_2^{N-1} \\ \vdots & \vdots & \vdots & \cdots & \vdots \\ 1 & W_{N-1} & W_{N-1}^2 & \cdots & W_{N-1}^{N-1} \end{bmatrix}, \quad W_k = e^{j2\pi\frac{k}{N}} \qquad (2.13)$$

and

$$\bar{a} = \begin{bmatrix} a_0 \\ a_1 \\ a_2 \\ \vdots \\ a_{N-1} \end{bmatrix}, \quad \bar{x} = \begin{bmatrix} x_0 \\ x_1 \\ x_2 \\ \vdots \\ x_{N-1} \end{bmatrix} \tag{2.14}$$

Similarly, in equation (2.11), the DFT can be seen as a linear transformation mapping the complex OFDM symbols $[x_0, x_1, ..., x_{N-1}]$ to detected data symbols $\left[a'_0, a'_1, ..., a'_{N-1}\right]$. This linear mapping can be represented in matrix form as follows:

$$\bar{a}' = \overline{W'}\bar{x} \tag{2.15}$$

where

$$\overline{W'} = \frac{1}{N}\begin{bmatrix} 1 & 1 & 1 & \cdots & 1 \\ 1 & W'_1 & W'^2_1 & \cdots & W'^{N-1}_1 \\ 1 & W'_2 & W'^2_2 & \cdots & W'^{N-1}_2 \\ \vdots & \vdots & \vdots & \cdots & \vdots \\ 1 & W'_{N-1} & W'^2_{N-1} & \cdots & W'^{N-1}_{N-1} \end{bmatrix}, \quad W'_n = e^{-j2\pi\frac{n}{N}} \tag{2.16}$$

and

$$\bar{a}' = \begin{bmatrix} a'_0 \\ a'_1 \\ a'_2 \\ \vdots \\ a'_{N-1} \end{bmatrix}, \quad \bar{x} = \begin{bmatrix} x_0 \\ x_1 \\ x_2 \\ \vdots \\ x_{N-1} \end{bmatrix} \tag{2.17}$$

2.2 OFDM over Time Varying Multipath Fading Channels

Time varying multipath fading channels cause impairments on the transmitted signals by creating ICI and ISI. In this section, it will be shown that ISI and ICI can be eliminated with the addition of a guard interval to the transmitted signal. In order to investigate these channel impairments, let us assume that the received signal r(t) is in the following form:

$$r(t) = \sum_{\ell=0}^{L-1} h_{\ell}(t)x(t - \ell\frac{T}{N}) \tag{2.18}$$

where x(t) denotes the transmitted OFDM signal, L is the number of taps, $h_{\ell}(t)$ denotes the attenuation process for the signal received on the ℓ^{th} path, and $\ell T/N$ is the propagation delay for the ℓ^{th} path. $h_{\ell}(t)$ are assumed to be uncorrelated zero mean complex valued Gaussian random processes. It is also assumed that the channel is slowly fading, i.e., $h_{\ell}(t)$ are constant during one OFDM symbol duration T.

At this point, let us define x(t) as a signal composed of consecutive OFDM symbols as shown in equation (2.19). It is a more general form of equation (2.2) [4].

$$x(t) = \sum_{m}\sum_{i=0}^{N-1} a_{i,m} e^{j\frac{2\pi i(t-mT)}{T}} s(t - mT) \tag{2.19}$$

Here, let us select s(t) as a rectangular pulse shape with the amplitude of 1. In order to demodulate the k^{th} subcarrier of the n^{th} OFDM symbol, equation (2.4) is used over the interval [nT,(n+1)T]. Due to the length of the time interval, based on the slowly fading channel assumption, $h_{\ell}(t)$ is constant and it is equal to h_{ℓ}. Then, at the end of the demodulation the following is obtained:

$$
\begin{aligned}
I_{k,n} &= \frac{1}{T}\int_{nT}^{(n+1)T} r(t)e^{-j\frac{2\pi k(t-nT)}{T}}dt \\
&= \frac{1}{T}\int_{nT}^{(n+1)T}\left[\sum_{\ell=0}^{L}h_\ell\sum_{m}\sum_{i=0}^{N-1}a_{i,m}e^{j\frac{2\pi i(t-\ell T/N-mT)}{T}}s(t-\ell\frac{T}{N}-mT)\right]e^{-j\frac{2\pi k(t-nT)}{T}}dt \\
&= \sum_{m}\sum_{i=0}^{N-1}a_{i,m}\sum_{\ell=0}^{L}h_\ell e^{-j2\pi i\frac{\ell}{N}}\frac{1}{T}\int_{0}^{T}e^{j2\pi(i-k)\frac{t}{T}}s(t-\ell\frac{T}{N}+(n-m)T)dt
\end{aligned}
\tag{2.20}
$$

It can be observed from equation (2.20) that due to the integral calculation only m=n and m=n–1 indices contribute to the summation over m. Hence, $I_{k,n}$ can be expressed as follows:

$$
\begin{aligned}
I_{k,n} &= \sum_{i=0}^{N-1}a_{i,n-1}\sum_{\ell=0}^{L}h_\ell e^{-j2\pi i\frac{\ell}{N}}\frac{1}{T}\int_{0}^{T}e^{j2\pi(i-k)\frac{t}{T}}s(t-\ell\frac{T}{N}+T)dt \\
&+\sum_{i=0}^{N-1}a_{i,n}\sum_{\ell=0}^{L}h_\ell e^{-j2\pi i\frac{\ell}{N}}\frac{1}{T}\int_{0}^{T}e^{j2\pi(i-k)\frac{t}{T}}s(t-\ell\frac{T}{N})dt
\end{aligned}
\tag{2.21}
$$

Since s(t) is assumed to be a rectangular pulse shape with amplitude 1, the following relation is obtained:

$$
\begin{aligned}
I_{k,n} &= \sum_{i=0}^{N-1}a_{i,n-1}\sum_{\ell=0}^{L}h_\ell e^{-j2\pi i\frac{\ell}{N}}\frac{1}{T}\int_{0}^{\ell T/N}e^{j2\pi(i-k)\frac{t}{T}}dt \\
&+\sum_{i=0}^{N-1}a_{i,n}\sum_{\ell=0}^{L}h_\ell e^{-j2\pi i\frac{\ell}{N}}\frac{1}{T}\int_{\ell T/N}^{T}e^{j2\pi(i-k)\frac{t}{T}}dt
\end{aligned}
\tag{2.22}
$$

If equation (2.22) is put in the following form

$$I_{k,n} = a_{k,n}\left(\sum_{\ell=0}^{L} h_\ell (1-\frac{\ell}{N})\, e^{-j2\pi k\frac{\ell}{N}}\right)$$
$$+\sum_{\substack{i=0\\ i\neq k}}^{N-1} a_{i,n}\sum_{\ell=0}^{L} h_\ell e^{-j2\pi i\frac{\ell}{N}}\frac{1}{T}\int_{\ell T/N}^{T} e^{j2\pi(i-k)\frac{t}{T}}dt \tag{2.23}$$
$$+\sum_{i=0}^{N-1} a_{i,n-1}\sum_{\ell=0}^{L} h_\ell e^{-j2\pi i\frac{\ell}{N}}\frac{1}{T}\int_{0}^{\ell T/N} e^{j2\pi(i-k)\frac{t}{T}}dt$$

then the first term represents the desired data, scaled by a complex quantity that depends on the complex channel taps. The second term represents ICI, which is caused by the other subcarriers belonging to the present OFDM symbol. And the third term represents ISI, which is caused by all the subcarriers belonging to the previous OFDM symbol.

For a satisfactory communication ISI and ICI should be removed. Let us consider first the removal of ISI. One method to remove the ISI is inserting a guard time interval at the beginning of each OFDM symbol, which is larger than the maximum possible delay spread of the channel [4]. Let T_b=T+T_g denote the length of the OFDM symbol where T_g is the guard interval. Then, the transmitted OFDM signal can be expressed as follows [4]:

$$x(t) = \sum_{m}\sum_{i=0}^{N-1} a_{i,m} e^{j\frac{2\pi i(t-T_g-mT_b)}{T}} s(t-T_g-mT_b) \tag{2.24}$$

The rectangular window s(t) is defined over [0,T] as before so that the n^{th} OFDM symbol is given by the following expression:

$$x_n(t) = \begin{cases} \sum_{i=0}^{N-1} a_{i,n} e^{j\frac{2\pi i(t-T_g-nT_b)}{T}}, & nT_b + T_g \le t \le (n+1)T_b \\ 0, \quad nT_b \le t \le nT_b + T_g \end{cases} \tag{2.25}$$

Hence, the result of demodulation for the k^{th} subcarrier of the n^{th} OFDM symbol is given by the following expression [4]:

$$
\begin{aligned}
I_{k,n} &= \frac{1}{T}\int_{nT_b+T_g}^{(n+1)T_b} r(t)e^{-j\frac{2\pi k(t-nT_b-T_g)}{T}}dt \\
&= \frac{1}{T}\int_{nT_b+T_g}^{(n+1)T_b}\left[\sum_{\ell=0}^{L} h_\ell \sum_{m}\sum_{i=0}^{N-1} a_{i,m} e^{j\frac{2\pi i(t-\ell T/N-mT_b-T_g)}{T}} s(t-\ell T/N-mT_b-T_g)\right] e^{-j\frac{2\pi k(t-nT_b-T_g)}{T}}dt \\
&= \sum_{m}\sum_{i=0}^{N-1} a_{i,m}\sum_{\ell=0}^{L} h_\ell e^{-j2\pi i\frac{\ell}{N}}\frac{1}{T}\int_0^T e^{j2\pi(i-k)\frac{t}{T}} e^{j2\pi i\frac{(n-m)T_b}{T}} s(t-\ell T/N+(n-m)T_b)dt
\end{aligned}
$$

(2.26)

In this case, if $LT/N<T_g$, i.e., if the guard interval is larger than maximum time delay of the channel LT/N, only the index m=n contributes to the sum. Hence, no ISI occurs. Since s(t) is assumed to be a rectangular pulse shape with amplitude 1, the following relation is obtained:

$$
\begin{aligned}
I_{k,n} &= \left(\sum_{\ell=0}^{L} h_\ell (1-\frac{\ell}{N})e^{-j2\pi k\frac{\ell}{N}}\right)a_{k,n} \\
&+ \sum_{i,i\neq k} a_{i,n}\sum_{\ell=0}^{L} h_\ell e^{-j2\pi i\frac{\ell}{N}}\frac{1}{T}\int_{\ell T/N}^{T} e^{j2\pi(i-k)\frac{t}{T}}dt
\end{aligned}
\qquad (2.27)
$$

The first term represents the desired symbol and the second term represents ICI. Therefore, a simple guard time gap between consecutive OFDM symbols removes ISI.

Now, in order to remove ICI, the OFDM signal can be extended to include the guard time. In this case, the transmitted OFDM signal is given as follows [4]:

$$x(t) = \sum_{m}\sum_{i=0}^{N-1} a_{i,m} e^{j\frac{2\pi i(t-T_g-mT_b)}{T}} s(t-mT_b) \tag{2.28}$$

where the rectangular window is now defined over $[0,T_b]$ with amplitude 1. Then, the result of demodulation for the kth subcarrier of the nth symbol becomes as follows [4]:

$$\begin{aligned}
I_{k,n} &= \frac{1}{T}\int_{nT_b+T_g}^{(n+1)T_b} r(t) e^{-j\frac{2\pi k(t-nT_b-T_g)}{T}} dt \\
&= \frac{1}{T}\int_{nT_b+T_g}^{(n+1)T_b} \left[\sum_{\ell=0}^{L} h_\ell \sum_{m}\sum_{i=0}^{N-1} a_{i,m} e^{j\frac{2\pi i(t-\ell T/N-mT_b-T_g)}{T}} s(t-\ell T/N-mT_b)\right] e^{-j\frac{2\pi k(t-nT_b-T_g)}{T}} dt \\
&= \sum_{m}\sum_{i=0}^{N-1} a_{i,m} \sum_{\ell=0}^{L} h_\ell e^{-j2\pi i\frac{\ell}{N}} \frac{1}{T}\int_{0}^{T} e^{j2\pi(i-k)\frac{t}{T}} e^{j2\pi i\frac{(n-m)T_b}{T}} s(t-\ell T/N+(n-m)T_b+T_g)dt
\end{aligned} \tag{2.29}$$

Due to the guard interval, which is larger than the maximum channel delay LT/N, only the index m=n contributes to the sum and ISI is eliminated. Since, the rectangular window s(t) is defined on $[0,T_b]$, the result of the demodulation is

$$\begin{aligned}
I_{k,n} &= \left(\sum_{\ell=0}^{L} h_\ell e^{-j2\pi k\frac{\ell}{N}}\right) a_{k,n} + \sum_{i,i\neq k} a_{i,n} \sum_{\ell=0}^{L} h_\ell e^{-j2\pi i\frac{\ell}{N}} \frac{1}{T}\int_{0}^{T} e^{j2\pi(i-k)\frac{t}{T}} dt \\
&= \left(\sum_{\ell=0}^{L} h_\ell e^{-j2\pi k\frac{\ell}{N}}\right) a_{k,n} \\
&= H_k a_{k,n}
\end{aligned} \tag{2.30}$$

where H_k corresponds to the channel frequency response at the kth subcarrier frequency. Since the rectangular window is defined over $[0,T_b]$, the correlator output does not contain ICI term but only the desired symbol.

Let $x_n(t)$ denote the nth OFDM symbol with guard interval. It is given in the following equation [4]:

$$x_n(t) = \sum_{i=0}^{N-1} a_{i,n} e^{j2\pi i \frac{t-T_g-nT_b}{T}} s(t-nT_b), \quad nT_b \le t \le (n+1)T_b \tag{2.31}$$

If the OFDM signal with guard interval is sampled with the sampling rate of N/T= $(N+G)/T_b = (N+G)/(T+T_g)$, where N is the number of samples of the OFDM symbol and G is the number of samples in the guard interval, then, the n^{th} OFDM symbol becomes as follows:

$$\begin{aligned}
x_n(k\frac{T_b}{N+G}) = x_n[k] &= \sum_{i=0}^{N-1} a_{i,n} e^{j2\pi i \frac{kT_b/(N+G)-T_g-nT_b}{T}} s(k\frac{T_b}{N+G} - nT_b) \\
&= \sum_{i=0}^{N-1} a_{i,n} e^{j2\pi i\left(\frac{k}{N+G}\frac{T_b}{T} - \frac{T_g+n(T+T_g)}{T}\right)} s(k\frac{T_b}{N+G} - nT_b) \\
&= \sum_{i=0}^{N-1} a_{i,n} e^{j2\pi i\left(\frac{k}{N+G}\frac{N+G}{N} - (n+1)\frac{G}{N}\right)} s(k\frac{T_b}{N+G} - nT_b) \\
&= \sum_{i=0}^{N-1} a_{i,n} e^{j2\pi i\left(\frac{k}{N} - (n+1)\frac{G}{N}\right)} s[k - n(N+G)] \\
&= \sum_{i=0}^{N-1} a_{i,n} e^{j2\pi i\left(\frac{(k-G)}{N} - \frac{nG}{N}\right)} s[k - n(N+G)] \\
& n(N+G) \le k \le (n+1)(N+G) - 1
\end{aligned} \tag{2.32}$$

where $s[k] = s(k\frac{T_b}{N+G})$. Each sample of the n^{th} OFDM symbol is given as follows:

$$\begin{aligned}
x_n[\,n(N+G)] &= \sum_{i=0}^{N-1} a_{i,n} e^{j2\pi i \frac{(nN-G)}{N}} s[0] = \sum_{i=0}^{N-1} a_{i,n} e^{j2\pi i \frac{-G}{N}} s[0] \\
x_n[\,n(N+G)+1] &= \sum_{i=0}^{N-1} a_{i,n} e^{j2\pi i \frac{(nN-G+1)}{N}} s[1] = \sum_{i=0}^{N-1} a_{i,n} e^{j2\pi i \frac{(-G+1)}{N}} s[1] \\
&\vdots \\
x_n[\,(n+1)(N+G)-1] &= \sum_{i=0}^{N-1} a_{i,n} e^{j2\pi i \frac{((n+1)N-1)}{N}} s[N+G-1] = \sum_{i=0}^{N-1} a_{i,n} e^{j2\pi i \frac{(-1)}{N}} s[N+G-1]
\end{aligned} \tag{2.33}$$

Then, using equation (2.33) with the assumption that s[k]=1 for k=1,2,…,N+G-1, the following relations are obtained:

$$
\begin{aligned}
x_n[\,n(N+G)] &= x_n[(n+1)(N+G)-G] = \sum_{i=0}^{N-1} a_{i,n} e^{j2\pi i\frac{(-G)}{N}} s[0] \\
x_n[\,n(N+G)+1] &= x_n[\,n(N+G)-G+1] = \sum_{i=0}^{N-1} a_{i,n} e^{j2\pi i\frac{(-G+1)}{N}} s[1] \\
&\vdots \\
x_n[\,(n+1)(N+G)-1] &= x_n[\,n(N+G)+G-1] = \sum_{i=0}^{N-1} a_{i,n} e^{j2\pi i\frac{(-1)}{N}} s[N+G-1]
\end{aligned}
\tag{2.34}
$$

That is, the sampled guard interval is nothing but the cyclic extension of the OFDM symbol such that the OFDM signal with this extension becomes as shown in Figure 2.1.

Guard interval				OFDM data			
$x_n[(n+1)N+G]$	. . .	$x_n[(n+1)(N+G)-2]$	$x_n[(n+1)(N+G)-1]$	$x_n[n(N+G)]$	$x_n[n(N+G)+1]$	. . .	$x_n[(n+1)(N+G)-1]$

Figure 2.1 Sampled nth OFDM symbol with cyclic extension

In order to see the use of the cyclic prefix in discrete time domain, let h_m of length M denotes the impulse response of the channel. Assume that the length of the cyclic prefix G is longer than the maximum channel delay M. This corresponds to $T_m<T_g$ in continuous time domain where T_m is the maximum channel delay in continuous time domain. Also, let x[n] denotes the sampled OFDM signal where x[n]= $x[n] = x(t)|_{t=n\frac{T}{N}}$ and x(t) is as given in equation (2.28). Then, the received OFDM signal becomes as follows [2]:

$$
r(t)|_{t=n\frac{T}{N}} = r[n] = h[n] * x[n] = \sum_{i=0}^{M-1} h[i]x[n-i] \tag{2.35}
$$

Here, there will be ISI in cyclic prefix part of the symbol but it will not affect the data part because cyclic prefix length is larger than maximum path delay T_m as shown in Figure 2.2 where X_i denotes the symbol at i^{th} subcarrier [5]:

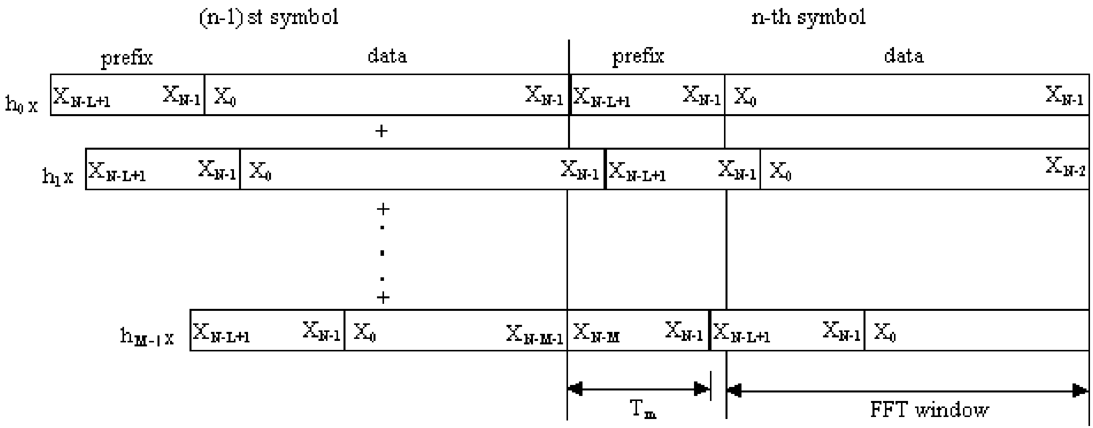

Figure 2.2 OFDM symbol with cyclic prefix on multipath channel [5]

At the receiver, the demodulated n^{th} symbol is obtained by taking the FFT of the received data part which falls in the FFT window as shown in Figure 2.3. The n^{th} demodulated symbol becomes as follows [2]:

$$r[n] = \sum_{i=0}^{M-1} h[i]x[((n-i))_N] = \sum_{i=0}^{N-1} h[i]x[((n-i))_N], \quad n = 0,1,...,N-1 \tag{2.36}$$

where $x[((.))_N]$ denotes the cyclically shifted samples of the OFDM symbol. Thus, after the removal of the cyclic prefix, it is observed that linear shift caused by the channel on the data part is converted to a cyclic shift, and received OFDM symbol is the cyclic convolution of the channel impulse response with the transmitted OFDM symbol. Using the DFT property that the circular convolution in time domain corresponds to multiplication in frequency domain,

$$DFT\{r[n]\} = DFT\{h[n]\}DFT\{x[n]\} = H_k X_k, \quad k = 0,1,...,N-1 \tag{2.37}$$

where

$$H_k = \sum_{m=0}^{M-1} h[n] e^{-j2\pi \frac{n}{N} k}, \quad k = 0,1,\ldots,N-1 \tag{2.38}$$

Equation (2.38) is the channel frequency response. Thus, it is clear that if a cyclic prefix with a length larger than channel impulse response length is used, both ISI and ICI terms can be eliminated.

2.3 Description of the OFDM Systems

The general block diagram of an OFDM system is shown in Figure 2.3. For each subcarrier, data can be modulated with different modulation methods such as BPSK, QPSK, QAM, etc. This process is performed in the symbol generator block of the transmitter. In the IFFT block the modulation is performed which is given by equation (2.12). After IFFT block, a guard interval of length k is added to each block of OFDM symbols. The use of guard interval was explained in section 2.2. This is followed by a pulse shaping operation. After pulse shaping operation the signal is converted to analog form by a digital to analog converter (DAC). In some systems, the digital to analog conversion is accomplished by baseband pulse shaping filters, excited by the IDFT output. Usually a raised cosine filter is used for this purpose. However, in this work rectangular pulse shape with an amplitude of 1 is used.

At the transmitter output, the OFDM signal is in the following form [4]:

$$x(t) = \sum_{i=0}^{N} a_i \exp\left(j \frac{2\pi i (t - T_g)}{T} \right) s(t), \quad 0 \le t \le T_b \tag{2.39}$$

where T_b is the symbol duration and T_g is the guard interval.

At the receiver side, first the OFDM signal is filtered with a passband receiver filter. Then, the output of the filter is fed to the analog to digital converter (ADC). The sampled OFDM signal is fed then to the FFT block. In this block the guard interval is removed and the signal is demodulated as shown in equation (2.15). As a result, the OFDM signals are obtained.

In some applications, coding can be used in OFDM systems. Such OFDM systems are called coded OFDM (COFDM) systems. [6] can be investigated for COFDM.

In this work, it is assumed that the timing is perfect in the OFDM system. That is, there is no timing error. Hence, there is no need for any synchronization process in the system. For this reason, synchronization for OFDM systems is not explained. But, [2,4,5,7] can be used in order to investigate this subject.

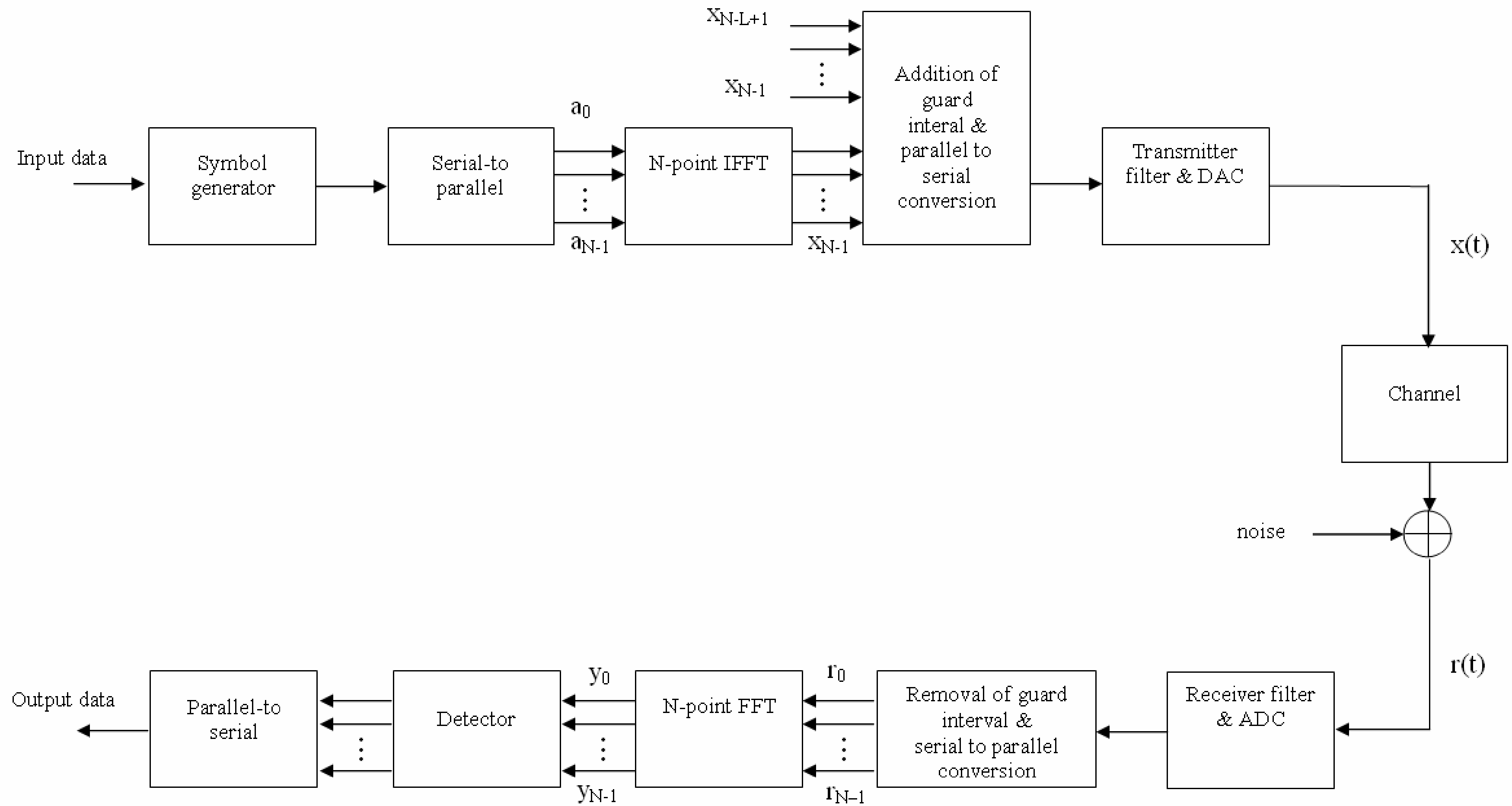

Figure 2.3 Baseband OFDM system structure [6]

CHAPTER 3

TIME VARYING MULTIPATH FADING CHANNEL AND HIGH FREQUENCY (HF) CHANNEL

In this work, high frequency (HF) channel is used as the communication medium. For this purpose, Watterson HF channel model is employed. HF channel is a time varying multipath fading channel [8]. Also, it has a time varying linear characteristics. Hence, it is also a time varying linear channel [9].

Since both the time varying multipath fading characteristics and time varying linear characteristics are embodied in the HF channels, in this chapter first the time varying multipath fading channels and their statistical modelling will be introduced, then the chapter will continue with the characterization of the time varying linear channels by defining their system functions and by classifying them with respect to their statistical properties. After that, in the light of the information about the time varying linear channels, the physical features of the time varying multipath fading channels will be investigated. After that, the time varying multipath fading channels will be classified according to their physical features affecting the input signal over frequency and/or time domain. Finally, the HF channel will be introduced and Watterson HF channel model will be explained.

3.1 Introduction to Time Varying Multipath Fading Channels [10]

If an extremely short pulse is transmitted, ideally an impulse, over a time varying multipath channel, the received signal might appear as a train of pulses. One characteristic of a time varying multipath fading medium is the time spread introduced in the signal that is transmitted through channel. A second characteristic is due to the time variations in the structure of the medium. As a result of such time variations, the nature of the multipath varies with time. That is, if the pulse sounding experiment is repeated over and over again, it will be observed changes in the received pulse train. These changes include changes in the sizes of the individual pulses, which is called fading, changes in the relative delays among the pulses, and changes in the number of pulses observed in the received pulse train. Moreover, the time variations appear to be unpredictable to the user of the channel. Therefore, it is reasonable to characterize the time varying multipath fading channel statistically [11].

Let s(t) denote the channel input and y(t) denote the channel output. These waveforms will usually be represented by their complex envelopes. For example,

$$s(t) = \mathrm{Re}\left\{s_{\ell}(t)e^{j\omega_0 t}\right\} \tag{3.1}$$

where $s_{\ell}(t)$ is the complex envelope of s(t) and ω_0 denotes the nominal carrier frequency in radians per second. From now on, the complex envelopes of the signals are used for calculations.

Let us consider a channel in which propagation is established by single scattering from a large number of elements or scatters. These scatterers might be orbital dipoles or differential elements of either the troposphere or the ionosphere.

Each scatterer is decribed by its reflection energy cross section ρ_i^2 and by its propagation delay $T_i(t)$ [10]. For convenience, it is assumed that $T_i(t)$ is a linear function of time, i.e.,

$$T_i(t) = \tau_i + \dot{\tau}_i t \tag{3.2}$$

where τ_i and $\dot{\tau}_i$ are the initial propagation delay and rate of change of delay, respectively. If the transmitter and the receiver are located at the same site, this assumption is equivalent to the assumption of a constant radial component of scatterer velocity. More general expressions for the delay can be employed, but it appears that their use does not appreciably affect the applicability of the model to the problem of interest, whereas it does complicate the analysis. Similar comments apply to the assumption that the energy cross section of a scatterer is constant. This cross section can be a function of time. However, it again appears that the additional complication introduced by these generalizations offsets the increased realism they afford.

Now, let us first consider the contribution of any single scatterer of the medium to the received waveform. Suppose that the contribution $\tilde{y}_i(t)$ of the i^{th} scatterer is just a delayed and attenuated replica of the transmitted waveform. In particular,

$$\tilde{y}_i(t) = A\rho_i \operatorname{Re}\left\{s_\ell(t-\tau_i-\dot{\tau}_i t)e^{j\omega_0(t-\tau_i-\dot{\tau}_i t)}\right\} \tag{3.3}$$

where A is an unimportant constant which is eliminated subsequently.

Now, suppose that the variation $\dot{\tau}_i$ t is appreciably less than the reciprocal bandwidth of s_ℓ(t). This supposition implies the following:

$$s_\ell\left(t-\tau_i-\dot{\tau}_i t\right) \approx s_\ell\left(t-\tau_i-\dot{\tau}_i t_0\right) \tag{3.4}$$

for any value of t_0 of t in the interval. In particular, without loss of generality, suppose that the time origin is contained in the interval. So, the following assumption holds:

$$s_\ell\left(t-\tau_i-\dot{\tau}_i t\right) \approx s_\ell\left(t-\tau_i\right) \tag{3.5}$$

That is, it is supposed that the time variation in the propagation delay of the i^{th} scatterer does not significantly alter the modulation of its contribution to the received waveform.

It is further assumed that the bandwidth of $s_\ell(t)$ is much less than the carrier frequency ω_0. This is the conditional "narrowband" condition encountered in most of the communication systems. It implies that variations of about π/ω_0 in the value of τ_i do not appreciably alter the value of $s_\ell(t-\tau_i)$, although they do drastically alter the value of $\tilde{y}_i(t)$ since they change the exponent $\omega_0(t-\tau_i-\dot{\tau}_i t)$ by π radians.

Since the precise value of τ_i is known seldomly and since small perturbations in the value are important, it appears reasonable to express each τ_i in the following form:

$$\tau_i = r_i + \frac{\theta_i}{\omega_0} \tag{3.6}$$

where r_i is taken to be known value of τ_i and it is accounted for the perturbations about this value by θ_i, whose values lie in the interval $-\pi$ to $+\pi$. Then, equation (3.3) becomes as follows:

$$\tilde{y}_i(t) = A\,\mathrm{Re}\left\{\rho_i s_\ell(t-r_i)e^{j\omega_0\left(t-r_i-\frac{\theta_i}{\omega_0}-\dot{\tau}_i t\right)}\right\} \tag{3.7}$$

Let $\omega_i = \dot{\tau}_i\omega_0$. Then for the i^{th} scatterer, the following expression can be written:

$$\tilde{y}_i(t) = A\,\mathrm{Re}\left\{\rho_i s_\ell(t-r_i)e^{j((\omega_0-\omega_i)t-\omega_0 r_i-\theta_i)}\right\} \tag{3.8}$$

In this expression ω_i is the Doppler shift of the scatterer measured in radians per second, and r_i is as before its mean time, or range, delay measured in seconds. If secondary scattering is unimportant, as supposed, the expression for the total received waveform is obtained by summing the above equation over all the scatterers composing the medium.

$$y(t) = A\,\mathrm{Re}\left\{\sum_i \rho_i s_\ell\left(t - r_i\right) e^{j\left((\omega_0 - \omega_i)t - \omega_0 r_i - \theta_i\right)}\right\} \tag{3.9}$$

More generally, the attenuation and the introduced delay of the transmitted signal may change with time, and the delay may not be a linear function of time. In this case, the received signal can be expressed as follows [11]:

$$y(t) = \mathrm{Re}\left\{\sum_i \alpha_i(t)\, s_\ell(t - \tau_i(t)) e^{j\omega_0 (t - \tau_i(t))}\right\} \tag{3.10}$$

where $\alpha_i(t)$ and $\tau_i(t)$ are the attenuation factor and the propagation delay for the signal received on the i^{th} path, respectively. Thus, the lowpass equivalent of the received signal, $y_\ell(t)$, can be expressed as follows:

$$y_\ell(t) = \sum_i \alpha_i(t)\, e^{-j\omega_0 \tau_i(t)}\, s_\ell(t - \tau_i(t)) \tag{3.11}$$

Since it is the response of an equivalent lowpass channel to the equivalent lowpass signal $s_\ell(t)$, the equivalent lowpass channel is described by the time varying impulse response:

$$c_\ell(\tau; t) = \sum_i \alpha_i(t)\, e^{-j\omega_0 \tau_i(t)}\, \delta(t - \tau_i(t)) \tag{3.12}$$

For some channels, such as the tropospheric scatter channel, it is more appropriate to view the received signal as consisting of continuum of multipath components. In this case, the received signal y(t) is expressed in the following integral form [11]:

$$y(t) = \int_{-\infty}^{\infty} \alpha(\tau; t)\, s(t - \tau)\, d\tau = \mathrm{Re}\left\{\left[\int_{-\infty}^{\infty} \alpha(\tau; t)\, e^{-j\omega_0 \tau}\, s_\ell(t - \tau)\, d\tau\right] e^{j\omega_0 t}\right\} \tag{3.13}$$

where $\alpha(\tau;t)$ is the attenuation of the signal components at delay τ and at time instant t. Then the lowpass equivalent impulse response of the channel becomes as follows [11]:

$$c_\ell(\tau;t) = \alpha(\tau;t)\, e^{-j\omega_0\tau} \tag{3.14}$$

As a result,

$$c_\ell(\tau;t) = \begin{cases} \sum_i \alpha_i(t)\, e^{-j\omega_0\tau_i(t)}\, \delta(t - \tau_i(t)), & \text{discrete multipath components exist} \\ \alpha(\tau;t)\, e^{-j\omega_0\tau}, & \text{continuous multipath components exist} \end{cases} \tag{3.15}$$

3.2 Statistical Model of the Time Varying Multipath Fading Channel [10]

Now, let us return to the channel model used in expression (3.9). It is observed that the uncertainty associated with each θ_i corresponds to a delay uncertainty of about half a wavelength. Since the total delay is usually many thousands of wavelength, the percentage uncertainty is exceedingly small, and there is good reason to assume that if θ_i is to be regarded as a random variable it should be uniformly distributed over the interval $-\pi$ to $+\pi$. The same argument applied to the difference in delay between scatterers suggests that θ_i should be presumed to be statistically independent of each other. Thus it only remains to specify the values, or statistical properties, of the scatterer cross sections ρ_i^2 [10].

Since cross sections ρ_i^2 account for such factors as the aspect of the scatters, it should be reasonable to treat them as unknown quantities and perhaps as random variables. If they are assumed to be random variables, there is little reason to assume that they are statistically dependent upon each other, or that their values are dependent upon the values of the random phase angles θ_i. Thus, it is appropriate to regard them as statistically independent random variables, each described by a probability density $p_i(\rho_i)$.

The assumptions made so far imply that the mean value $E\{y(t)\}$ of y(t), given in equation (3.9), is zero. They also imply that the correlation function

$$R_y(t,\tau) = E\{y(t)y^*(\tau)\} \tag{3.16}$$

of y(t) is given by the following expression:

$$R_y(t,\tau) = \mathrm{Re}\left\{\sum_i \frac{A^2}{2} E\{\rho_i^2\} s_\ell(t-r_i) s_\ell^*(\tau-r_i) e^{j(\omega_0-\omega_i)(t-\tau)}\right\} \tag{3.17}$$

where asterisk denotes complex conjugation of the indicated quantity.

The mean and correlation function of y(t) do not provide a complete statistical description of the received process. There are arguments for supposing that the received process is Gaussian and hence completely described by its mean and correlation function.

Experimental evidence suggests that for troposcatter and ionoscatter channels the received process may be Gaussian. Specifically the envelope and phase of the process often exhibit the behaviour to be expected from a Gaussian random process. Also sometimes there are reasons to believe that the scatterer cross sections ρ_i^2 are chi-squared variates or equivalently that ρ_i are Rayleigh distributed random variables. This supposition, in conjunction with previous assumptions concerning ρ_i and θ_i, implies that the received process is a Gaussian one.

Alternately, if the number of scatterers is exceedingly large and the cross section of each scatterer is exceedingly small, the previous assumptions pertaining to θ_i ensure that the received process is Gaussian.

It is clear that equation (3.17) depends only upon the total average cross section associated with each pair of values of r_i and ω_i; the number of scatterers involved is immaterial. Therefore it is convenient to introduce the average scatterer cross section $\tilde{\sigma}(r,f)$ associated with each such pair, that is, then following equation holds:

$$\tilde{\sigma}(r,f) = \sum_i \overline{\rho_i^2} \tag{3.18}$$

where the summation is over all scatterers for which

$$r_i = r \text{ and } \omega_i = 2\pi f = \omega \tag{3.19}$$

The correlation function $R_y(t,\tau)$ may then be expressed as follows:

$$R_y(t,\tau) = \mathrm{Re}\left\{\sum \frac{A^2}{2}\tilde{\sigma}(r,f)s_\ell(t-r)s_\ell^*(\tau-r)e^{j(\omega_0-\omega)(t-\tau)}\right\} \tag{3.20}$$

where the summation is over all pairs r and f for which $\tilde{\sigma}(r,f)$ is nonzero.

In order to satisfy mathematical convergence, it is assumed that the number of scatterers composing the medium is finite. On the other hand, there can be some situations in which it is impossible to distinguish the contributions to the received waveform of the different scatterers. This occurs when, for any given scatterer with range delay r and Doppler shift f, there are many other scatterers whose range delay differs from r by much less than the reciprocal bandwidth of $s_\ell(t)$ and when there are also many scatterers whose Doppler shift differ from f by much less than the reciprocal time duration of $s_\ell(t)$.

When this situation occurs the channel behaves as if the point function $\tilde{\sigma}(r,f)$ is replaced by a smooth density and the summation of equation (3.20) is replaced by an integral. So, $\tilde{\sigma}(r,f)$ is taken to be a density defined for all values of r and f. The cross section associated with values of delay and Doppler in the interval r to r+dr and f to f+df is then $\tilde{\sigma}(r,f)$ drdf, and equation (3.20) becomes as follows.

$$R_y(t,\tau) = \mathrm{Re}\left\{\frac{A^2}{2}\iint \tilde{\sigma}(r,f)\, s_\ell(t-r)\, s_\ell^*(\tau-r)\, e^{j(\omega_0-\omega)(t-\tau)} dr\, df\right\} \tag{3.21}$$

The function $\tilde{\sigma}(r,f)$ describes both the distribution of average cross section and also the total amount of such cross section. The following equation gives the normalized $\tilde{\sigma}(r,f)$ which is called the channel scattering function.

$$\sigma(r,f) = \tilde{\sigma}(r,f)\left[\iint \tilde{\sigma}(r,f)\, dr\, df\right]^{-1} \tag{3.22}$$

3.3 Characterization of the Time Varying Linear Channels [9]

Time varying linear channels are the channel models used for the troposcatter, ionoscatter, chaff and moon communication links and radar astronomy systems. Since these types of channels are randomly time varying the various system functions become random processes.

Let z(t) and Z(f) denote the input time function and spectrum, and w(t) and W(f) denote the output time function and spectrum of a device. In the case of a linear device, such as a linear time varying channel, the following relations can be expressed:

$$w(t) = \int z(s) K_1(t,s) ds \tag{3.23}$$

$$W(f) = \int Z(l) K_2(f,l) dl \tag{3.24}$$

$$w(t) = \int Z(f) K_3(t,f) df \tag{3.25}$$

$$W(f) = \int z(t) K_4(f,t) dt \tag{3.26}$$

The above system functions have simple physical interpretations in terms of the response of the channel to impulses and cissoids. Thus, it is readily determined that if the channel is excited with a unit impulse at t=s, the resulting channel output is the time function $K_1(t,s)$ with spectrum $K_4(f,s)$, while if the channel is excited with the cissoid $e^{j2\pi lt}$ (i.e., frequency impulse at f=l), the resulting channel output is the time function $K_3(t,f)$ with spectrum $K_2(f,l)$.

Consider the following input output relationship for a linear time varying channel obtained from the equation (3.23) by the transformation $s = t - \xi$.:

$$w(t) = \int z(t-\xi)g(t,\xi)d\xi \tag{3.27}$$

where

$$g(t, \xi) = K_1(t,t-\xi) \tag{3.28}$$

Equation (3.27) leads to a physical picture of the channel as a continuum of nonmoving scintillating scatterers. Note that the input signal is firstly delayed and then multiplied by the differential scattering gain. $g(t, \xi)$ is called input delay spread function.

If z(t) is first multiplied by a differential gain function $h(t,\xi)d\xi$ and then delayed by ξ with a continuum of ξ values, the following input output relationship is obtained:

$$w(t) = \int z(t-\xi)h(t-\xi,\xi)d\xi \tag{3.29}$$

where

$$h(t, \xi) = K_1(t+\xi,t) = g(t+\xi,\xi) \tag{3.30}$$

An entirely dual and just as general channel characterization exists in terms of frequency variables by employing the input delay spread function. Consider the following input output relationship for a linear time varying channel obtained from the equation (3.24) by the transformation l = f - υ:

$$W(f) = \int Z(f - \upsilon)H(f, \upsilon)d\upsilon \tag{3.31}$$

where

$$H(f, \upsilon) = K_2(f, f-\upsilon) \tag{3.32}$$

This dual characterization involves a representation of the output spectrum W(f) as a superposition of infinitesimal Doppler shifted (the dual of delayed) replicas of the input spectrum Z(f). H(f, υ) is called input Doppler spread function.

From equation (3.29), the dual of the output delay spread function can be deduced as follows:

$$W(f) = \int Z(f - \upsilon)G(f - \upsilon, \upsilon)d\upsilon \tag{3.33}$$

where

$$G(f, \upsilon) = K_2(f+\upsilon, f) = H(f+\upsilon, f) \tag{3.34}$$

Now, let z(t) be the input with the following inverse Fourier transform relation:

$$z(t) = \int Z(f)e^{j2\pi ft}df \tag{3.35}$$

where Z(f) is the spectrum of z(t).

Moreover,

$$\int g(t,\xi)e^{j2\pi f(t-\xi)}d\xi = e^{j2\pi ft}T(f,t) \tag{3.36}$$

where

$$T(f,t) = \int g(t,\xi)e^{-j2\pi f\xi}d\xi \tag{3.37}$$

is the Fourier transform of the input delay spread function with respect to the delay parameter. By using equations (3.27), (3.35) and (3.37), the network output can be found as follows:

$$w(t) = \int Z(f)T(f,t)e^{j2\pi ft}df \tag{3.38}$$

Since T(f,t) depends on time, it is called time varying transfer function. With equations (3.25) and (3.38), the following relation can be obtained easily:

$$T(f,t)e^{j2\pi ft} = K_3(t,f) \tag{3.39}$$

Similarly,

$$Z(f) = \int z(t)e^{j2\pi ft}dt \tag{3.40}$$

Moreover,

$$\int H(f,\upsilon)e^{-j2\pi t(f-\upsilon)}d\upsilon =^{-j2\pi ft} M(t,f) \tag{3.41}$$

where

$$M(t,f) = \int H(f,\upsilon)e^{j2\pi t\upsilon}d\upsilon \tag{3.42}$$

is the Fourier transform of the input Doppler spread function with respect to the Doppler shift variable. By using equations (3.29), (3.40), and (3.42), the network output spectrum is given by the following:

$$W(f) = \int z(t)M(t,f)e^{j2\pi ft}dt \tag{3.43}$$

In equation (3.43), M(t,f) is a frequency dependent time function used as a multiplier. Hence, it is called frequency dependent modulation function. With equations (3.26) and (3.43), the following relation can be obtained easily:

$$M(t,f).e^{-j2\pi ft} = K_4(f,t) \tag{3.44}$$

So far, it has been shown that any linear time varying channel may be interpreted either as a continuum of nonmoving scintillating scatterers with the aid of the delay spread functions, or as a continuum of hypothetical Doppler shifting elements with associated filters with the aid of the Doppler spread functions. However, any linear time varying channel may also be represented as a continuum of elements which simultaneously provide both a corresponding delay and Doppler shift. In this case, since both the delay and the Doppler shift occur, only two system functions exist. These are the input delay output Doppler shift function and input Doppler shift output delay function.

In order to determine the input delay output Doppler shift function, the input delay spread function $g(t,\xi)$ is expressed as the inverse Fourier transform of its spectrum (where ξ is considered to be a fixed parameter).

$$g(t,\xi) = \int U(\xi,\upsilon)e^{j2\pi\upsilon t}d\upsilon \tag{3.45}$$

Then, using equation (3.45) in equation (3.27), the following input output relationship is obtained:

$$w(t) = \int\int z(t-\xi)e^{j2\pi\upsilon t}U(\xi,\upsilon)d\upsilon d\xi \tag{3.46}$$

If equation (3.46) is examined, it can be seen that the output is represented as a sum of delayed and then Doppler shifted elements where $U(\xi,\upsilon)d\upsilon d\xi$ is the amplitude of the differential scattering. Hence, $U(\xi,\upsilon)$ is called delay Doppler spread function.

In an entirely analogous way, in order to determine the dual system function, i.e., that corresponding to the input Doppler shift output delay function, the input Doppler spread function $H(f, \upsilon)$ is expressed as a Fourier transform

$$H(f,\upsilon) = \int V(\upsilon,\xi)e^{-j2\pi\xi f}d\xi \tag{3.47}$$

Then, using equation (3.47) in equation (3.31), the following input output relationship is obtained:

$$W(f) = \int\int Z(f-\upsilon)e^{-j2\pi\xi f}V(\upsilon,\xi)d\xi d\upsilon \tag{3.48}$$

If equation (3.48) is examined, it can be seen that the output is represented as a sum of Doppler shifted and then delayed elements where $V(\upsilon, \xi)d\xi d\upsilon$ is the amplitude of the differential scattering. Hence, $V(\upsilon, \xi)$ is called Doppler delay spread function.

When the channel is randomly time varying, the system functions become stochastic processes. An exact statistical characterization of a randomly time varying linear channel in terms of multidimensional probability density distributions for system functions presupposes more knowledge than is likely to be available in physical situations. A practical way for this statistical characterization is based on correlation functions for the various system functions since these correlation functions allow a determination of the autocorrelation function of the channel output.

The correlation functions for the system functions explained so far are defined as follows:

$$
\begin{aligned}
R_g(t,s;\xi,\eta) &= E\{g(t,\xi)g^*(s,\eta)\} \\
R_h(t,s;\xi,\eta) &= E\{h(t,\xi)h^*(s,\eta)\} \\
R_H(f,l;\upsilon,\mu) &= E\{H(f,\upsilon)H^*(l,\mu)\} \\
R_G(f,l;\upsilon,\mu) &= E\{G(f,\upsilon)G^*(l,\mu)\} \\
R_T(f,l;t,s) &= E\{T(f,t)T^*(l,s)\} \\
R_M(t,s;f,l) &= E\{M(t,f)M^*(s,l)\} \\
R_U(\xi,\eta;\upsilon,\mu) &= E\{U(\xi,\upsilon)U^*(\eta,\mu)\} \\
R_V(\upsilon,\mu;\xi,\eta) &= E\{V(\upsilon,\xi)V^*(\mu,\eta)\}
\end{aligned}
\qquad (3.49)
$$

According to this statistical characterization, the channels can be divided into three practical classes. These are wide sense stationary (WSS) channel, the uncorrelated scattering (US) channel, and the wide sense stationary uncorrelated scattering (WSSUS) channel.

In many physical channels the fading statistics may be assumed approximately stationary for time intervals sufficiently long to make it meaningful to define a subclass of channels, called WSS channels.

A WSS channel has the property that the channel correlation functions $R_g(t,s;\xi,\eta)$, $R_h(t,s;\xi,\eta)$, $R_T(f,l;t,s)$, and $R_M(f,l;t,s)$ are invariant under a translation in time; i.e., these correlation functions depend on the variables t and s only through the difference τ=s-t. Thus, for the WSS channel

$$
\begin{aligned}
R_g(t,t+\tau;\xi,\eta) &= R_g(\tau;\xi,\eta) \\
R_h(t,t+\tau;\xi,\eta) &= R_h(\tau;\xi,\eta) \\
R_T(f,l;t,t+\tau) &= R_T(f,l;\tau) \\
R_M(t,t+\tau;f,l) &= R_M(\tau;f,l)
\end{aligned}
\tag{3.50}
$$

The restricted nature of these correlation functions constrains the remaining four channel correlation functions to have a singular behavior in the Doppler shift variables. As an example, let us consider the double Fourier transform relationship between $R_g(t,s;\xi,\eta)$ and $R_U(\xi,\eta;\upsilon,\mu)$:

$$
R_U(\xi,\eta;\upsilon,\mu) = \iint R_g(t,s;\xi,\eta)e^{j2\pi(\upsilon t-\mu s)}dtds \tag{3.51}
$$

When the variable change τ=s-t is made in equation (3.51) and using equation (3.50), the following relation can found:

$$
R_U(\xi,\eta;\upsilon,\mu) = \int e^{j2\pi t(\upsilon-\mu)}dt\int R_g(\tau;\xi,\eta)e^{j2\pi\tau\mu}d\tau \tag{3.52}
$$

By using the equation (3.52), $R_U(\xi,\eta;\upsilon,\mu)$ can be written as follows:

$$
R_U(\xi,\eta;\upsilon,\mu) = P_U(\xi,\eta;\upsilon)\delta(\upsilon-\mu) \tag{3.53}
$$

where $P_U(\xi,\eta;\upsilon)$ is the Fourier transform of $R_g(\tau;\xi,\eta)$ with respect to the variable τ.

In a similar way, the following equations can be written:

$$
\begin{aligned}
R_G(f,l;\upsilon,\mu) &= P_G(f,l;\upsilon)\delta(\upsilon-\mu) \\
R_V(\upsilon,\mu;\xi,\eta) &= P_V(\upsilon;\xi,\eta)\delta(\upsilon-\mu) \\
R_H(f,l;\upsilon,\mu) &= P_H(f,l;\upsilon)\delta(\upsilon-\mu)
\end{aligned}
\tag{3.54}
$$

where $P_G(f,l;\upsilon)$, $P_V(\upsilon;\xi,\eta)$, and $P_H(f,l;\upsilon)$ are Fourier transforms of $P_T(f,l;\tau)$, $P_h(\tau;\xi,\eta)$, and $P_M(\tau;f,l)$, respectively, with respect to the delay variable τ.

For several channels (e.g., troposcatter, chaff, moon reflection) the channel may be modeled approximately as a continuum of uncorrelated scattering (US). Thus, for the US channel the autocorrelation function of the input and output delay spread functions:

$$\begin{aligned} R_g(t,s;\xi,\eta) &= R_g(t,s;\xi)\delta(\eta-\xi) \\ R_h(t,s;\xi,\eta) &= R_h(t,s;\xi)\delta(\eta-\xi) \end{aligned} \tag{3.55}$$

The equations (3.55) imply that the autocorrelation functions of the Doppler delay spread and delay Doppler spread functions must have the following form:

$$\begin{aligned} R_U(\xi,\eta;\upsilon,\mu) &= P_U(\xi;\upsilon,\mu)\delta(\eta-\xi) \\ R_V(\upsilon,\mu;\xi,\eta) &= P_V(\upsilon,\mu;\xi)\delta(\eta-\xi) \end{aligned} \tag{3.56}$$

The forms of the correlation functions for the remaining four system functions which are readily determined from the Fourier transform relationships are given as follows:

$$\begin{aligned} R_T(f,f+\Omega;t,s) &= R_T(\Omega;t,s) \\ R_M(t,s;f,f+\Omega) &= R_M(t,s;\Omega) \\ R_G(f,f+\Omega;\upsilon,\mu) &= R_G(\Omega;\upsilon,\mu) \\ R_H(f,f+\Omega;\upsilon,\mu) &= R_H(\Omega;\upsilon,\mu) \end{aligned} \tag{3.57}$$

The simplest type of randomly time varying linear channel is the WSSUS channel. As its name implies, WSSUS channel is both WSS and US. Thus, for the WSSUS channel the correlation functions of the delay spread functions must have the following form:

$$\begin{aligned} R_g(t,t+\tau;\xi,\eta) &= R_g(\tau;\xi)\delta(\eta-\xi) \\ R_h(t,t+\tau;\xi,\eta) &= R_h(\tau;\xi)\delta(\eta-\xi) \end{aligned} \tag{3.58}$$

The correlation functions of the Doppler spread functions must have the following form:

$$
\begin{aligned}
R_G(f, f+\Omega; \upsilon, \mu) &= P_G(\Omega; \upsilon)\delta(\upsilon - \mu) \\
R_H(f, f+\Omega; \upsilon, \mu) &= P_H(\Omega; \upsilon)\delta(\upsilon - \mu)
\end{aligned}
\tag{3.59}
$$

For the WSSUS channel, the correlation functions of the delay Doppler spread and Doppler delay spread functions becomes simplified as follows:

$$
\begin{aligned}
R_U(\xi, \eta; \upsilon, \mu) &= P_U(\xi; \upsilon)\delta(\mu - \upsilon)\delta(\eta - \xi) \\
R_V(\upsilon, \mu; \xi, \eta) &= P_V(\upsilon; \xi)\delta(\mu - \upsilon)\delta(\eta - \xi)
\end{aligned}
\tag{3.60}
$$

Finally, for the WSSUS channel, the correlation functions of the time varying transfer function and the frequency dependent modulation function take the following simple forms:

$$
\begin{aligned}
R_T(f, f+\Omega; t, t+\tau) &= R_T(\Omega; \tau) \\
R_M(t, t+\tau; f, f+\Omega) &= R_M(\tau; \Omega)
\end{aligned}
\tag{3.61}
$$

Now, let us consider the time varying multipath channel general expression (3.62), which was also given in equation (3.17) [11], and repeated here for convenience.

$$
c_\ell(\tau; t) = \begin{cases} \sum\limits_i \alpha_i(t)\, e^{-j\omega_0\tau_i(t)}\, \delta(t - \tau_i(t)), & \text{discrete multipath components exist} \\ \alpha(\tau; t)\, e^{-j\omega_0\tau}, & \text{continuous multipath components exist} \end{cases}
\tag{3.62}
$$

Now, let us consider the transmission of an unmodulated carrier at frequency f_0, i.e., $s(t) = e^{j\omega_0 t}$. Then, $s_\ell(t) = 1$. Hence, the received signal for the case of discrete multipath is given as follows (see equation (3.11)):

$$
y_\ell(t) = \sum_n \alpha_n(t)\, e^{-j\omega_0\tau_n(t)} = \sum_n \alpha_n(t)\, e^{-j\theta_n(t)}
\tag{3.63}
$$

Thus, the received signal consists of the sum of a number of time varying vectors having amplitudes $\alpha_n(t)$ and phases $\theta_n(t)$. Since both these quantities change with an unpredictable manner, the received signal can be modeled as a random process. When there are a large number of paths, with the central limit theorem $y_\ell(t)$ can be modeled as a complex valued Gaussian random process. This means that the time varying impulse response of the channel $c_\ell(\tau;t)$ is a complex valued Gaussian random process in the *t* variable. The autocorrelation function of $c_\ell(\tau;t)$ is defined, assuming that the channel is wide sense stationary (WSS), as given below [11]:

$$\Phi_c(\tau_1,\tau_2;\Delta t) = \frac{1}{2} E[c_\ell^*(\tau_1;t)c_\ell(\tau_2;t+\Delta t)] \tag{3.64}$$

In most transmission media, the attenuation and phase shift of the channel associated with path delay τ_1 is uncorrelated with the attenuation and phase shift associated with path delay τ_2. So, the channel can be assumed to be an uncorrelated scattering (US) channel. Moreover, it is assumed that $c_\ell(\tau;t)$ is wide sense stationary. Hence, the channel autocorrelation function becomes as follows:

$$\Phi_c(\tau_1,\tau_2;\Delta t) = \frac{1}{2} E[c_\ell^*(\tau_1;t)c_\ell(\tau_2;t+\Delta t)] = \Phi_c(\tau_1;\Delta t)\,\delta(\tau_1-\tau_2) \tag{3.65}$$

If $\Delta t = 0$, then $\Phi_c(\tau;0) \equiv \Phi_c(\tau)$ is simply the average power output of the channel as a function of time delay τ. For this reason $\Phi_c(\tau)$ is called "multipath intensity profile" or "delay power spectrum". The range value of τ over which $\Phi_c(\tau)$ is essentially nonzero is called the "multipath spread of the channel" and is denoted by T_m. $\Phi_c(\tau)$ is shown in Figure 3.1.

In practice, the function $\Phi_c(\tau;\Delta t)$ is measured by transmitting very narrow pulses or, equivalently, a wideband signal and cross correlating the received signal with a delayed version of itself.

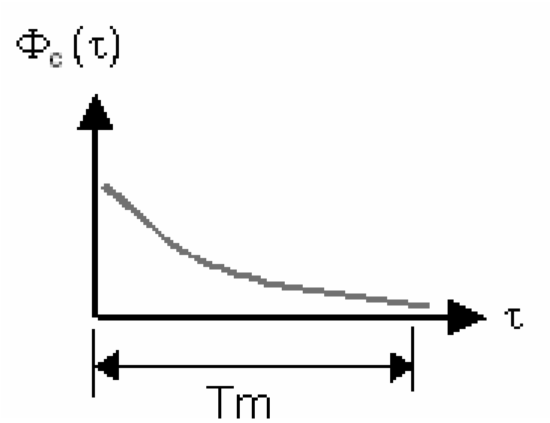

Figure 3.1 Multipath intensity profile

A completely analogous characterization of the time varying multipath channel begins in the frequency domain. By taking the Fourier transform of $c_\ell(\tau;t)$ the time varying transfer function $C_\ell(f;t)$ is obtained, where f is the frequency variable. Thus,

$$C_\ell(f;t) = \int_{-\infty}^{\infty} c_\ell(\tau;t)\, e^{-j2\pi f\tau} d\tau \tag{3.66}$$

If $c_\ell(\tau;t)$ is modeled as a complex valued zero mean Gaussian random process in the t variable, $C_\ell(f;t)$ has the same statistics. Under the assumption that the channel is wide sense stationary, autocorrelation function is expressed as follows:

$$\Phi_C(f_1, f_2; \Delta t) = \frac{1}{2} E[C_\ell^*(f_1;t) C_\ell(f_2; t+\Delta t)] \tag{3.67}$$

Moreover, the following relation exists:

$$\begin{aligned}\Phi_C(f_1, f_2; \Delta t) &= \frac{1}{2} \int_{-\infty}^{\infty}\int_{-\infty}^{\infty} E[c_\ell^*(\tau_1;t) c_\ell(\tau_2; t+\Delta t)]\, e^{j2\pi(f_1\tau_1 - f_2\tau_2)} d\tau_1 d\tau_2 \\ &= \frac{1}{2} \int_{-\infty}^{\infty}\int_{-\infty}^{\infty} \Phi_c(\tau_1;\Delta t)\, \delta(\tau_1 - \tau_2)\, e^{j2\pi(f_1\tau_1 - f_2\tau_2)} d\tau_1 d\tau_2\end{aligned}$$

$$= \frac{1}{2}\int_{-\infty}^{\infty}\Phi_c(\tau_1;\Delta t)\, e^{j2\pi(f_1-f_2)\tau_1} d\tau_1$$
$$= \frac{1}{2}\int_{-\infty}^{\infty}\Phi_c(\tau_1;\Delta t)\, e^{-j2\pi\Delta f\tau_1} d\tau_1 \equiv \Phi_C(\Delta f;\Delta t) \tag{3.68}$$

where $\Delta f = f_2 - f_1$. $\Phi_C(\Delta f;\Delta t)$ is the spaced frequency, spaced time correlation function of the channel.

$\Phi_C(f_1,f_2;\Delta t)$ can be measured in practice by transmitting a pair of sinusoids separated by Δf and crosscorrelating the two separately received signals with a relative delay Δt.

Now, if $\Delta t=0$, then, with $\Phi_C(\Delta f;0) \equiv \Phi_C(\Delta f)$ and $\Phi_c(\tau;0) \equiv \Phi_c(\tau)$, the transformation shown in equation (3.69) can be written.

$$\Phi_C(\Delta f) = \int_{-\infty}^{\infty}\Phi_c(\tau)\, e^{-j2\pi\Delta f\tau} d\tau \tag{3.69}$$

Since $\Phi_C(\Delta f)$ is an autocorrelation function in the frequency variable, it provides the measure of the frequency coherence of the channel. The relationship between $\Phi_C(\Delta f)$ and $\Phi_c(\tau)$ is shown in Figure 3.2.

$\Phi_C(\Delta f)$ is the spaced frequency correlation function, and $(\Delta f)_c \approx 1/T_m$ is the coherence bandwith of the channel. Two sinusoids with frequency separation greater than $(\Delta f)_c$ are affected differently by the channel.

Now, for the time variations of the channel, the time variations in the channel are evidenced as Doppler broadening and perhaps a Doppler shift of a spectral line. In order to relate the Doppler effects to the time variations of the channel, the Fourier transform of $\Phi_C(\Delta f;\Delta t)$ with respect to the variable Δt is defined as follows:

$$S_C(\Delta f;\lambda) = \int_{-\infty}^{\infty} \Phi_C(\Delta f;\Delta t)\, e^{-j2\pi\lambda\Delta t} d\Delta t \tag{3.70}$$

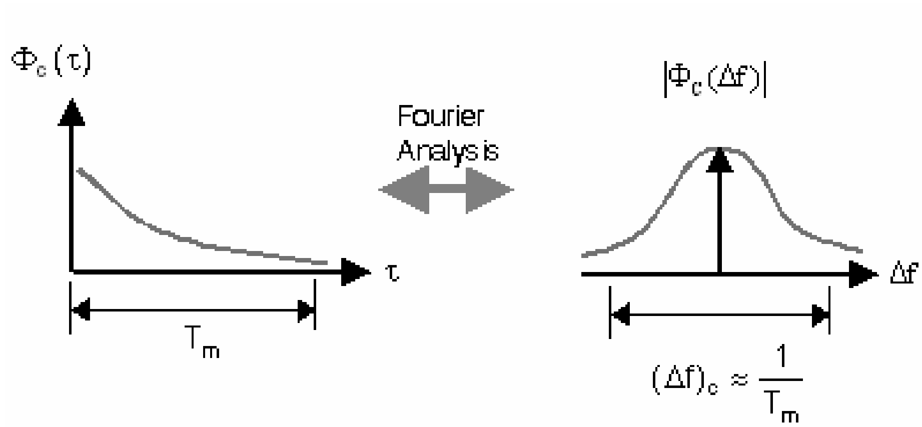

Figure 3.2 Multipath intensity profile and spaced frequency correlation function

If $\Delta f=0$, then $S_C(0;\lambda) \equiv S_C(\lambda)$ and $S_C(\lambda) = \int_{-\infty}^{\infty} \Phi_C(\Delta t)\, e^{-j2\pi\lambda\Delta t} d\Delta t$. Here, $S_C(\lambda)$ is the Doppler power spectrum of the channel.

It can be observed that if the channel is time invariant, $\Phi_C(\Delta t) = 1$ and $S_C(\lambda) = \delta(\lambda)$. Therefore, there is no spectral broadening observed in the transmission of a pure frequency tone.

The range of values λ over which $S_C(\lambda)$ is essentially nonzero is called the Doppler spread B_d of the channel. Since $S_C(\lambda)$ is related to $\Phi_C(\Delta t)$ by the Fourier transform, the reciprocal of B_d is a measure of the coherence time of the channel. They are shown in the Figure 3.3.

So far, a Fourier transform relation between $\Phi_C(\Delta f;\Delta t)$ and $\Phi_c(\tau;\Delta t)$ involving the variables $(\tau,\Delta f)$, a Fourier transform relation between $\Phi_C(\Delta f;\Delta t)$ and $S_C(\Delta f;\lambda)$ involving the variables $(\Delta t,\lambda)$ have been established. Now, a relationship between $\Phi_c(\tau;\Delta t)$ and $S_C(\Delta f;\lambda)$ can be defined and close the loop. This relationship is obtained by defining a new function, denoted by S(τ; λ) to be the Fourier transform of $\Phi_c(\tau;\Delta t)$ in the Δt variable given as follows:

$$S(\tau;\lambda)=\int_{-\infty}^{\infty}\Phi_c(\tau;\Delta t)\,e^{-j2\pi\lambda\Delta t}d\Delta t \qquad (3.71)$$

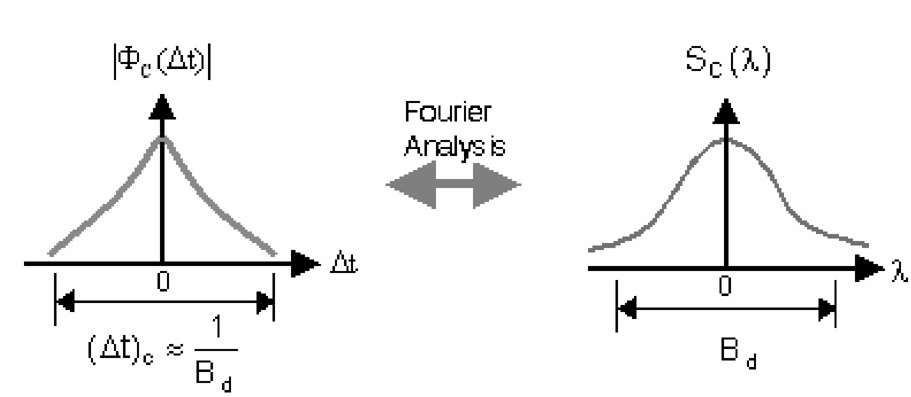

Figure 3.3: Spaced time correlation function and Doppler power spectrum

It can be seen that S(τ; λ) and $S_C(\Delta f;\lambda)$ are a Fourier transform pair. That is,

$$S(\tau;\lambda)=\int_{-\infty}^{\infty}S_C(\Delta f;\lambda)\,e^{j2\pi\tau\Delta f}d\Delta f \qquad (3.72)$$

Furthermore,

$$S(\tau;\lambda)=\int_{-\infty}^{\infty}\int_{-\infty}^{\infty}\Phi_C(\Delta f;\Delta t)\,e^{j2\pi\tau\Delta f}e^{-j2\pi\lambda\Delta t}d\Delta t d\Delta f \qquad (3.73)$$

Here, $S(\tau;\lambda)$ is called the scattering function of the channel which was defined in section 3.2.

A sample scattering function is shown in Figure 3.4. The physical explanation of scattering function was given in section 3.2.

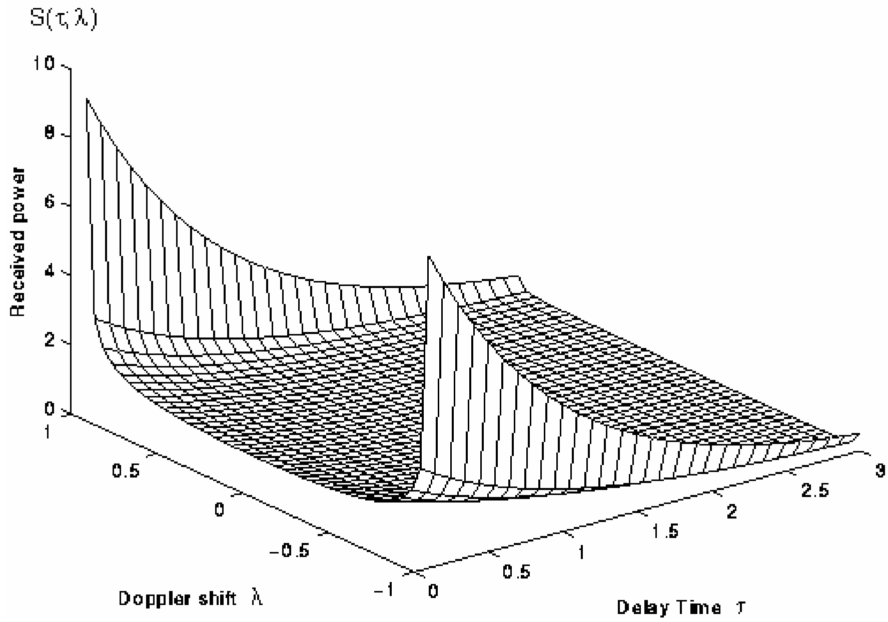

Figure 3.4 Scattering function

3.4 Channel Classifications [10]

3.4.1. Nondispersive Channels

A nondispersive channel can be defined with the following scattering function:

$$\sigma(\tau;f) = \delta(\tau)\delta(f) \tag{3.74}$$

So, the channel output y(t) in response to the following transmitted waveform

$$s(t) = \mathrm{Re}\left\{s_\ell(t)e^{j\omega_0 t}\right\} \tag{3.75}$$

is

$$y(t) = A\rho\,\mathrm{Re}\left\{s_\ell(t)e^{j(\omega_0 t-\theta)}\right\} \tag{3.76}$$

where θ and ρ are statistically independent random variables that are not functions of time and frequency. ρ is Rayleigh distributed and θ is uniformly distributed between -π to +π. A nondispersive channel is sometimes called flat flat fading channel. This type of channels only creates time invariant attenuation and phase shift.

3.4.2. Channels Dispersive Only in Time

A channel is said to be dispersive only in time, or not dispersive in frequency, if its scattering function is defined as follows:

$$\sigma(\tau; f) = \sigma(\tau)\delta(f) \tag{3.77}$$

This type of channel is also called frequency selective slowly fading channel. The channel output y(t) in response to the following transmitted waveform

$$s(t) = \mathrm{Re}\left\{s_\ell(t)e^{j\omega_0 t}\right\} \tag{3.78}$$

is

$$y(t) = \mathrm{Re}\left\{\sum_i A\rho_i s_\ell(t - r_i)e^{j(\omega_0(t - r_i) - \theta_i)}\right\} \tag{3.79}$$

If the following condition holds

$$T_m W << 1 \tag{3.80}$$

where T_m is multipath spread of the channel and W is the signal bandwidth, then the following holds:

$$s_\ell(t - r_i) \approx s_\ell(t) \tag{3.81}$$

Hence,

$$\begin{aligned} y(t) &\approx \mathrm{Re}\left\{\sum_i A\rho_i s_\ell(t) e^{j(\omega_0 t-\theta_i)} e^{-j\omega_0 r_i}\right\} \\ &\approx \mathrm{Re}\left\{\left[s_\ell(t) e^{j\omega_0 t}\left[\sum_i A\rho_i e^{-j\theta_i} e^{-j\omega_0 r_i}\right]\right]\right\} \end{aligned} \tag{3.82}$$

That is, the received waveform differs from the transmitted waveform only by a scale factor (or fade) and a carrier phase shift. On the other hand, if W is increased the product $T_m W$ increases and at some point the approximation given in (3.81) will not hold anymore and the returns from some of the scatterers combine destructively, or interfere.

In summary, one manifestation of time dispersion in a channel is the presence of time spreading or distortion or both in the received waveform. As W increases distortion of the waveform appears firstly and then time spreading (dispersion) appears. This results in ISI. The severity of these effects depends upon both the nature of the transmitted waveform and the channel scattering function.

Now, in order to see the effect of time dispersion in frequency domain, let us take one realization of the transmitted waveform. The Fourier transform S(f) of the transmitted waveform is given as follows:

$$S(f) = \frac{1}{2}\left[S_\ell(f-f_0) + S_\ell^*(-f-f_0)\right] \tag{3.83}$$

Then, by virtue of (3.82), the expression of the received waveform is as follows:

$$\begin{aligned} y(t) &= \mathrm{Re}\left\{\sum_i A\rho_i s_\ell(t-r_i) e^{j(\omega_0(t-\tau_i)-\theta_i)}\right\} \\ &= \mathrm{Re}\left\{\sum_i \eta_i s_\ell(t-r_i) e^{j\omega_0(t-\tau_i)}\right\} \\ &= \frac{1}{2}\sum_i \eta_i s_\ell(t-r_i) e^{j(\omega_0(t-\tau_i))} + \frac{1}{2}\sum_i \eta_i^* s_\ell^*(t-r_i) e^{-j(\omega_0(t-\tau_i))} \end{aligned} \tag{3.84}$$

where

$$\eta_i = A\rho_i e^{-j\theta_i} \tag{3.85}$$

Then, the Fourier transform of the received waveform y(t) can be written as follows:

$$\begin{aligned} Y(f) &= \frac{1}{2} S_\ell(f - f_0) \sum_i \eta_i e^{-j2\pi\tau_i f} + \frac{1}{2} \sum_i S_\ell^*(-f - f_0) \eta_i^* e^{j2\pi\tau_i f} \\ &= \frac{1}{2} S_\ell(f - f_0) H(f) + \frac{1}{2} S_\ell^*(-f - f_0) H^*(-f) \end{aligned} \tag{3.86}$$

where

$$H(f) = \sum_i \eta_i e^{-j2\pi f\tau_i} \tag{3.87}$$

Equations (3.83) and (3.86) show the effect of time dispersion as the attenuation of certain frequency components of the transmitted waveform. This interpretation provides a more precise description of the distortion introduced by the constructive and destructive combination of the contributions from different scatterers. Because of this description, the manifestation of time dispersion is often called *frequency selective fading*.

If $T_m W \ll 1$ then the exponential term in equation (3.87) becomes nearly 1. Hence, the following approximation can be made:

$$H(f) \approx \sum_i \eta_i \,, \quad \text{for } |f| < W \tag{3.88}$$

That is, Y(f) differs from S(f) only by a complex constant. So, if $T_m W$ is much less than unity then the channel is nondispersive in time.

A scattering function sample of the frequency selective slowly fading channel is shown in Figure 3.5. As shown in this figure, it introduces changes over frequency but it does not cause changes over time.

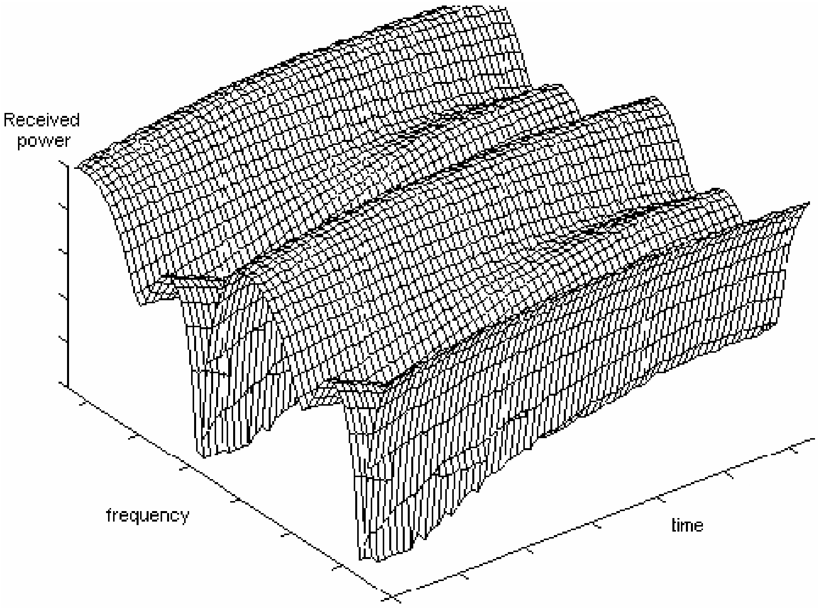

Figure 3.5 Frequency selective, slowly fading channel

3.4.3. Channels Dispersive Only in Frequency

A channel is said to be dispersive only in frequency, or not dispersive in time, if its scattering function is defined as follows:

$$\sigma(\tau;f) = \delta(\tau)\sigma(f) \tag{3.89}$$

This type of channel is also called frequency nonselective fast fading channels. The channel output y(t) in response to the following transmitted waveform

$$s(t) = \mathrm{Re}\left\{s_\ell(t)e^{j\omega_0 t}\right\} \tag{3.90}$$

is

$$
\begin{aligned}
y(t) &= \mathrm{Re}\left\{\sum_i A\rho_i s_\ell(t)e^{j\omega_0(t-\dot{\tau}_i t)}\right\} \\
&= \mathrm{Re}\left\{\sum_i A\rho_i s_\ell(t)e^{j(\omega_0-\omega_i)t}\right\}
\end{aligned}
\tag{3.91}
$$

where $\dot{\tau}_i = \dfrac{\omega_i}{\omega_0}$.

If the following condition holds

$$W_i T << 1 \tag{3.92}$$

where W_i is the Doppler spread of the channel the and T is the signal duration, then

$$e^{jt(\omega_0-\omega_i)} \approx e^{j\omega_0 t}, \ \text{for } |\omega_i| < W_i/2 \tag{3.93}$$

Hence,

$$
\begin{aligned}
y(t) &\approx \mathrm{Re}\left\{\sum_i A\rho_i s_\ell(t)e^{j\omega_0 t}\right\} \\
&\approx \mathrm{Re}\left\{s_\ell(t)e^{j\omega_0 t}\sum_i A\rho_i\right\}
\end{aligned}
\tag{3.94}
$$

That is, the received process differs from the transmitted waveform only by a scale factor (or fade). On the other hand, if T is increased the product W_iT increases and at some point the approximation given in (3.93) will not hold anymore and there will be frequency spreading. That is, as T increases distortion of the waveform appears first and then frequency spreading (dispersion) appears.

Now, in order to see the effect of frequency dispersion in frequency domain, let us take one realization of the received waveform. If W_iT is near to unity then the Fourier transform of the received waveform y(t) given in equation (3.91) will be expressed as follows:

$$Y(f) = \frac{1}{2}\sum_i A\rho_i U\left(f-(f_0-f_i)\right)+\frac{1}{2}\sum_i A\rho_i^* U^*\left(-f-(f_0-f_i)\right) \qquad (3.95)$$

The inverse Fourier transform (IFFT) of equation (3.95) shows the effect of frequency dispersion as the attenuation of certain time components of the transmitted waveform due to f_i. As in the time dispersion case, this interpretation provides a more precise description of the distortion introduced by the constructive and destructive combination of the contributions from different scatterers. Because of this description, the manifestation of frequency dispersion is called *time selective fading*.

A scattering function sample of the frequency nonselective fast fading channel is shown in Figure 3.6. As shown in this figure, it introduces changes over time but it does not cause changes over frequency.

3.4.4 Time Frequency Dispersive Channels

A channel is said to be time frequency dispersive if it is both time dispersive and frequency dispersive, in other words the channel is frequency selective and fast fading. If the channel is frequency selective and fast fading, then its scattering function will be like in Figure 3.7. In this case, channel introduces changes both over time and frequency.

3.5 HF Channel [13]

HF channel scattering function has been experimentally examined for the wideband case by Wagner and Basler in 1988. Various models are also available for use in estimating channel properties. An early model has found restricted use for analysis of narrowband channels by Watterson in 1970 [8]. Some more recent wideband HF channel models are discussed in [13 - 16].

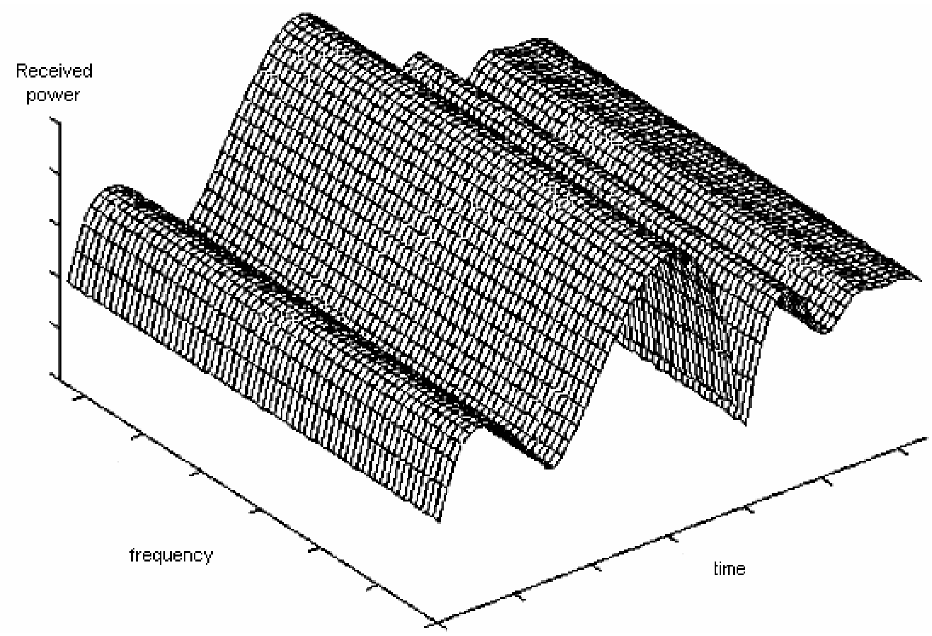

Figure 3.6 Frequency nonselective, fast fading channel

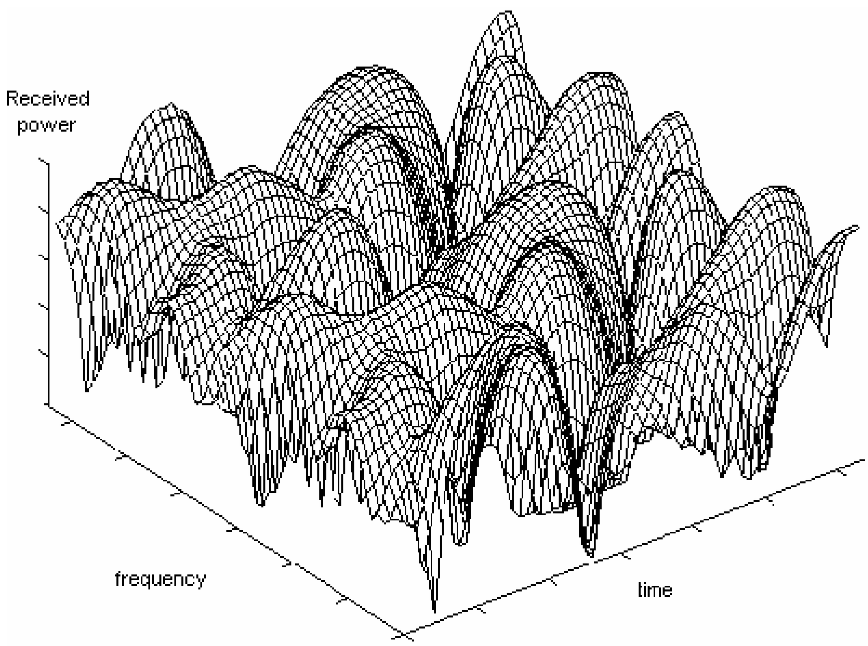

Figure 3.7 Frequency selective, fast fading channel

Knowledge of the ionospheric multipath structure has been greatly enhanced through investigation by wideband probes and sounders. As FMCW type sounder has been developed by Salous [1989], and a wideband HF system study has been carried out by MITRE. In addition, Rome Air Development Center (RADC) has investigated a variety of adaptive probing techniques and SRI has developed a set of channel probe parameters for disturbed media.

As far as the HF channel is concerned, two forms of propagation effects are noteworthy, losses and distortion. Losses include spreading loss, focusing loss, ducting loss, and absorption loss. Major sources of distortion include time variation of channel parameters, multipath, and signal dispersion. In general it may be said that the multipath introduces two forms of impairment depending upon whether or not the multipath delay is intermodal or intramodal. Intermodal delays are due to multimode and multihop propagation, and give rise to ISI. Here, multimode propagation is a multipath condition in which RF energy is received from two (or more) ionospheric layers simultaneously and multihop propagation is a multipath condition in which the radio wave undergoes multiple bounces from a specified ionospheric layer. Intramodal delays are due to geomagnetic field effects, range spread due to ionospheric inhomogeneities, and the dispersive property of the ionospheric medium (independent of any structure present). Intramodal delays cause distortion of the pulse and place limits on channel bandwidth. Time dispersion is the result of variation of signal velocity with frequency. Thus, individual frequency components transmitted at a time t_0 will arrive at a destination within a time envelope defined by $t_0+T+\delta t$, where T is the median time delay, and δt is the time delay spread of the individual components. Time dispersion has a greater impact on wideband systems than narrowband ones and is generally felt to be responsible for a limitation in the coherence bandwidth. Indeed, a nonlinear phase and group delay properties of the channel transfer function will distort wideband waveforms significantly, and this may be observed both as broadening of the received pulse and a reduction in its amplitude. Dispersion is considerably greater for short skywave paths than for long-haul paths. Another form of signal distortion is that which is introduced by Faraday rotation or polarization interference. If the transmission bandwidth is equal to or larger than the polarization bandwidth (but not large enough to resolve the two magnetoionic modes responsible for the effect) considerable distortion and fading may be introduced. The physical characteristics of the HF channel can be investigated further in [13].

Multipath arises when the received signal obeys one of the following conditions: (1) the signal is nondispersively distended by multiple reflections from the ionosphere with or without ground reflections (more than 1 hop or layer is involved); or (2) the signal is distorted by the superposition of multiple and near equal amplitude sources within a single layer. Fading is involved in two cases. Although amplitude fading is an important deleterious effect attributed to ionospheric multipath, the most serious impact of multipath in digital systems is intersymbol interference (ISI). It is also worth noting that ionospheric irregularities within a single layer are generally in pseudorandom motion, and there can be Doppler spreads when micromultipath returns are evident.

In this work, HF channel model is selected as the communication medium and Watterson HF channel model is used. Hence, at this point it is convenient to study this channel model.

3.5.1 Watterson HF Channel Model [8, 13]

HF ionospheric channels are nonstationary in both frequency and time, but for band-limited channels (10 kHz) and sufficiently short times (10 minutes), most channels are nearly stationary and they can be represented by a stationary model. For this fortunate characteristic, the Watterson channel model is widely used in order to represent narrowband and short duration HF channels. The ionosphere exhibits another fortunate characteristic: In a substantial percentage of the channels, propagation is over a limited number of relatively discrete modes. These characteristics allow to select the stationary channel model.

The Watterson channel can be modelled as a tapped delay line as shown in Figure 3.8. The signal at each tap is modulated in amplitude and phase by a suitable baseband tap-gain function $G_i(t)$, and the several delayed and modulated signals are summed to form the received signal. One tap or path is used for each modal component, wave reflecting from an ionospheric layer, that is resolvable in time. While each mode in general contains two components, the ordinary magnetoionic component (corresponds to the low ray) and extraordinary magnetoionic component (corresponding to the high ray), both when present are not necessarily resolvable. Any pair of components is resolvable only when their differential propagation time is greater than about one fourth of the reciprocal of the bandwidth of interest.

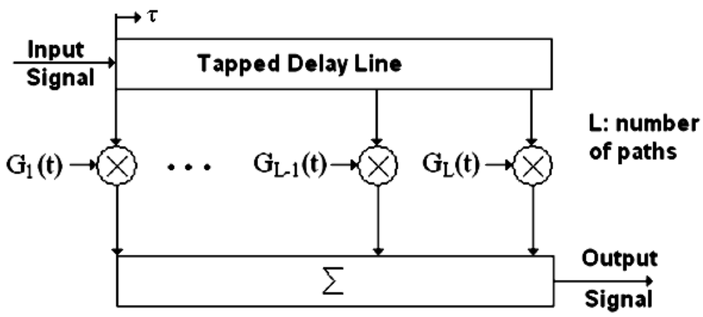

Figure 3.8 Watterson HF channel model

Two magnetoionic components are resolvable in frequency, then Gaussian spectrum components can be used. Hence, according to CCIR 549-2, the tap $G_i(t)$ may be represented as the sum of two independent complex (bivariate) Gaussian ergodic random processes, each with zero mean values and independent real and imaginary components with equal r.m.s. values that produce Rayleigh fading.

$$G_i(t) = G_{ia}(t)e^{j2\pi f_{ia}t} + G_{ib}(t)e^{j2\pi f_{ib}t} \tag{3.96}$$

where a and b represent the two possible magnetoionic components, and the exponentials allow for Doppler shifts for the components.

Let $G_{ia}(t)$ is defined in terms of its real and imaginary components as

$$G_{ia}(t) = g_{iar}(t) + j\, g_{iai}(t) \tag{3.97}$$

where $g_{iar}(t)$ and $g_{iai}(t)$ are independent real Gaussian processes with the following single time jointly density function:

$$p(g_{iar}, g_{iai}) = \frac{1}{\pi C_{ia}(0)} e^{-\frac{g_{iar}^2 + g_{iai}^2}{C_{ia}(0)}} \tag{3.98}$$

where $C_{ia}(0)$ is the autocorrelation of $G_{ia}(t)$ at $\Delta t = 0$. Furthermore, the spectra of $g_{iar}(t)$ and $g_{iai}(t)$ are equal.

Since $g_{iar}(t)$ and $g_{iai}(t)$ are independent, $G_{ia}(t)$ has a spectrum that is the sum of the identical spectra of $g_{iar}(t)$ and $g_{iai}(t)$ and it has even symmetry about $\nu=0$.

The tap gain correlation function is given as follows:

$$C_i(\Delta t) = C_{ia}(0) e^{-2\pi^2 \sigma_{ia}^2 (\Delta t)^2 + j2\pi f_{ia} \Delta t} + C_{ib}(0) e^{-2\pi^2 \sigma_{ib}^2 (\Delta t)^2 + j2\pi f_{ib} \Delta t} \tag{3.99}$$

The tap gain spectrum is given as follows:

$$S_{G_i}(f) = \frac{C_{ia}(0)}{(2\pi)^{1/2} \sigma_{ia}} e^{-\frac{(f - f_{ia})^2}{2\sigma_{ia}^2}} + \frac{C_{ib}(0)}{(2\pi)^{1/2} \sigma_{ib}} e^{-\frac{(f - f_{ib})^2}{2\sigma_{ib}^2}} \tag{3.100}$$

Equation (3.100) is shown in Figure 3.9. Now, of course, it must be recognized that each $G_i(t)$ is associated with a nominal time delay τ_i. Thus, the transfer function for a single mode is given by the following:

$$H_i(f;t) = G_i(t) e^{j2\pi f_i t} e^{j2\pi f \tau_i} \tag{3.101}$$

where the presence of two unresolved magnetoionic modes have been suppressed.

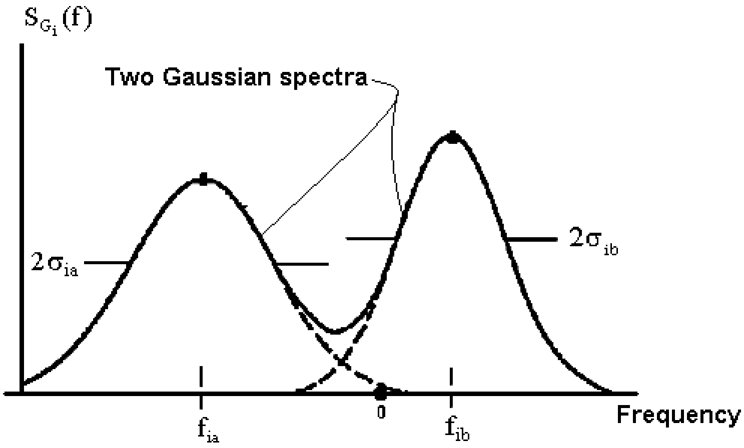

Figure 3.9 Tap gain spectra of Watterson HF channel

It should be noted that the Watterson model is applicable only under conditions of channel stability and stationarity. For use in the Watterson model, the following limits should be considered:

- Channel bandwidth ≈ 12 kHz or smaller
- Channel is time and frequency stationary
- Channel has low delay dispersion
- Only low rays are considered.

CHAPTER 4

CHANNEL ESTIMATION AND TRACKING

In this chapter, the investigated channel estimation and tracking methods will be explained. First the literature survey about the channel estimation and tracking methods will be summarized. Then, the problem statement will be given. After that, least squares (LS) and linear minimum mean square error (LMMSE) channel estimation methods will be explained. After that, least mean squares (LMS), recursive least square (RLS), and Kalman filter channel tracking methods will be explained in order. For LMS and RLS methods some adaptive schemes will also be investigated. Moreover, according to the state variables two types of Kalman filter will be investigated.

4.1 Literature Survey for Channel Estimation and Tracking

OFDM systems employing coherent detection require estimation and tracking of fading channel. In order to eliminate the need for channel estimation and tracking, differential noncoherent demodulation can be used in OFDM, at the expense of a 3 dB loss BER performance compared with coherent detection scheme. However, for spectrally efficient OFDM systems, coherent modulation is more appropriate. Furthermore, by using channel state information adaptive loading algorithms can be used to improve performance under Rayleigh fading [3, 17, 18].

Channel estimation methods are used to obtain channel state information (CSI). They can be divided into two main methods: Pilot symbol aided (PSA) channel estimation and blind (semiblind) channel estimation. Depending on the characteristics of the channel these two methods can be applied in various ways. The channel may be frequency selective, or fast fading (time selective), or frequency selective and fast fading, or frequency nonselective and slowly fading as described in section 3.4.

In PSA channel estimation techniques, some known pilot symbols are transmitted in the given positions of the time frequency grid. Then, in the receiver the channel is estimated over the pilot subcarriers. After that, this estimate is interpolated or smoothed over the entire time frequency grid [19, 20]. Besides interpolation methods, channel estimation can be performed through the estimation of the channel impulse response via inverse fast Fourier transform (IFFT) [21].

In the literature, some investigated PSA estimation methods are least squares (LS) channel estimation, minimum mean square error (MMSE) channel estimation, decision directed channel estimation, interpolation based channel estimation. Besides the investigations of various channel estimation methods, various pilot frequency time patterns are investigated for a given channel estimation method and channel [20].

MMSE channel estimation method is used by exploiting time domain correlation or frequency domain correlation or both, depending on the characteristics of the channel [3, 18, 21-23]. Since the MMSE channel estimation method is a computationally complex method, various simplifications are proposed. Instead of MMSE channel estimation method, linear minimum mean square error (LMMSE) channel estimation method with singular value decomposition (SVD) can be used [25].

Least squares (LS) channel estimation method is not as computationally complex as the MMSE channel estimation method is. However, the performance of the former is poorer than the performance of the latter [22].

Decision directed channel estimation methods [17, 25-27] and interpolation based [28, 29] channel estimation methods are other alternative channel estimation methods. They can be used for frequency selective channels and fast fading channels.

For the PSA channel estimation methods, selection of the pilot frequency time pattern is one of the crucial steps. The selection is performed depending on the characteristics of the channel. For example, for fast fading channels it is appropriate to put pilot symbols into some subcarriers but for all OFDM symbols. Whereas, for frequency selective flat fading channels it is appropriate to put the pilot symbols not for all OFDM symbols but into each subcarriers. So that, fast variations of the channel in time domain or in frequency domain can be tracked [30].

Besides channel estimation methods, channel tracking techniques can be employed for time varying multipath fading channels so that channel variations can be tracked and also channel variations can be filtered up to some level in order to reduce the channel impairments caused by noise and interference. In the literature, least mean square (LMS), recursive least squares (RLS) and Kalman filter based methods exist [31-35]. These methods can be used also for OFDM systems [23, 36-39].

As for blind (semi blind) channel estimation techniques, no pilot symbols are used. This satisfies more efficient use of the bandwidth and provides stealthy communication. In the literature, some blind channel estimation methods are maximum likelihood approach [27, 40, 41], expectation maximization approach [42], subspace approaches using cyclic prefix subspace approach, subspace based approaches exploiting virtual carriers [43], cyclic prefix [44], and noise subspace [45]. Additionally, blind channel estimation based on receiver diversity [46] and white preamble [47] also exist.

In case of HF channels, the given channel estimation methods for time varying multipath fading channels are applicable [17, 48-50].

4.2 Channel Estimation and Tracking Methods

4.2.1 Problem statement

After the demodulation process in the OFDM receiver, the following demodulated OFDM signal, whose derivation was explained in section 2.2, is obtained.

$$y_{k,n} = H_{k,n} a_{k,n} + N_{k,n} \tag{4.1}$$

Here, $H_{k,n}$ is the channel frequency response at k^{th} subcarrier for n^{th} OFDM symbol. $y_{k,n}$ and $a_{k,n}$ are the received and the transmitted symbol at k^{th} subcarrier for n^{th} OFDM symbol, respectively. $N_{k,n}$ is the zero mean AWGN at k^{th} subcarrier for n^{th} OFDM symbol. The channel is assumed to be Rayleigh distributed. Hence, the mean of $H_{k,n}$ is zero.

During channel estimation and tracking process some known pilot symbols are transmitted and at the position of these pilot symbols $H_{k,n}$ are estimated. For packet based communication, the estimated $H_{k,n}$ can be tracked after some initialization procedure.

Let us define the following matrices:

$$\overline{y}_n = \begin{bmatrix} y_{0,n} \\ y_{1,n} \\ \vdots \\ y_{N-1,n} \end{bmatrix}, \ \overline{a}_n = \begin{bmatrix} a_{0,n} & 0 & \cdots & 0 \\ 0 & a_{1,n} & \cdots & 0 \\ \vdots & \vdots & \ddots & \vdots \\ 0 & 0 & \cdots & a_{N-1,n} \end{bmatrix}, \ \overline{H}_n = \begin{bmatrix} H_{0,n} \\ H_{1,n} \\ \vdots \\ H_{N-1,n} \end{bmatrix}, \ \overline{N}_n = \begin{bmatrix} N_{0,n} \\ N_{1,n} \\ \vdots \\ N_{N-1,n} \end{bmatrix} \tag{4.2}$$

Then, equation (4.1) can be written in matrix form as

$$\overline{y}_n = \overline{a}_n \overline{H}_n + \overline{N}_n \tag{4.3}$$

Channel estimation and channel tracking equations are solved for pilot symbols for each subchannel, separately. After finding $H_{k,n}$ values at the pilot symbols, other $H_{k,n}$ values can be found using interpolation. Hence, the main problem is to find all $H_{k,n}$ for n^{th} OFDM symbol during this symbol is investigated.

4.2.2 Channel Estimation Methods

4.2.2.1 Least Squares (LS) Estimation [22]

In LS estimation, the cost function given in equation (4.4) should be minimized with respect to $\overline{H}_n$. Hence, the estimated channel can be found by minimizing

$$C = \left\| \overline{a}_n \overline{H}_n - \overline{y}_n \right\|^2 = \left(\overline{a}_n \overline{H}_n - \overline{y}_n \right)^H \left(\overline{a}_n \overline{H}_n - \overline{y}_n \right) \tag{4.4}$$

with respect to $\overline{H}_n$ and the following result is obtained (for derivation see Appendix C):

$$\hat{\overline{H}}_n = \left[\left(\overline{a}_n^H \overline{a}_n \right)^{-1} \overline{a}_n^H \right] \overline{y}_n \tag{4.5}$$

Here, $\overline{a}_n$ is a diagonal matrix with entries being pilot symbol values. For this reason, it is nonsingular and it has an inverse. As a result, the following expression can be written as the solution of LS estimation method:

$$\hat{\overline{H}}_n = \begin{bmatrix} \hat{H}_{0,n} \\ \hat{H}_{1,n} \\ \vdots \\ \hat{H}_{N-1,n} \end{bmatrix} = \overline{a}_n^{-1} \overline{y}_n = \begin{bmatrix} 1/a_{0,n} & 0 & \cdots & 0 \\ 0 & 1/a_{1,n} & \cdots & 0 \\ \vdots & \vdots & \ddots & \vdots \\ 0 & 0 & \cdots & 1/a_{N-1,n} \end{bmatrix} \begin{bmatrix} y_{0,n} \\ y_{1,n} \\ \vdots \\ y_{N-1,n} \end{bmatrix} = \begin{bmatrix} y_{0,n}/a_{0,n} \\ y_{1,n}/a_{1,n} \\ \vdots \\ y_{N-1,n}/a_{N-1,n} \end{bmatrix} \tag{4.6}$$

4.2.2.2 Linear Minimum Mean Square Error (LMMSE) Estimation [22]

Let $\hat{H}_{k,n}$ denote the estimate of $H_{k,n}$ and let the estimator is in the following form:

$$\hat{H}_{k,n} = Ay_{k,n} \tag{4.7}$$

In LMMSE estimation, the cost function, given in equation (4.8), should be minimized with respect to A.

$$C = E\left\{\left|H_{k,n} - \hat{H}_{k,n}\right|^2\right\} = E\left\{\left(H_{k,n} - \hat{H}_{k,n}\right)^*\left(H_{k,n} - \hat{H}_{k,n}\right)\right\} \tag{4.8}$$

Here, $H_{k,n}$ is the unknown to be estimated and $y_{k,n}$ is the observation.

$A=A_r+jA_i$ where A_r and A_i denote the real and imaginary parts of A, respectively. Then, the following gradient equation can be written:

$$\begin{aligned}\nabla C &= \frac{\partial C}{\partial A_r} + j\frac{\partial C}{\partial A_i} \\ &= E\{-H^*_{k,n}y^*_{k,n} - j(jH^*_{k,n}y^*_{k,n}) - y^*_{k,n}H_{k,n} - j(-jy^*_{k,n}H_{k,n}) \\ &\quad + y^*_{k,n}Ay_{k,n} + j(-jy^*_{k,n}Ay_{k,n}) + A^*y^*_{k,n}y_{k,n} + j(jA^*y^*_{k,n}y_{k,n})\} \\ &= E\{-2y^*_{k,n}H_{k,n} + 2Ay^*_{k,n}y_{k,n}\} \\ &= 0\end{aligned} \tag{4.9}$$

From (4.9), A can be found as follows:

$$\begin{aligned}AE\{y_{k,n}y^*_{k,n}\} &= E\{H_{k,n}y^*_{k,n}\} \\ A &= R_{Hy}R^{-1}_{yy}\end{aligned} \tag{4.10}$$

where $R_{Hy} = E\{H_{k,n} y^*_{k,n}\}$ is the cross correlation of H_k and $y_{k,n}$ and $R_{yy} = E\{y_{k,n} y^*_{k,n}\}$ is the autocorrelation of $y_{k,n}$.Then, the estimation result becomes

$$\hat{H}_{k,n} = Ay_{k,n} = R_{Hy} R^{-1}_{yy} y_{k,n} \tag{4.11}$$

4.2.3 Channel Tracking Methods

4.2.3.1 Least Mean Squares (LMS) Method [39]

Let $y_{k,n}$ denote the demodulated OFDM signal as given in equation (4.1). In order to estimate $H_{k,n}$, the cost function to be minimized with respect to $H_{k,n}$ is as follows:

$$C = E\{e_{k,n} e^*_{k,n}\} \tag{4.12}$$

Here, $e_{k,n}$ is the error between the desired signal $d_{k,n}$ and $H_{k,n}a_{k,n}$.

$H_{k,n} = R_{k,n} + jI_{k,n}$ where $R_{k,n}$ and $I_{k,n}$ are the real and imaginary parts of $H_{k,n}$, respectively. Then, the gradient of the cost function is given as follows:

$$\begin{aligned}
\nabla C &= \frac{\partial C}{\partial R_{k,n}} + j\frac{\partial C}{\partial I_{k,n}} \\
&= E\{d_{k,n}(-a^*_{k,n}) - jd_{k,n}(-ja^*_{k,n}) - a_{k,n}d^*_{k,n} - j(ja_{k,n}d^*_{k,n}) \\
&\quad + a^*_{k,n}a_{k,n}H_{k,n} + j(-ja^*_{k,n}a_{k,n}H_{k,n}) + a^*_{k,n}H^*_{k,n}a_{k,n} + j(ja^*_{k,n}H^*_{k,n}a_{k,n})\} \\
&= E\{-2d_{k,n}a^*_{k,n} + 2a^*_{k,n}a_{k,n}H_{k,n}\}
\end{aligned} \tag{4.13}$$

According to the steepest descent algorithm, the following recursive expression is used:

$$\begin{aligned}
H_{k,n+1} &= H_{k,n} - \frac{1}{2}\mu\nabla C \\
&= H_{k,n} + \mu\left(E\{d_{k,n}a^*_{k,n}\} - E\{a_{k,n}a^*_{k,n}\}H_{k,n}\right)
\end{aligned} \tag{4.14}$$

where μ is the step size. Then, for the LMS algorithm, instantaneous values are used as estimates. Hence, (4.14) becomes

$$H_{k,n+1} = H_{k,n} + \mu a^*_{k,n}\left(d_{k,n} - a_{k,n}H_{k,n}\right) \tag{4.15}$$

In this work, $d_{k,n}$ is selected to be the measurement itself.

In [39], it is shown that the step size μ can be selected optimally when the details of the physical model of the system and its variability with time are known. But, if the information is not known, then an adaptive scheme is proposed as a solution for the selection of the step size. This adaptive scheme is investigated in the following section.

4.2.3.1.1 LMS Method with Adaptive Step Size [39]

The purpose of the adaptive scheme is to find an estimate for the particular value of the step size parameter μ that minimizes the cost function $C(n) = \frac{1}{2}E\left\{e_{k,n}e^*_{k,n}\right\}$ where $e_{k,n} = d_{k,n} - H_{k,n}a_{k,n}$. Here, 1/2 scaling is used for convenience for the following equations.

Differentiating the cost function with respect to μ yields the following scalar gradient:

$$\nabla_\mu C(n) = \frac{\partial C(n)}{\partial \mu} = \frac{1}{2}E\left\{\frac{\partial e_{k,n}}{\partial \mu}e^*_{k,n} + \frac{\partial e^*_{k,n}}{\partial \mu}e_{k,n}\right\} \tag{4.16}$$

$$\frac{\partial e_{k,n}}{\partial \mu} = -\frac{\partial H_{k,n}}{\partial \mu}a_{k,n} = -\Psi_{k,n}a_{k,n} \tag{4.17}$$

So, equation (4.16) becomes

$$\nabla_{\mu} C(n) = \frac{\partial C(n)}{\partial \mu} = -\frac{1}{2} E\left\{\Psi_{k,n} a_{k,n} e_{k,n}^{*} + \Psi_{k,n}^{*} a_{k,n}^{*} e_{k,n}\right\} \tag{4.18}$$

In the similar computation of the LMS algorithm, the recursive formulation of the step size can be expressed as follows:

$$\mu(n+1) = \mu(n) - \alpha \hat{\nabla}_{\mu} C(n) \tag{4.19}$$

Here, α is a small positive learning parameter and $\hat{\nabla}_{\mu} C(n)$ is an estimate of the scalar gradient $\nabla_{\mu} C(n)$. The instantaneous estimate $\hat{\nabla}_{\mu} C(n)$ can be expressed as follows:

$$\hat{\nabla}_{\mu} C(n) = -\frac{1}{2}\left[\hat{\Psi}_{k,n} a_{k,n} e_{k,n}^{*} + \hat{\Psi}_{k,n}^{*} a_{k,n}^{*} e_{k,n}\right] = -\mathrm{Re}\left\{\hat{\Psi}_{k,n} a_{k,n} e_{k,n}^{*}\right\} \tag{4.20}$$

where $\hat{\Psi}_{k,n}$ is the estimate of $\Psi_{k,n}$.

Finally, the steps of the adaptive LMS algorithm are as follows:

a- $H_{k,n}$ are updated as given in (4.15) and its derivative's estimate $\hat{\Psi}_{k,n}$ are updated as

$$\begin{aligned} \hat{\Psi}_{k,n+1} &= \hat{\Psi}_{k,n} + a_{k,n}^{*} e_{k,n} + \mu(n) a_{k,n}^{*} \frac{\partial e_{k,n}}{\partial \mu(n)} \\ &= \hat{\Psi}_{k,n} + a_{k,n}^{*} e_{k,n} - \mu(n) a_{k,n}^{*} a_{k,n} \hat{\Psi}_{k,n} \end{aligned} \tag{4.21}$$

b- The step size is updated as

$$\mu(n+1) = \mu(n) + \alpha\, \mathrm{Re}\left\{\hat{\Psi}_{k,n} a_{k,n} e_{k,n}^{*}\right\} \tag{4.22}$$

Here, $\mu(n+1)$ is limited from upper and lower in order to preserve the stability condition.

For the adaptive LMS algorithm, an initialization period is needed. In this work, since packet based communication is used, a header for each packet will be used for the initialization of the algorithm. For detailed information about the packet based data structure, section 5.2.2 can be investigated.

4.2.3.2 Recursive Least Squares (RLS) Method [39]

Let $y_{k,n}$ denote the demodulated OFDM signal as given in equation (4.1). For the estimation of $H_{k,n}$, the cost function to be minimized with respect to $H_{k,n}$ is expressed as follows:

$$C_{k,n} = \sum_{i=1}^{n} \beta(n,i) \left| e_{k,i} \right|^2 \tag{4.23}$$

Here $e_{k,i}$ is the error between the desired signal $d_{k,i}$ and $H_{k,n}a_{k,i}$. $\beta(n,i)$ is the weighting factor. It has the property that $0 < \beta(n,i) \leq 1,\ \ i = 0,1,2,...,n$. The commonly used form of weighting is the exponential weighting factor or forgetting factor. It is defined by the following expression:

$$\beta(n,i) = \lambda^{n-i}, \quad i = 0,1,2,...,n \tag{4.24}$$

where λ is a positive constant less than 1. Thus, when using the exponential weighting factor, the cost function becomes

$$C_{k,n} = \sum_{i=1}^{n} \lambda^{n-i} \left| e_{k,i} \right|^2 \tag{4.25}$$

$H_{k,n} = R_{k,n} + jI_{k,n}$ where $R_{k,n}$ and $I_{k,n}$ are the real and imaginary parts of $H_{k,n}$, respectively.

$$
\begin{aligned}
\nabla C_{k,n} &= \frac{\partial C_{k,n}}{\partial R_{k,n}} + j\frac{\partial C_{k,n}}{\partial I_{k,n}} \\
&= \sum_{i=1}^{n} \lambda^{n-i}\left(\left(d_{k,i} - H_{k,n}a_{k,i}\right)\left(-a_{k,i}^{*}\right) + \left(d_{k,i}^{*} - H_{k,n}^{*}a_{k,i}^{*}\right)\left(-a_{k,i}\right)\right) \\
&+ j\sum_{i=1}^{n} \lambda^{n-i}\left(\left(d_{k,i} - H_{k,n}a_{k,i}\right)\left(ja_{k,i}^{*}\right) + \left(d_{k,i}^{*} - H_{k,n}^{*}a_{k,i}^{*}\right)\left(-ja_{k,i}\right)\right) \\
&= \sum_{i=1}^{n} \lambda^{n-i}\left(\left(d_{k,i} - H_{k,n}a_{k,i}\right)\left(-2a_{k,i}^{*}\right)\right) \\
&= 0
\end{aligned}
\tag{4.26}
$$

Then, the following relation is obtained:

$$
\begin{aligned}
\sum_{i=1}^{n} \lambda^{n-i} d_{k,i}a_{k,i}^{*} &= \sum_{i=0}^{n} \lambda^{n-i} H_{k,n}a_{k,i}a_{k,i}^{*} \\
Z_{k,n} &= H_{k,n}\Phi_{k,n} \\
H_{k,n} &= \Phi_{k,n}^{-1}Z_{k,n}
\end{aligned}
\tag{4.27}
$$

$Z_{k,n}$ and $\Phi_{k,n}$ can be expressed recursively as follows:

$$
Z_{k,n} = \sum_{i=1}^{n} \lambda^{n-i} d_{k,i}a_{k,i}^{*} = \lambda\sum_{i=1}^{n-1} \lambda^{n-1-i} d_{k,i}a_{k,i}^{*} + d_{k,n}a_{k,n}^{*} = \lambda Z_{k,n-1} + d_{k,n}a_{k,n}^{*} \tag{4.28}
$$

Similarly,

$$
\Phi_{k,n} = \sum_{i=1}^{n} \lambda^{n-i} a_{k,i}a_{k,i}^{*} = \lambda\sum_{i=1}^{n-1} \lambda^{n-1-i} a_{k,i}a_{k,i}^{*} + a_{k,n}a_{k,n}^{*} = \lambda\Phi_{k,n-1} + a_{k,n}a_{k,n}^{*} \tag{4.29}
$$

Then, equation (4.27) can be expressed as follows (for derivation see Appendix D):

$$H_{k,n} = H_{k,n-1} + k_n \left(d_{k,n} \frac{a_{k,n}^*}{a_{k,n}} - a_{k,n}^* H_{k,n-1} \right) \tag{4.30}$$

where

$$k_n = \frac{\lambda^{-1} \Phi_{k,n-1}^{-1} a_{k,n}}{1 + \lambda^{-1} a_{k,n}^* \Phi_{k,n-1}^{-1} a_{k,n}} \tag{4.31}$$

As in the LMS case, in this work, the desired symbol $d_{k,n}$ is selected to be the measurement itself.

In [39], it is shown that the forgetting factor λ can be selected optimally when the details of the physical model of the system and its variability with time are known. But if the information is not known, then an adaptive scheme is proposed as a solution for the selection of the forgetting factor as in the case of LMS method for the selection of the step size. This adaptive scheme is investigated in the following section.

4.2.3.2.1 RLS Method with Adaptive Forgetting Factor [39]

The purpose of the adaptive scheme is to find an estimate for the particular value of the forgetting factor λ that minimizes the cost function $C(n) = \frac{1}{2} E\left\{ e_{k,n} e_{k,n}^* \right\}$ where $e_{k,n} = d_{k,n} \frac{a_{k,n}^*}{a_{k,n}} - a_{k,n}^* H_{k,n-1}$. Here, 1/2 scaling is used for convenience for the following equations.

Differentiating the cost function with respect to λ yields the following scalar gradient:

$$\nabla_{\lambda} C(n) = \frac{\partial C(n)}{\partial \lambda} = \frac{1}{2} E\left\{ \frac{\partial e_{k,n}}{\partial \lambda} e^{*}_{k,n} + \frac{\partial e^{*}_{k,n}}{\partial \lambda} e_{k,n} \right\} \tag{4.32}$$

Here,

$$\frac{\partial e_{k,n}}{\partial \lambda} = -\frac{\partial H_{k,n-1}}{\partial \lambda} a^{*}_{k,n} = -\Omega_{k,n-1} a^{*}_{k,n} \tag{4.33}$$

So, equation (4.32) becomes as follows:

$$\nabla_{\lambda} C(n) = \frac{\partial C(n)}{\partial \lambda} = -\frac{1}{2} E\left\{ \Omega_{k,n-1} a^{*}_{k,n} e^{*}_{k,n} + \Omega^{*}_{k,n-1} a_{k,n} e_{k,n} \right\} \tag{4.34}$$

Let $S_{k,n}$ denote the derivative of the inverse correlation matrix $\Phi^{-1}_{k,n}$. That is, $S_{k,n} = \frac{\partial \Phi^{-1}_{k,n}}{\partial \lambda}$. Then, using equation (4.30) and $S_{k,n}$ the derivative of $H_{k,n}$ becomes as follows:

$$\frac{\partial H_{k,n}}{\partial \lambda} = (1 - k_n a^{*}_{k,n}) \Omega_{k,n-1} + S_{k,n} a_{k,n} e_{k,n} \tag{4.35}$$

Hence, by differentiating

$$\Phi^{-1}_{k,n} = \lambda^{-1} \Phi^{-1}_{k,n-1} - \frac{\lambda^{-2} \Phi^{-1}_{k,n-1} a_{k,n} a^{*}_{k,n} \Phi^{-1}_{k,n-1}}{1 + \lambda^{-1} a^{*}_{k,n} \Phi^{-1}_{k,n-1} a_{k,n}} \tag{4.36}$$

with respect to λ then collecting terms the following equation is obtained:

$$S_{k,n} = \lambda^{-1} (1 - k_n a^{*}_{k,n}) S_{k,n-1} (1 - k^{*}_{n} a_{k,n}) + \lambda^{-1} k_n k^{*}_{n} - \lambda^{-1} \Phi^{-1}_{k,n} \tag{4.37}$$

The derivation of equation (4.36) can be found in Appendix D.

As in the case of the LMS method, the recursive formulation of the forgetting factor can be expressed as follows:

$$\lambda(n) = \lambda(n-1) - \alpha\hat{\nabla}_{\lambda}C(n) \tag{4.38}$$

Here, α is a small positive learning parameter and $\hat{\nabla}_{\lambda}C(n)$ is an estimate of the scalar gradient $\nabla_{\lambda}C(n)$. By using equation (4.34), the instantaneous estimate $\hat{\nabla}_{\lambda}C(n)$ can be expressed as

$$\hat{\nabla}_{\lambda}C(n) = -\frac{1}{2}\left(\hat{\Omega}_{k,n-1}a^{*}_{k,n}e^{*}_{k,n} + \hat{\Omega}^{*}_{k,n-1}a_{k,n}e_{k,n}\right) = -\operatorname{Re}\left\{\hat{\Omega}_{k,n-1}a^{*}_{k,n}e^{*}_{k,n}\right\} \tag{4.39}$$

Here, $\hat{\Omega}_{k,n}$ is the estimate of $\Omega_{k,n}$.

Finally, the steps of the adaptive RLS algorithm becomes as follows:

a- $H_{k,n}$ and $\Phi^{-1}_{k,n}$ are updated as given in (4.30) and (4.36), respectively.

b- The forgetting factor, the derivative of the inverse correlation $\Phi^{-1}_{k,n}$, and the estimate of the derivative of $H_{k,n}$ are updated according to the following equations:

$$\lambda(n) = \lambda(n-1) + \alpha\operatorname{Re}\left\{\hat{\Omega}_{k,n-1}a^{*}_{k,n}e^{*}_{k,n}\right\} \tag{4.40}$$

$$S_{k,n} = \lambda^{-1}(1 - k_n a^{*}_{k,n})S_{k,n-1}(1 - k^{*}_{n}a_{k,n}) + \lambda^{-1}k_n k^{*}_{n} - \lambda^{-1}\Phi^{-1}_{k,n} \tag{4.41}$$

$$\hat{\Omega}_{k,n} = (1 - k_n a^{*}_{k,n})\hat{\Omega}_{k,n-1} + S_{k,n}a_{k,n}e_{k,n} \tag{4.42}$$

As in the adaptive LMS case, for the adaptive RLS algorithm, an initialization period is needed. In this work, since packet based communication is used, a header for each packet will be used for the initialization of the algorithm. For detailed information about the packet based data structure, section 5.2.2 can be investigated.

4.2.3.3 Kalman Filter Method [39]

Let $\overline{x}(n)$ denote the state matrix with a size M-by-1 at time n. The process equation is expressed as follows.

$$\overline{x}(n+1) = \overline{F}(n+1,n)\overline{x}(n) + \overline{\Gamma}\overline{v}_1(n) \tag{4.43}$$

In the above expression, $\overline{F}(n+1,n)$ is a known M-by-M state transition matrix relating the state of the system at times n+1 and n. $\overline{\Gamma}$ is the M-by-1 process noise coefficient and $\overline{v}_1(n)$ is the process noise which is modeled as a zero mean white noise process whose correlation matrix is defined by the following expression:

$$E\left\{\overline{v}_1(n)\overline{v}_1^H(k)\right\} = \begin{cases} \overline{Q}_1(n), & n = k \\ 0, & n \neq k \end{cases} \tag{4.44}$$

The channel transfer function for a selected frequency can be seen as a maneuvering target over time domain. In order to track the target, in this work two types of Kalman filter are employed. These are Kalman filter with constant position model and Kalman filter with constant velocity model [51]. In the former, the system uses the position of the tracked data, which is nothing but the channel transfer function for a selected frequency, as state. So, the dimension of the state matrix is 1 by 1. In the latter, the system uses the velocity of the tracked data as well as its position as states. So, in this case the dimesion of the state matrix is 2 by 1. The velocity of the tracked data is the first time derivative of the channel transfer function for a selected frequency. In each case, the uncertainty in state estimation is represented by the process noise covariance matrix. There is also a third model, constant acceleration model [51]. But it is not investigated here.

For Kalman filter with constant position model, the state matrix $\overline{x}(n)$, the state transition matrix $\overline{F}(n+1,n)$, and process noise coefficient Γ are expressed as follows:

$$\overline{x}(n) = x(n) \tag{4.45}$$

$$\overline{F}(n+1,n) = 1 \tag{4.46}$$

$$\Gamma = 1 \tag{4.47}$$

On the other hand, for the Kalman filter with constant velocity model, the state matrix $\overline{x}(n)$, the state transition matrix $\overline{F}(n+1,n)$ and process noise coefficient Γ are expressed as follows:

$$\overline{x}(n) = \begin{bmatrix} x(n) \\ v(n) \end{bmatrix} \tag{4.48}$$

$$\overline{F}(n+1,n) = \begin{bmatrix} 1 & T \\ 0 & 1 \end{bmatrix} \tag{4.49}$$

$$\Gamma = \begin{bmatrix} T^2/2 \\ T \end{bmatrix} \tag{4.50}$$

In the above expressions, v(n) is the velocity obtained from the position x(n). T is the sampling duration used for the calculation of the velocity v(n) of x(n).

Since velocity is included as an additional state in the constant velocity model based Kalman filter, uncertainty in state estimation due to the target dynamics is less compared to that in the constant position model based Kalman filter. That is, the former uses more information about the target dynamics compared to the latter. Hence, it is expected that the former has higher tracking performance compared to the latter.

The measurement equation, describing the observation vector, is expressed as follows:

$$\bar{y}(n) = \bar{C}(n)\bar{x}(n) + \bar{v}_2(n) \tag{4.51}$$

where $\bar{C}(n)$ is a known N-by-M measurement matrix. The N-by-1 vector $\bar{v}_2(n)$ is called measurement noise, which is modeled as a zero mean, white noise process whose correlation matrix is given as follows:

$$E\{\bar{v}_2(n)\bar{v}_2^H(k)\} = \begin{cases} \bar{Q}_2(n), & n = k \\ 0, & n \neq k \end{cases} \tag{4.52}$$

In this work, the measurement matrix is taken as shown in equation (4.53) for the constant position model based Kalman filter and it is taken as shown in equation (4.54) for the constant velocity model based Kalman filter for a subchannel at n^{th} symbol.

$$\bar{C}(n) = [\text{pilot symbol}] \tag{4.53}$$

$$\bar{C}(n) = [\text{pilot symbol} \quad 0] \tag{4.54}$$

It is assumed that $\bar{x}(0)$, the initial value of the state, is uncorrelated with both $\bar{v}_1(n)$ and $\bar{v}_2(n)$ for n≥0. The noise vectors $\bar{v}_1(n)$ and $\bar{v}_2(n)$ are statistically independent. So, the following can be written:

$$E\{\bar{v}_1(n)\bar{v}_2^H(k)\} = 0 \qquad \text{for all n and k} \tag{4.55}$$

Now, let $\hat{\bar{x}}(n-1 \mid Y_{n-1})$ denote the filtered estimate of the state vector at time n-1, given the observation vectors $Y_{n-1} = \{\bar{y}(1), \bar{y}(2), ..., \bar{y}(n-1)\}$ and let $\hat{\bar{x}}(n \mid Y_{n-1})$ denote the predicted estimate of the state vector at time n, given the observation vectors $Y_{n-1} = \{\bar{y}(1), \bar{y}(2), ..., \bar{y}(n-1)\}$. Then, the following expression can be written:

$$\bar{\hat{x}}(n \mid Y_{n-1}) = \bar{F}(n, n-1)\bar{\hat{x}}(n-1 \mid Y_{n-1}) \tag{4.56}$$

Also, let us define the filtered state error vector $\bar{e}(n)$ and predicted state error vector $\bar{e}(n, n-1)$ as follows:

$$\bar{e}(n) = \bar{x}(n) - \bar{\hat{x}}(n \mid Y_n) \tag{4.57}$$

$$\bar{e}(n, n-1) = \bar{x}(n) - \bar{\hat{x}}(n \mid Y_{n-1}) \tag{4.58}$$

Moreover, let $\bar{K}(n)$ denote the correlation matrix of the error vector $\bar{e}(n)$ and let $\bar{K}(n, n-1)$ denote the correlation matrix of the error vector $\bar{e}(n, n-1)$. Then

$$\bar{K}(n, n-1) = \bar{F}(n, n-1)\bar{K}(n-1)\bar{F}^{H}(n, n-1) + \bar{Q}_1(n) \tag{4.59}$$

Additionally, let $\bar{G}(n)$ denote the Kalman gain at time n. After finding $\bar{K}(n, n-1)$, $\bar{G}(n)$ can be written as follows:

$$\bar{G}(n) = \bar{K}(n, n-1)\bar{C}^{H}(n)\left[\bar{C}(n)\bar{K}(n, n-1)\bar{C}^{H}(n) + \bar{Q}_2(n)\right]^{-1} \tag{4.60}$$

After that, the filtered estimate of the state vector at time n $\bar{\hat{x}}(n \mid Y_n)$ becomes as follows:

$$\bar{\hat{x}}(n \mid Y_n) = \bar{\hat{x}}(n \mid Y_{n-1}) + \bar{G}(n)\left[\bar{y}(n) - C(n)\bar{\hat{x}}(n \mid Y_{n-1})\right] \tag{4.61}$$

Finally, $\bar{K}(n)$ is found as follows:

$$\bar{K}(n) = \left[\bar{I} - \bar{G}(n)\bar{C}(n)\right]\bar{K}(n, n-1) \tag{4.62}$$

In order to track the target, the equations starting from (4.56) up to (4.62) are used iteratively.

As in the adaptive LMS and RLS cases, for the constant position and constant velocity model based Kalman filter, an initialization period is needed. In this work, since packet based communication is used, a header for each packet will be used for the initialization of the algorithm. For detailed information about the packet based data structure, section 5.2.2 can be investigated.

CHAPTER 5

SIMULATION RESULTS

5.1 Aim of the Simulations

The aim of the simulations is to compare the performances of least squares (LS) channel estimation method, linear minimum mean square error (LMMSE) channel estimation method, least mean square (LMS) channel tracking method, recursive least squares (RLS) channel tracking method, constant position model based Kalman filter channel tracking method, and constant velocity model based Kalman filter channel tracking method in high frequency (HF) channel. For this purpose, Monte Carlo simulations were performed. During the simulations, adaptive versions of LMS and RLS channel tracking methods were also investigated.

These methods are compared by using the symbol error rate (SER) and the normalized mean square error (NMSE) performance metrics. These metrics were calculated over a range of signal to noise ratio (SNR) values. For signal detection maximum a posteriori probability (MAP) estimator was used. The MAP estimator is explained in Appendix B in detail. After the SER and the NMSE tests, the channel estimation and tracking behaviour of the methods were investigated by observing the estimates over time. Finally, convergence duration of LMS, RLS and Kalman filter were investigated and an initialization method is proposed in order to reduce the convergence duration. In the simulations it was assumed that timing is perfect. That is, there is no timing error.

In the simulations, the channel is assumed to be CCIR poor HF channel. The structure of this channel is described in section 5.2.1. Moreover, the channel design is explained in Appendix A.

In the simulations packet based data communication was used. The data packet is composed of a header part and a data part. The header contains known pilot symbols and the data part contains data symbols and some pilot symbols. The data packet structure is explained in section 5.2.2 in more detail.

Channel estimation and tracking are performed in each data packet. For the channel tracking methods, LS method is used in order to obtain measurements. Moreover, LS method is used in the header in order to perform initialization steps of the tracking algorithms.

5.2 Simulations

5.2.1 Description of the CCIR Poor HF Channel

For HF channel, the CCIR poor HF channel recommendation was used. In this recommendation, the channel is taken to be two path with 1 Hz Doppler spread in each path. There is no Doppler shift. One path has zero delay and the other path has 2 milliseconds delay. The HF channel design steps are given in Appendix A.

The coherent time and coherent frequency of the channel are 1/Doppler spread = 1/(0.5 Hz) = 2 seconds and 1/(symbol duration) = $1/(8.10^{-3})$ = 125 Hz, respectively.

Considering the channel structure used in the simulations, it is now convenient to calculate the channel transfer function because the aim of channel estimation and tracking process is finding the channel transfer function. In equation (5.1), the impulse response of the channel is shown.

$$c_{\ell}(\tau;t) = \sum_{n=1}^{2} \alpha_n(t)\delta(\tau - \tau_n) \tag{5.1}$$

where τ_1=0, τ_2=2 msec. Then, by taking the Fourier transform of the channel impulse response for τ variable, the channel transfer function is found as shown in equation (5.2):

$$C_\ell(f;t) = \int_{-\infty}^{\infty} c_\ell(\tau;t)e^{-j2\pi f\tau}d\tau = \sum_{n=1}^{2}\alpha_n(t)e^{-j2\pi f\tau_n} \tag{5.2}$$

After that, since all calculations are made over discrete time and discrete frequency domain in the simulations, $C_\ell(f;t)$ should be sampled over time and frequency domain. For this purpose, it is sampled with the period 1/T over frequency domain and T/N over time domain. Here, T is the duration of the OFDM symbol duration and N is the number of subcarriers. The sampled channel transfer function is shown in equation (5.3).

$$C_\ell(m;k) = C_\ell(f;t)\Big|_{\substack{f=m/T \\ t=kT/N}} = \sum_{n=1}^{2}\alpha'_n(k)e^{-j2\pi\frac{m}{T}(\tau'_n\frac{T}{N})} \tag{5.3}$$

where $\alpha'_n(k) = \alpha_n(t)\Big|_{t=kT/N}$ and $\tau'_n = \dfrac{\tau_n}{T/N}$.

5.2.2 Description of the OFDM System

In the OFDM system there were N=256 subchannels in one OFDM symbol. The duration of one OFDM symbol is T=8 milliseconds. Hence, the sampling period is T/N=31.25 microseconds. The total bandwidth of the OFDM symbol is N/T= 32 kHz. The length of guard interval is chosen to be N_gT/N= 3 milliseconds in order to cover the 2 milliseconds delay of the channel. By choosing the guard interval as 3 milliseconds N_g becomes 96. If the values of T and N are put in equation (5.3), the channel transfer function becomes as follows:

$$C_\ell(m;k) = \sum_{n=1}^{2} \alpha_n^{'}(k) e^{-j2\pi \frac{m}{8.10^{-3}}(2.10^{-3})} = \sum_{n=1}^{2} \alpha_n^{'}(k) e^{-j2\pi \frac{m}{4}} \tag{5.4}$$

Here, since $C_\ell(f;t)$ is sampled with a period of 1/ T, which is the bandwidth of the subchannels, the channel transfer function is periodic over frequency domain with a period of 4 subchannels as shown in equation (5.4).

Data packet consists of 100 symbols, 10 of which constitute the header part and the remaining are the data part. In the header part, the subcarriers of all the symbols are composed of known pilots. In the data part, only the subcarriers of some symbols are composed of pilot symbols. These symbols are equally spaced in time grid. In the simulations, the period of pilot symbols is taken to be 5. Naturally, it can be increased to some extend. The frequency time grid of the symbols is shown in Figure 5.1.

The packets are sent one after another. That is, there is no time gap between the packets. Two modulation techniques are used in the simulations. These are QPSK (46.55 kbps) and 16QAM (93.09 kbps). Their constellations are shown in Figure 5.2 and Figure 5.3, respectively.

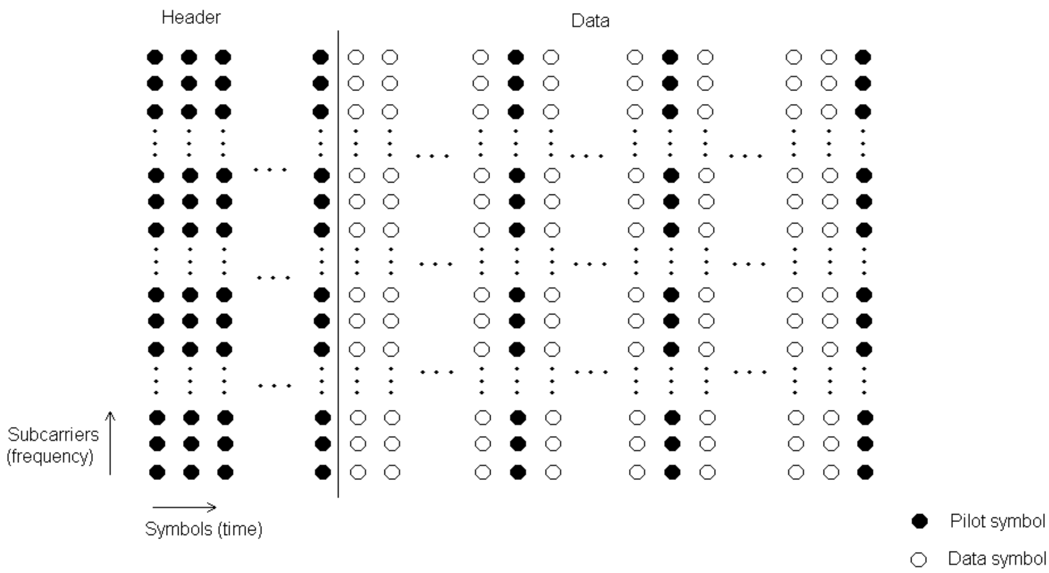

Figure 5.1 Structure of data packet

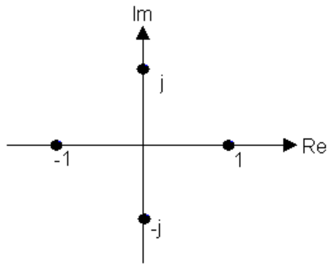

Figure 5.2 QPSK constellation

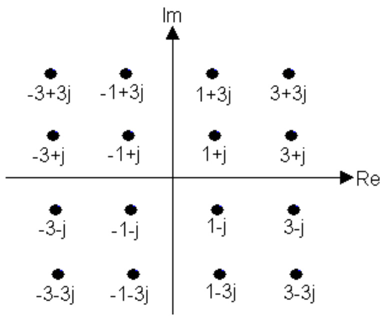

Figure 5.3 16QAM constellation

For QPSK modulation, the pilot symbol is selected as 1 and for 16QAM modulation, the pilot symbol is selected as 3+3j.

After demodulation the following expression is obtained:

$$y_{k,n} = H_{k,n}a_{k,n} + I_{k,n} + N_{k,n} \tag{5.5}$$

In equation (5.5), $H_{k,n}$ is the channel transfer function for k^{th} subcarrier at n^{th} OFDM symbol, $I_{k,n}$ and $N_{k,n}$ are interference and noise at k^{th} subcarrier and n^{th} OFDM symbol, respectively. After estimating $H_{k,n}$, $a_{k,n}$ are found by using maximum a posteriori (MAP) estimator, which is explained in Appendix B.

5.2.3 Implementation of Investigated Methods

During the packet based data communication, the channel estimation and tracking processes start every time a new data packet is received. As soon as these processes are completed and a new data packet is received, these processes start for that data packet again and the channel information obtained during the previous data packet is not used. In this way, it is guaranteed that the effect of the changes of the channel characteristics on these processes is eliminated.

For LS method, the channel transfer function is estimated in the whole header part and at the pilot symbols in the data part. This estimation is performed for each subcarrier. After estimating the channel transfer function at the pilot symbols in the data part, linear interpolation is used over time domain in order to estimate the channel transfer function at data symbols in data part. After the interpolation step the channel estimation is completed.

For LMMSE method, firstly the channel transfer function is estimated in the whole header part and at the pilot symbols in the data part by using LS method in one packet data. Then, these estimates are used in the final estimation of the channel. Finally, linear interpolation is used over time domain in order to estimate the channel transfer function at data symbols in data part. After this interpolation step the channel estimation is completed. As a new data packet is received, the correlation functions are found again and the process continues in the similar way.

For LMS and adaptive LMS methods, firstly the channel transfer function is estimated until to 5^{th} symbol in the header part using LS method. Then, at the 5^{th} symbol of the header part, channel tracking starts. Since the time gap between the pilot symbols is 5, at 5^{th} symbol in the header part, the channel transfer function is estimated for 10^{th} symbol. In this way, channel tracking with LMS or adaptive LMS methods starts within the header part. So that, the transient part of the LMS method is pushed to the header part. Then, the channel transfer function is estimated by LS method from the remaining 6^{th} symbol until 9^{th} symbol in the header part.

RLS and adaptive RLS methods work similar to the LMS method. At 5^{th} symbol, the initialization of the tracking is performed and channel tracking starts in the header part.

In the same way, constant position and constant velocity model based Kalman filters start channel tracking at the 5^{th} symbol of the header part. Before that, the process noise covariance matrix is calculated. Measurement noise covariance matrix is found by using SNR value of the channel. Here, SNR is assumed to be known. During channel tracking, the measurement noise covariance matrix is fixed. Whereas, the process noise covariance matrix is updated every time a new measurement is obtained. As a new data packet is received, the covariance matrices are calculated again and all the process continues in the similar way.

As soon as the channel estimation process is finished with any of the estimation and tracking method explained so far, the estimated channel transfer function is used in the MAP symbol estimation process.

In Table 5.1, the parameters of the LMS, RLS, and Kalman filter channel tracking methods used in the simulations for QPSK and 16QAM modulation methods are listed.

5.2.4 Simulation Results

Symbol error rate (SER) and normalized mean square error (NMSE) were calculated for 90 packet data over the signal to noise ratio (SNR) range of 0 dB – 36 dB. SER, NMSE and SNR were found by using the equations (5.6), (5.7) and (5.8), respectively. The simulations were performed for QPSK and 16QAM modulations, separately. The SER versus SNR results are shown in Figure 5.4 and Figure 5.5 for QPSK and QAM, respectively. The NMSE versus SNR results are shown in Figure 5.6 and Figure 5.7 for QPSK and QAM, respectively.

$$\mathrm{SER} = \frac{\text{Number of erroneously received symbols}}{\text{Number of all received symbols - Number of pilot symbols}} \tag{5.6}$$

$$\mathrm{NMSE} = \frac{1}{N}\sum_{k=1}^{N}\frac{\frac{1}{M}\sum_{n=1}^{M}\left|\hat{H}_{k,n} - H_{k,n}\right|^2}{\frac{1}{M}\sum_{n=1}^{M}\left|H_{k,n}\right|^2} \tag{5.7}$$

$$\mathrm{SNR} = \frac{\mathrm{Avg}\left|H_{k,n}a_{k,n}\right|^2}{\sigma^2_{noise}} \tag{5.8}$$

where M is the number of transmitted OFDM symbols and N is the number of subchannels. k and n are the subchannel number and symbol number indices.

Table 5.1 Parameters used in the simulations

Channel tracking method	**Parameters**	
	QPSK (pilot value=1)	**16QAM (pilot value=3+3j)**
LMS	Step size (μ) = 1.4	Step size (μ) = 0.078
Adaptive LMS	Initial step size (μ) = 1.4 Learning rate parameter (α)=0.03 Step size upper limit=2 Step size lower limit=0.01	Initial step size (μ) = 0.078 Learning rate parameter (α)=4.10^{-6} Step size upper limit=0.11 Step size lower limit=5.10^{-4}
RLS	Forgetting factor (λ) = 0.1 Inverse of correlation (Φ^{-1}) = 1	Forgetting factor (λ) = 0.1 Inverse of correlation (Φ^{-1}) = 1
Adaptive RLS	Initial forgetting factor (λ) = 0.1 Inverse of correlation (Φ^{-1}) = 1 Learning rate parameter (α)=0.05 Forgetting factor upper limit=0.95 Forgetting factor lower limit=0.02	Initial forgetting factor (λ) = 0.1 Inverse of correlation (Φ^{-1}) = 1 Learning rate parameter (α)=0.002 Forgetting factor upper limit=0.95 Forgetting factor e lower limit=0.02
Constant position model based Kalman filter	Measurement noise covariance = Noise variance Process noise covariance = 20. measurement variance	Measurement noise covariance = Noise variance Process noise covariance = 20. measurement variance
Constant velocity model based Kalman filter	Measurement noise covariance = Noise variance Process noise covariance = 20. measurement variance	Measurement noise covariance = Noise variance Process noise covariance = 20. measurement variance

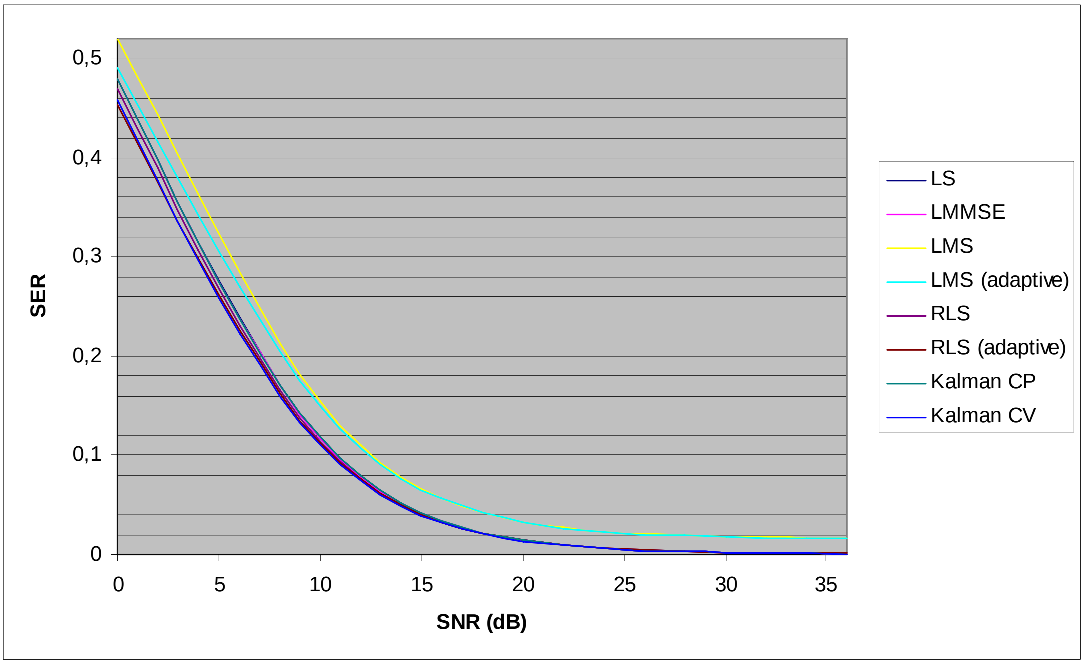

Figure 5.4 SER vs. SNR graph for QPSK

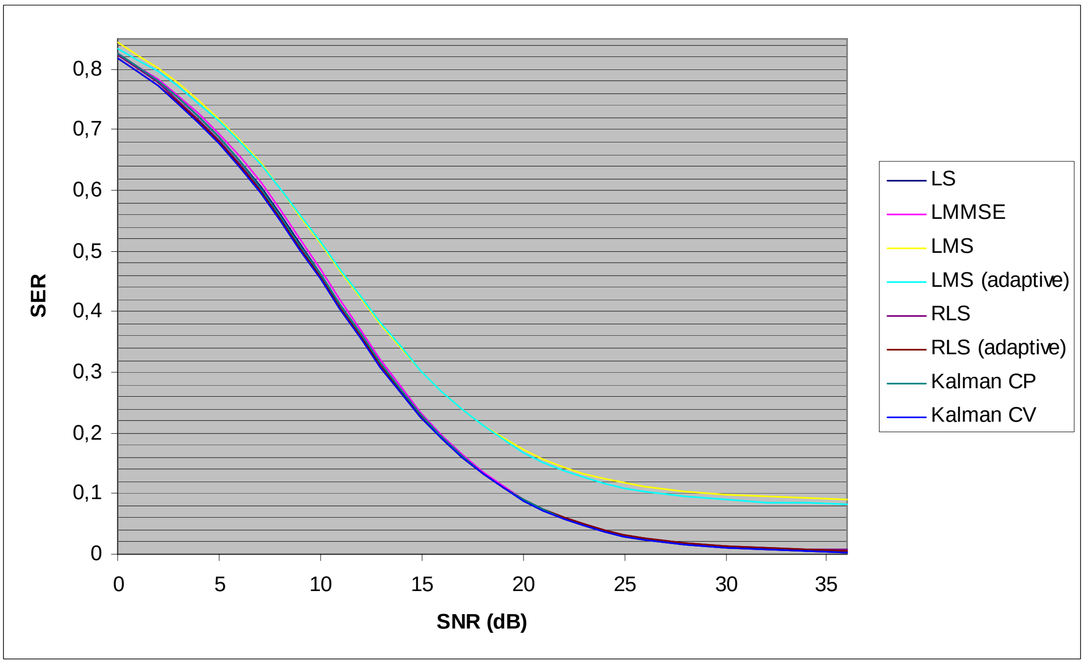

Figure 5.5 SER vs. SNR graph for 16QAM

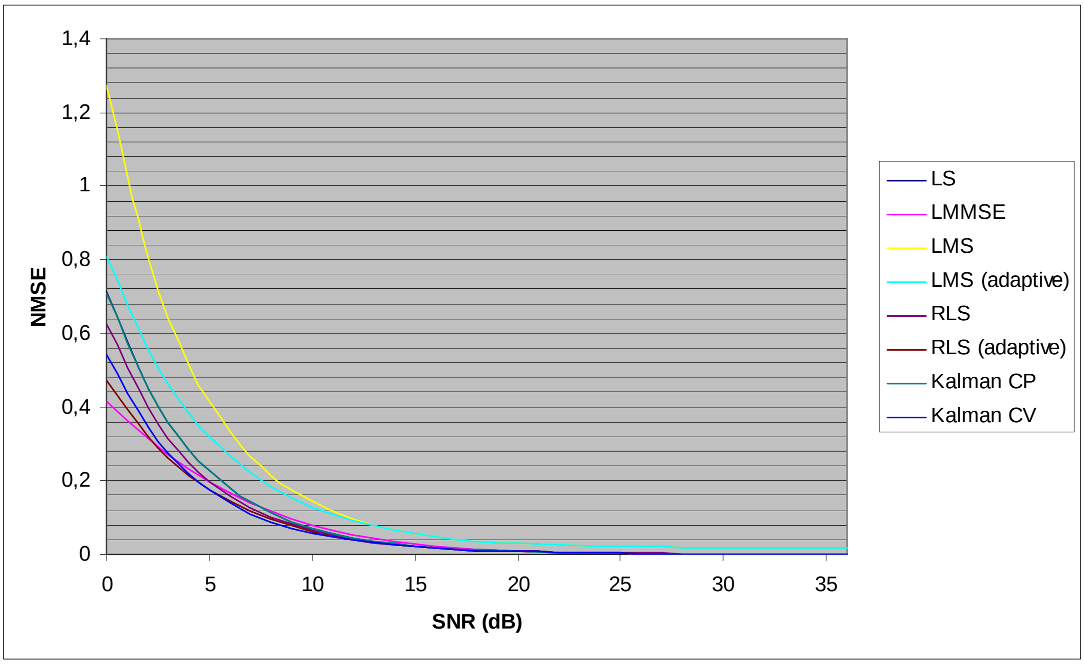

Figure 5.6 NMSE vs. SNR graph for QPSK

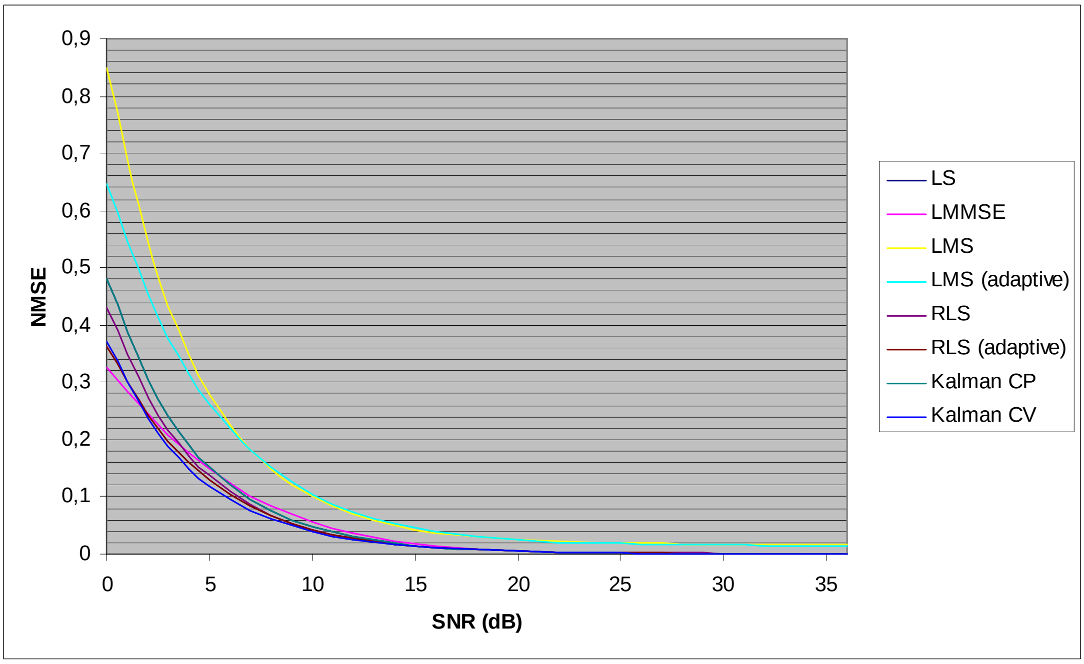

Figure 5.7 NMSE vs. SNR graph for 16QAM

As shown in figures from 5.4 to 5.7, constant velocity model based Kalman filter and adaptive RLS are the best methods. They are followed by RLS, constant velocity model based Kalman filter, LMMSE, and LS methods. As SNR becomes lower than

4 dB, the performance of the LMMSE becomes the best. The worst method is the LMS method. It is followed by the adaptive LMS method. It is because of the delay introduced by these methods during tracking. This delay reduces the performance. If the time gap between the pilot symbols is decreased, then the effect of the delay can be reduced and the performances of the LMS and adaptive LMS methods increase.

In these simulations, the process and noise covariance matrices of the Kalman filters, giving lowest NMSE, are found at the SNR value of 18 dB by trial and error. For other SNR values, the same covariance matrices are used. If for each SNR the covariance matrices giving the lowest NMSE were found, the performance of the Kalman filters might become better.

In order to get further insight for the studied channel estimation and tracking methods, these methods were investigated for 600 OFDM symbols over time and frequency. In these simulations, first 10 symbol long header was transmitted and after that 590 data symbols were transmitted with the same frequency time pilot grid as before. SNR is fixed at 18 dB in order to visually observe the estimation and tracking and filtering results of the methods easily. QPSK is the modulation technique used in these simulations. It should be noted that the results of these simulations should not be treated as an information source for performance comparison because the number of the OFDM symbols are too small for a reliable performance determination.

In order to observe the estimation and tracking behaviour of the methods, firstly the channel transfer function of the 1^{st} subcarrier to be estimated (with noise and without noise), the estimated channel transfer function of the 1^{st} subcarrier and the normalized square error which is averaged over all subcarriers are plotted over time. Here, each time instant represents one OFDM symbol. The channel transfer function to be estimated is named as “real channel transfer function” for noisy case and as “original channel transfer function” for noiseless case in the graphs. In order to observe the phase and amplitude of the channel transfer function, its real part, its imaginary part and its absolute values are plotted separately. Then, the channel transfer function to be estimated and the estimated channel transfer function are plotted over frequency for 20th symbol. So that, the estimation and tracking results and performance can be investigated for one symbol over frequency. Here, each frequency sample represents one OFDM subcarrier. Additionally, for adaptive LMS and RLS algorithms, the change of the step size and the forgetting factor are plotted for 1st subchannel over time. Finally, the absolute value of the channel transfer function is plotted over time and frequency. This three dimensional graph shows the whole estimation result over the frequency time grid.

In Figure 5.8, the absolute value of the transfer function of the channel to be estimated is shown over the whole frequency time grid. Here, there is no noise. Then, from Figure 5.10 to Figure 5.67, the graphs explained in the previous paragraph are shown.

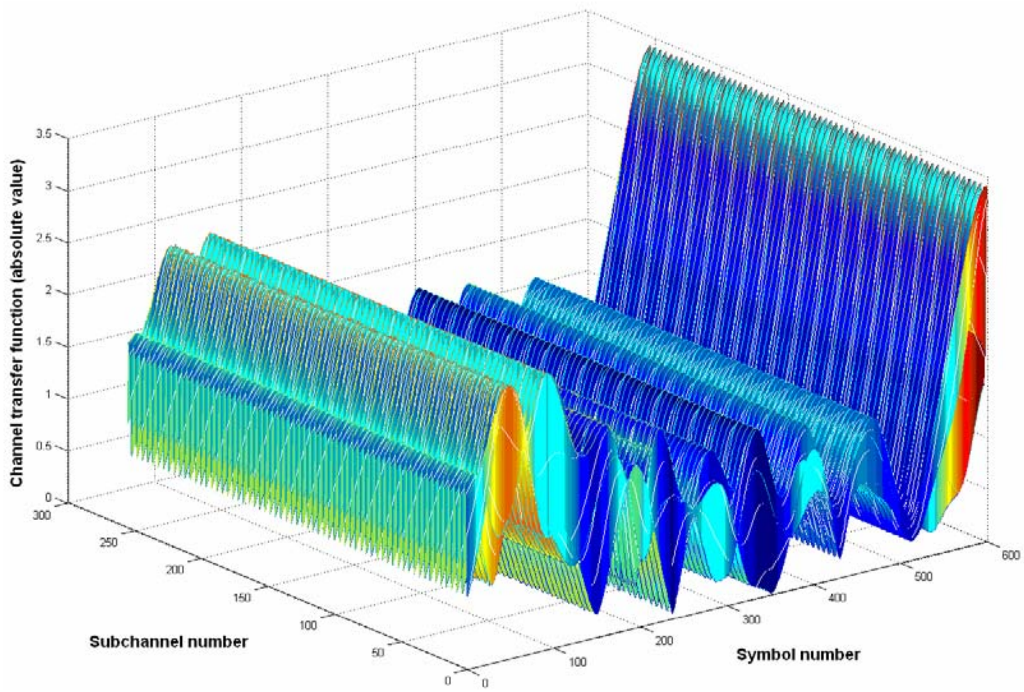

Figure 5.8 Absolute value of the HF channel transfer function over whole frequency time grid (no noise)

In Figure 5.8, the channel transfer function seems smooth over frequency domain. However, it is not smooth and so the channel is not frequency nonselective. As explained in section 5.2.2, the channel transfer function is periodic over frequency domain with a period of 4 subchannels. In order to see this periodicity, Figure 5.9 can be investigated. This figure shows the absolute value of the channel transfer function over frequency domain for 20th OFDM symbol. If the peaks are counted, it can be seen that there are 64 peaks out of 256 subchannels.

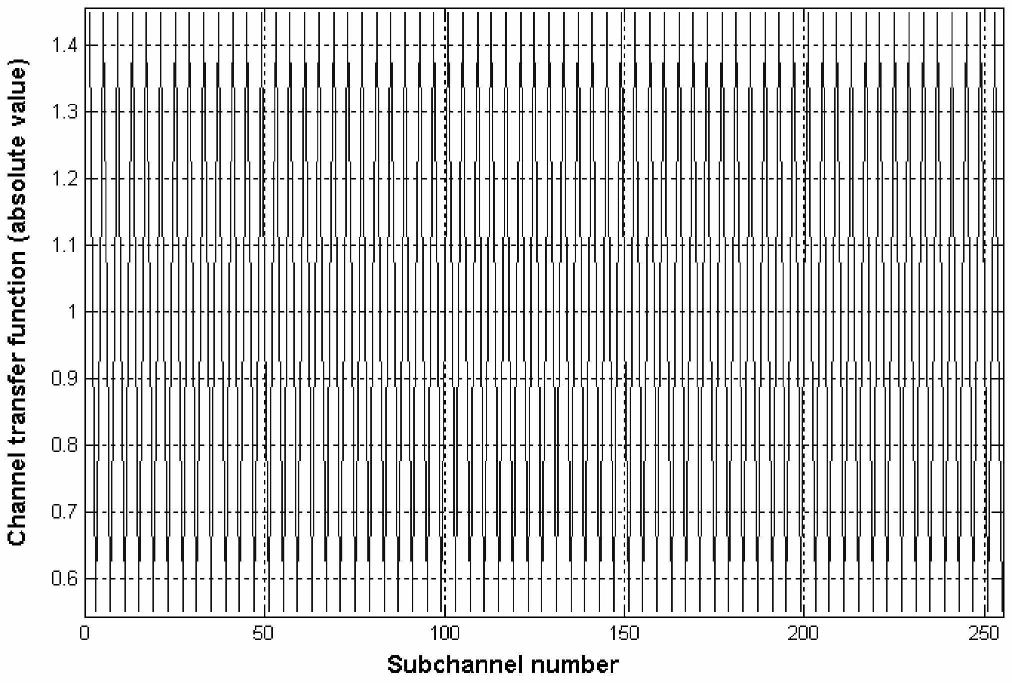

Figure 5.9 Absolute value of the original channel transfer function at 20th symbol versus subchannel number graph (no noise)

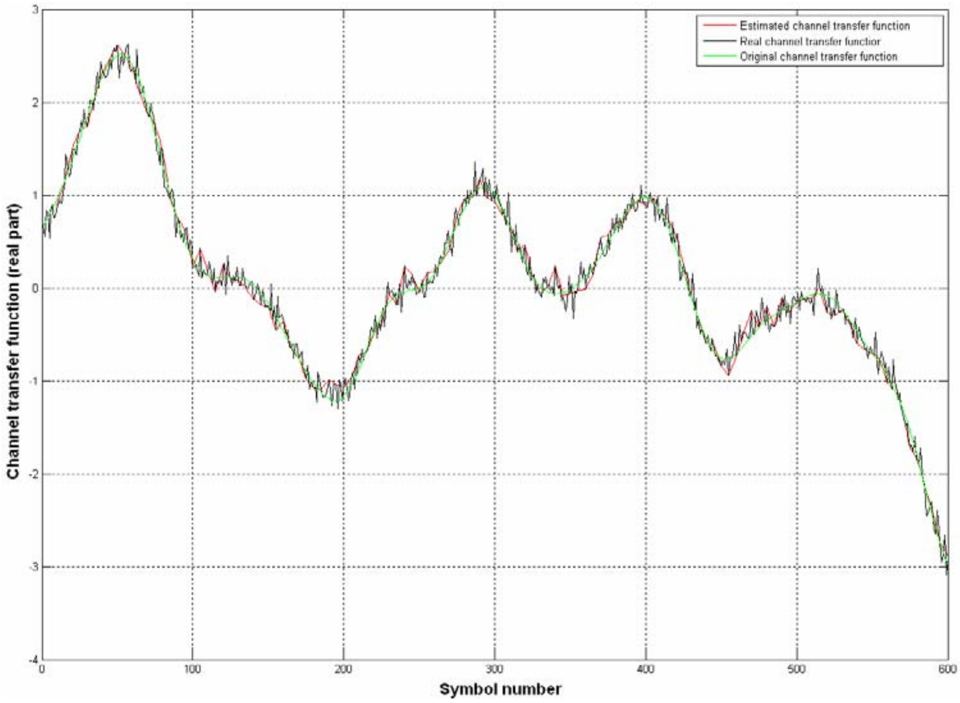

Figure 5.10 Real part of estimated (LS result), real and original channel transfer functions at 1st subchannel versus symbol number graph (SNR = 18 dB)

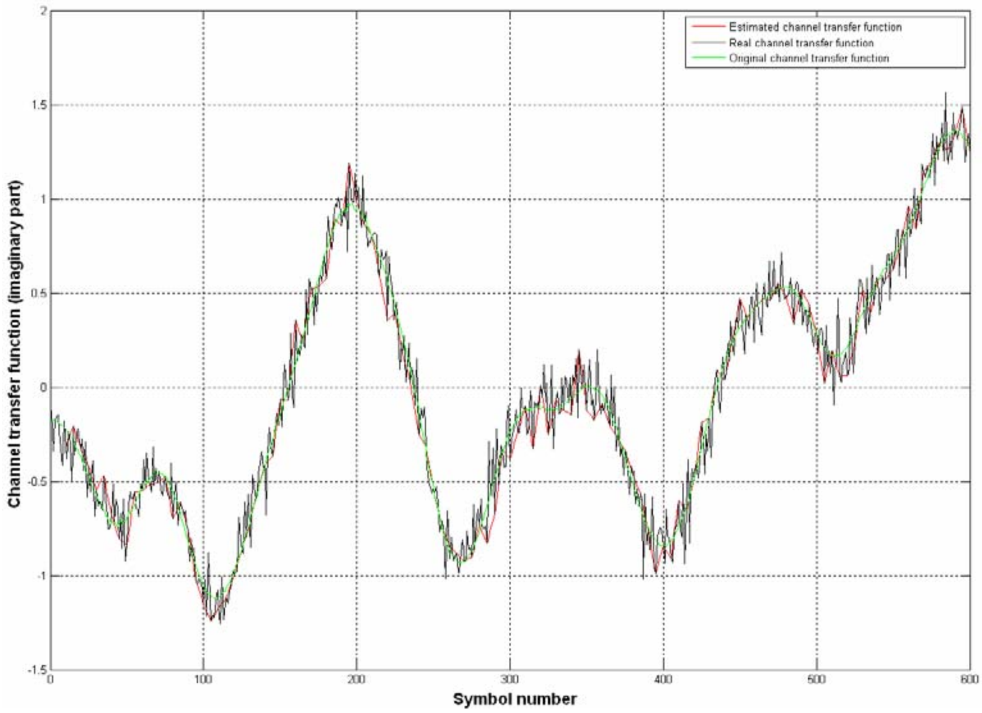

Figure 5.11 Imaginary part of estimated (LS result), real and original channel transfer functions at 1st subchannel versus symbol number graph (SNR = 18 dB)

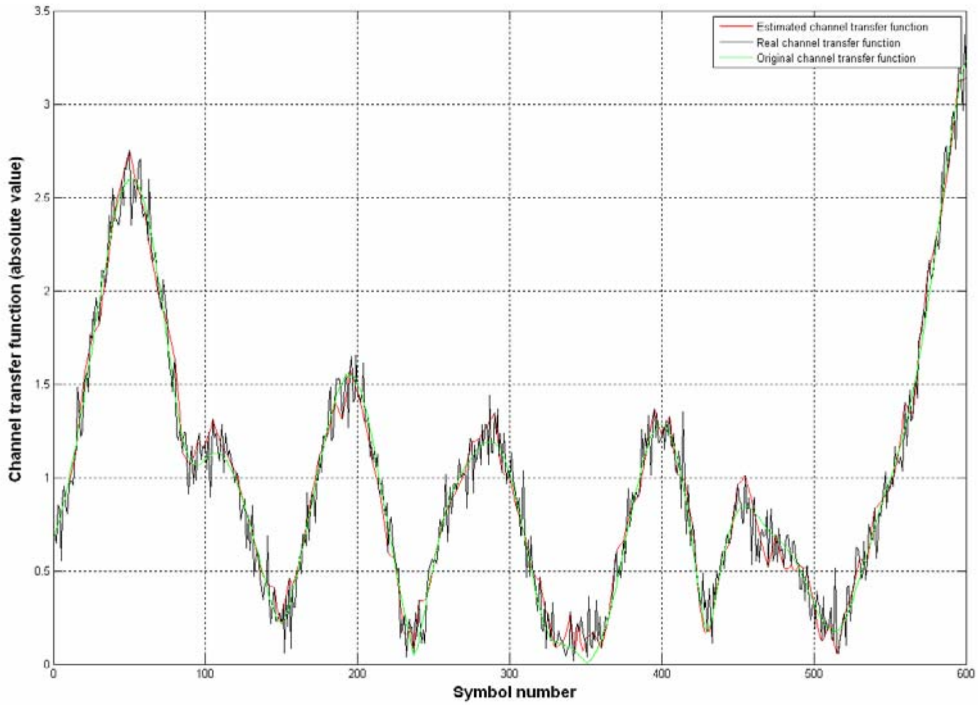

Figure 5.12 Absolute value of estimated (LS result), real and original channel transfer functions at 1st subchannel versus symbol number graph (SNR = 18 dB)

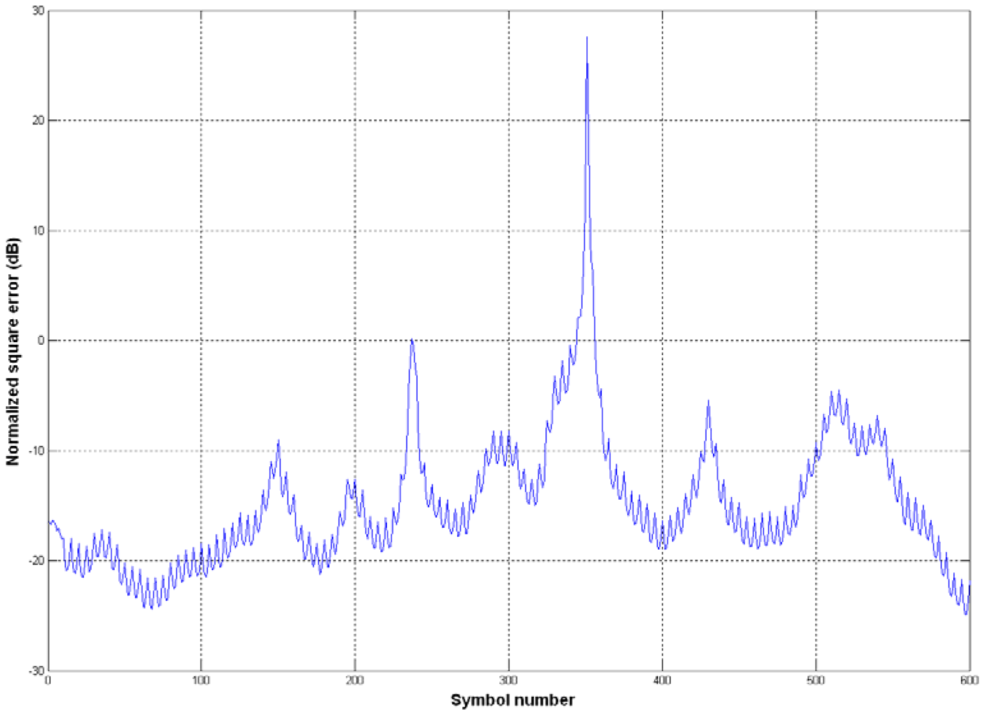

Figure 5.13 Normalized square error averaged over all subchannels (LS result) versus symbol number graph (SNR = 18 dB)

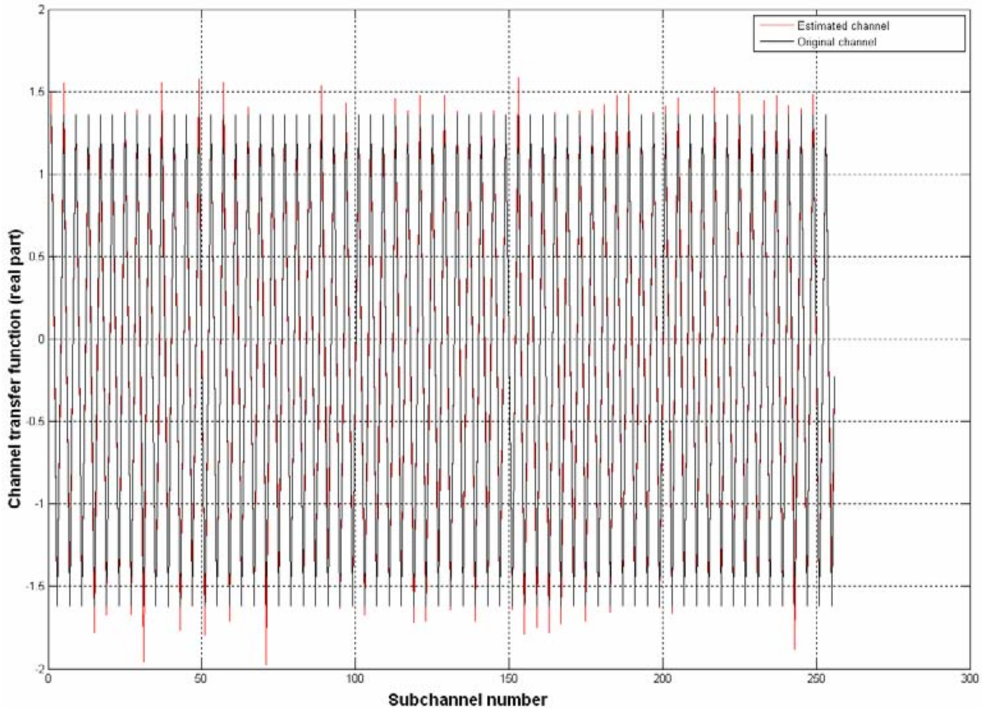

Figure 5.14 Real part of estimated (LS result) and original channel transfer functions at 20th symbol versus subchannel number graph (SNR = 18 dB)

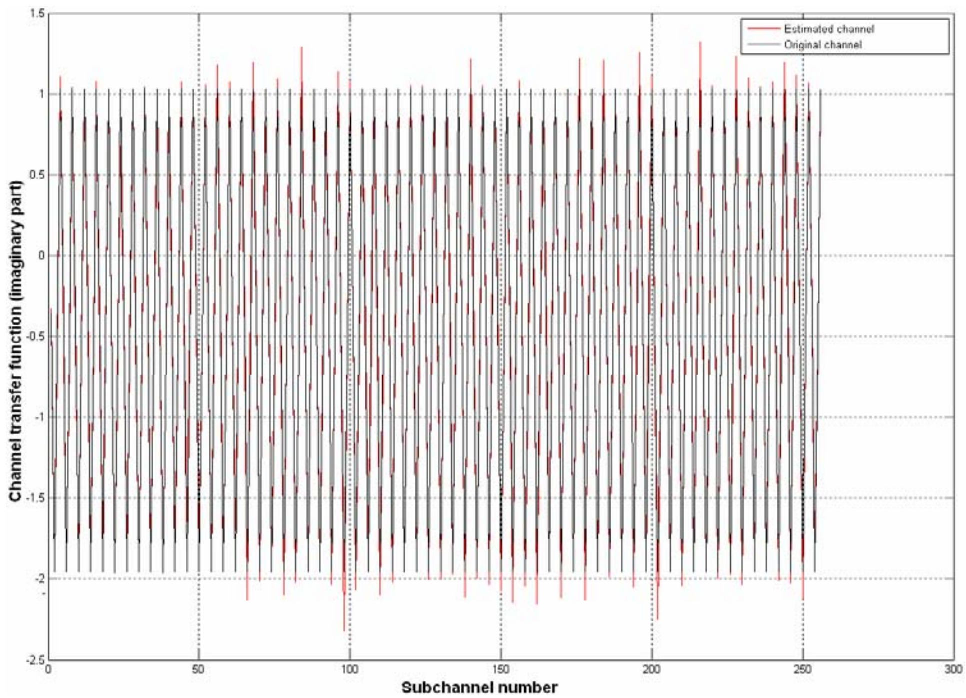

Figure 5.15 Imaginary part of estimated (LS result) and original channel transfer functions at 20th symbol versus subchannel number graph (SNR = 18 dB)

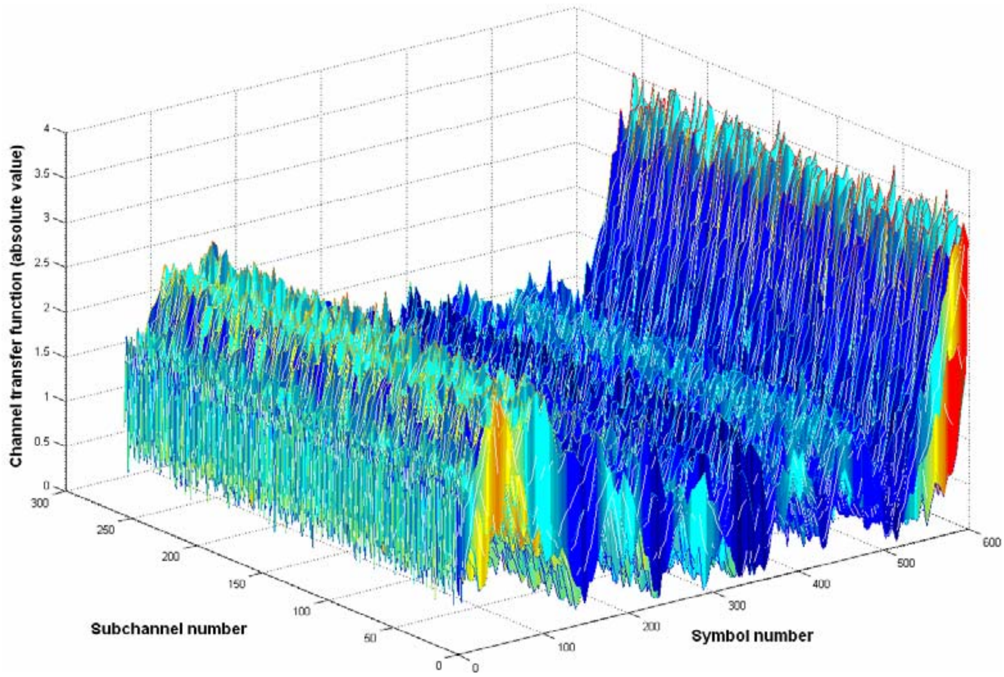

Figure 5.16 Absolute value of the estimated HF channel transfer function (LS result) over whole frequency time grid (SNR=18 dB)

When the results shown in figures from 5.10 to 5.16 are investigated, it can be observed that NSE has peaks where deep fades occur. Moreover, the small ripples exist due to the linear interpolation. These small ripples have peaks in the middle of the linear interpolation because the largest difference between the tracked data and tracking result, which is the tracking error, mostly occurs at that position.

Moreover, if the peaks in Figures 5.14 - 5.15 are count, it is seen that there are 64 peaks in 256 data. This shows that the channel transfer function is periodic with a period of 4 subchannels. This observation meets the theoretical calculation obtained in equation (5.4).

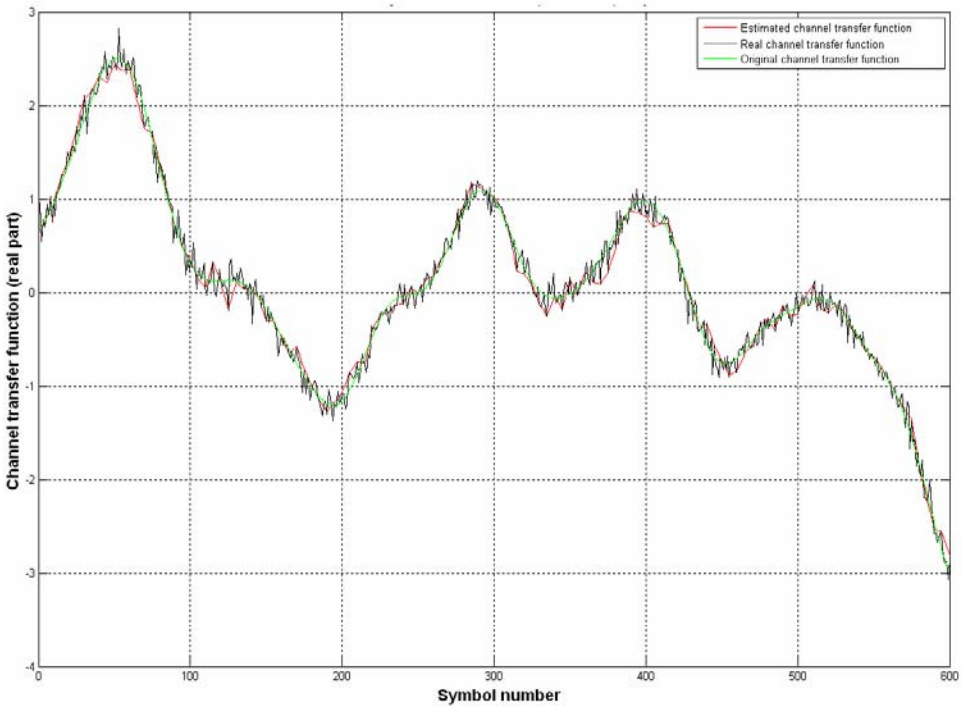

Figure 5.17 Real part of estimated (LMMSE result), real and original channel transfer functions at 1st subchannel versus symbol number graph (SNR = 18 dB)

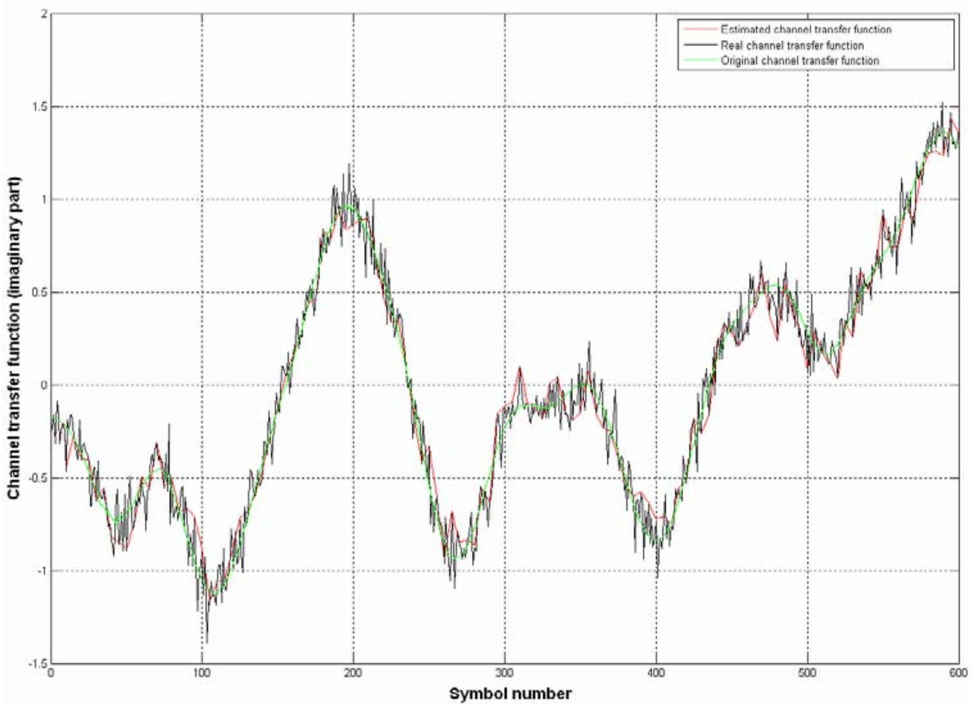

Figure 5.18 Imaginary part of estimated (LMMSE result), real and original channel transfer functions at 1st subchannel versus symbol number graph (SNR = 18 dB)

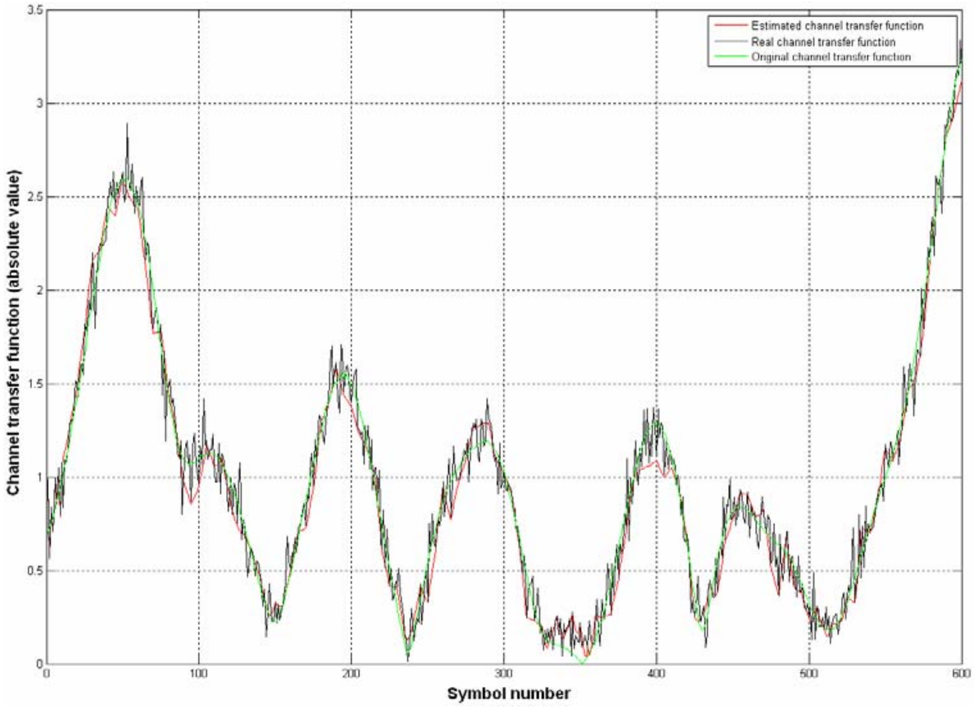

Figure 5.19 Absolute value of estimated (LMMSE result), real and original channel transfer functions at 1st subchannel versus symbol number graph (SNR = 18 dB)

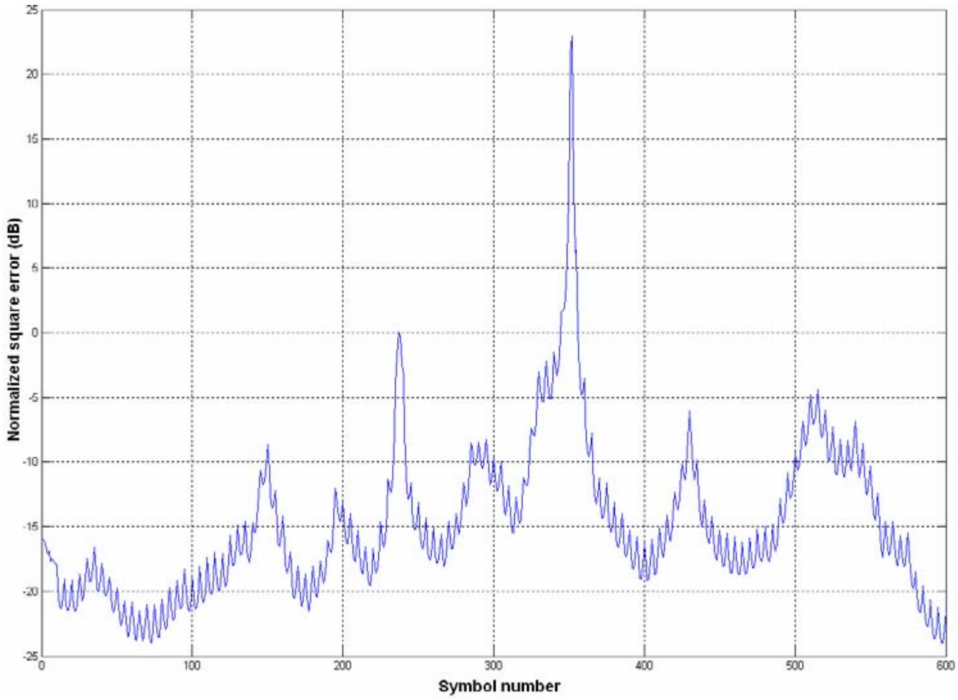

Figure 5.20 Normalized square error averaged over all subchannels (LMMSE result) versus symbol number graph (SNR = 18 dB)

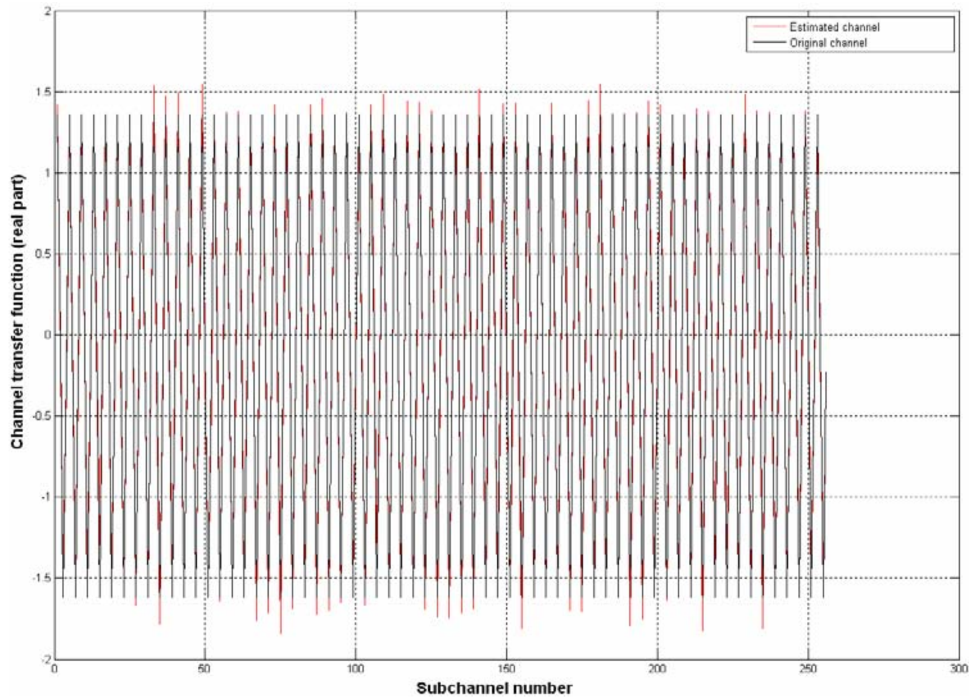

Figure 5.21 Real part of estimated (LMMSE result) and original channel transfer functions at 20th symbol versus subchannel number graph (SNR = 18 dB)

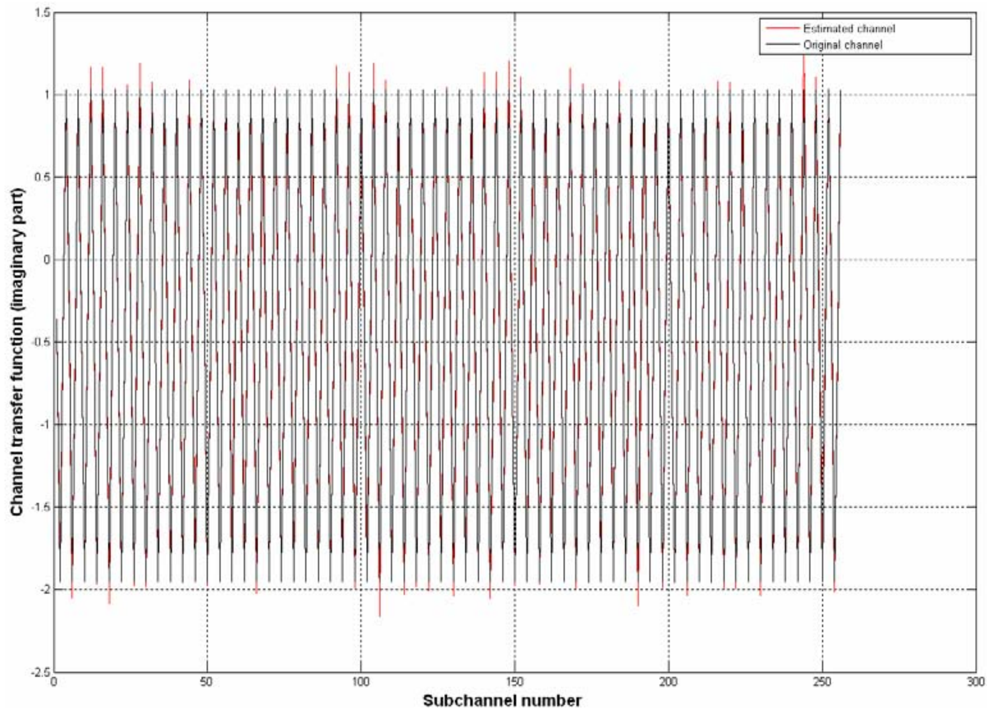

Figure 5.22 Imaginary part of estimated (LMMSE result) and original channel transfer functions at 20th symbol versus subchannel number graph (SNR = 18 dB)

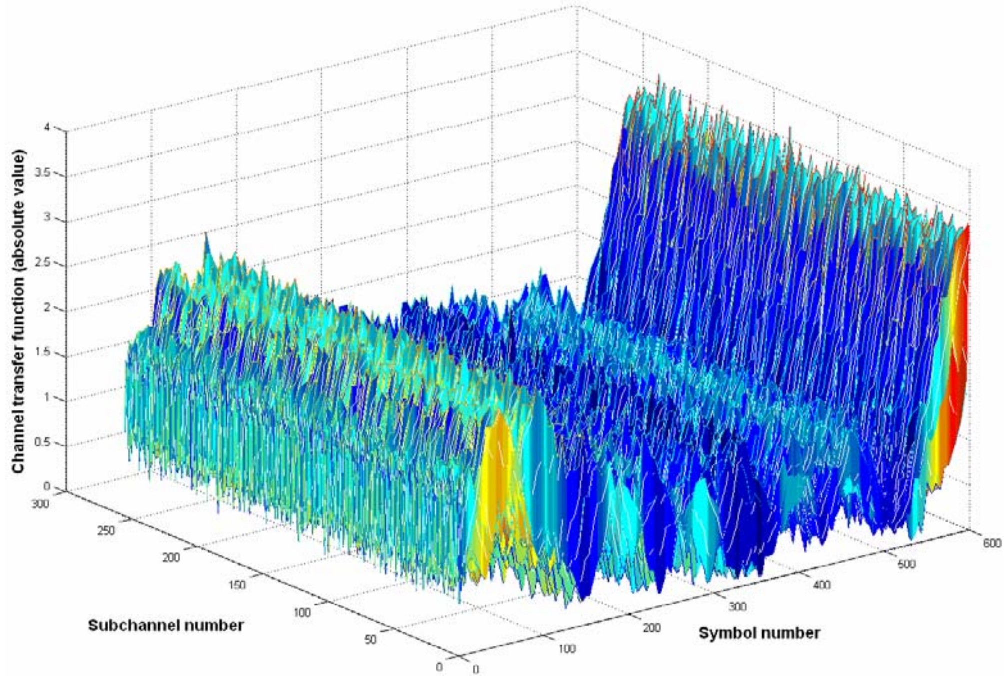

Figure 5.23 Absolute value of the estimated HF channel transfer function (LMMSE result) over whole frequency time grid (SNR=18 dB)

In the LS method case, the estimates are obtained with instantaneous values of the channel transfer function at the pilot symbols. However, for the LMMSE method the estimates are obtained with some processing of the measurements after obtaining some statistical information about these measurements (see equation (4.11)). As a result, if figures from (5.10) to (5.23) are observed closely, it can be seen that the estimation results of LMMSE are more smooth compared to the results of the LS method. That is, filtering process works better in this case.

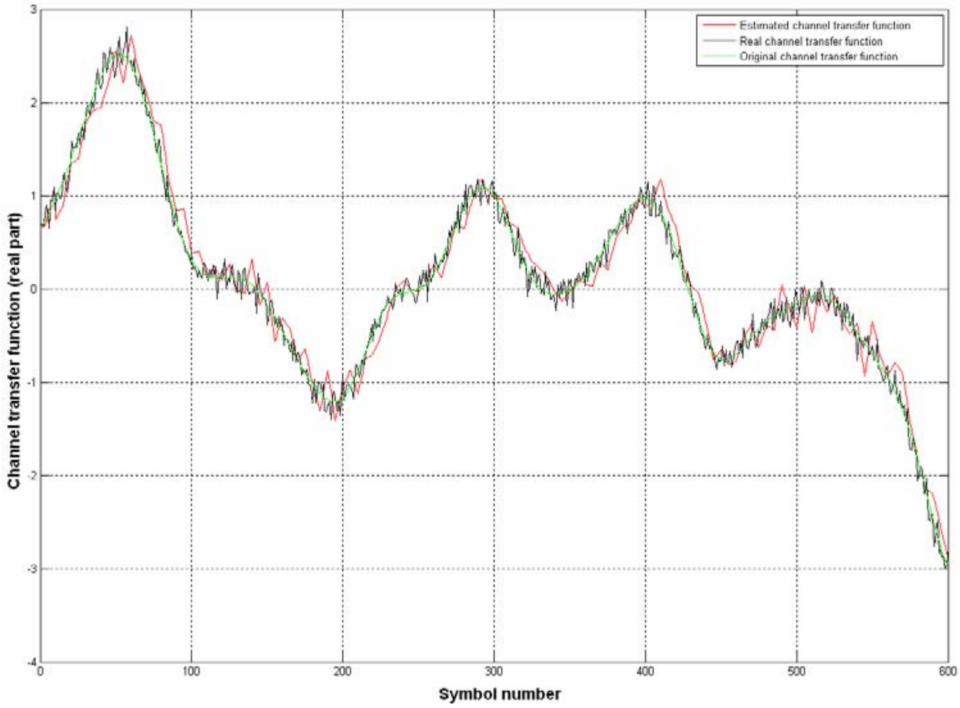

Figure 5.24 Real part of estimated (LMS result), real and original channel transfer functions at 1st subchannel versus symbol number graph (SNR = 18 dB)

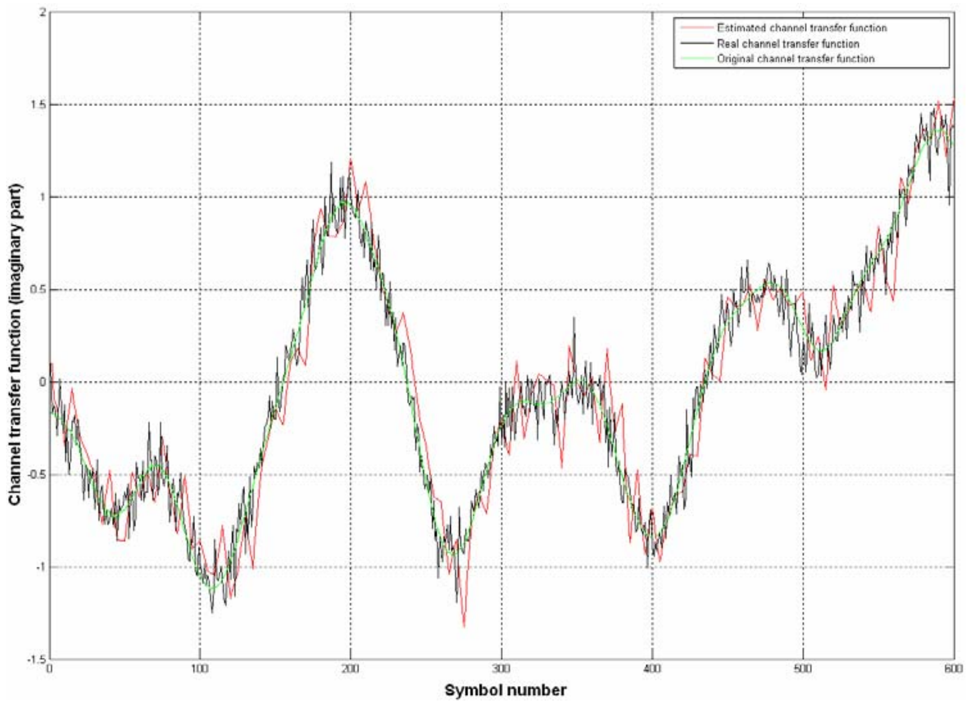

Figure 5.25 Imaginary part of estimated (LMS result), real and original channel transfer functions at 1st subchannel versus symbol number graph (SNR = 18 dB)

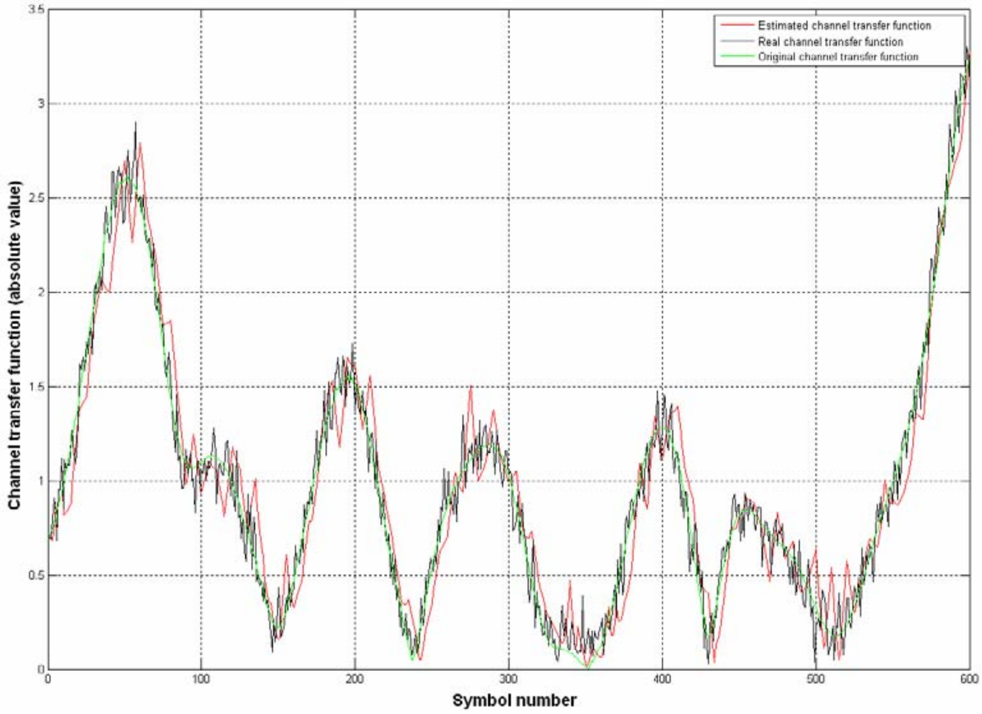

Figure 5.26 Absolute value of estimated (LMS result), real and original channel transfer functions at 1st subchannel versus symbol number graph (SNR = 18 dB)

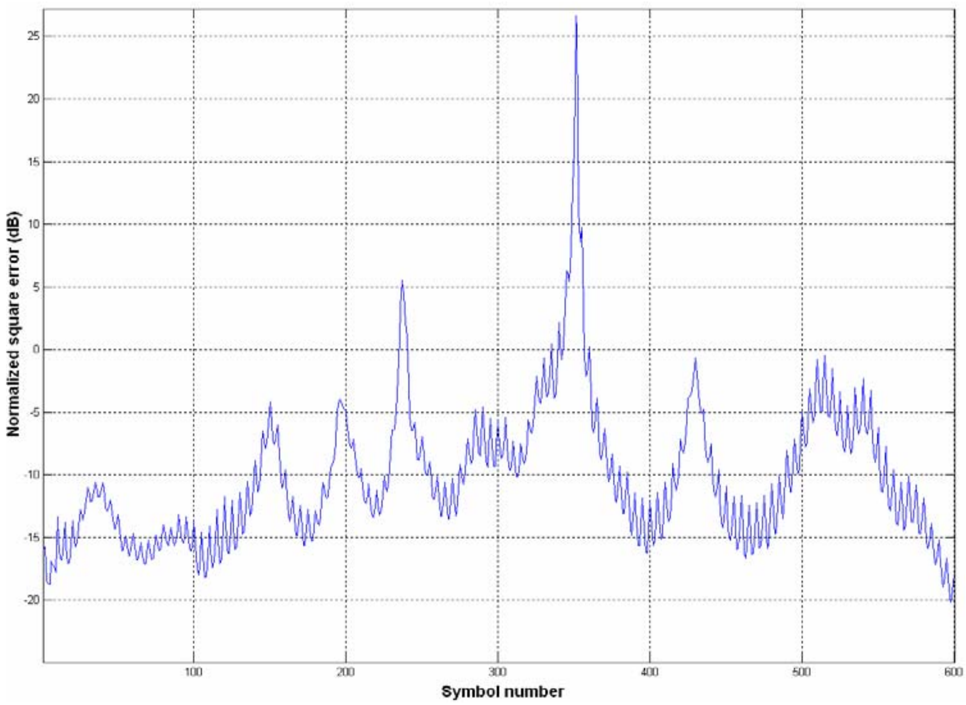

Figure 5.27 Normalized square error averaged over all subchannels (LMS result) versus symbol number graph (SNR = 18 dB)

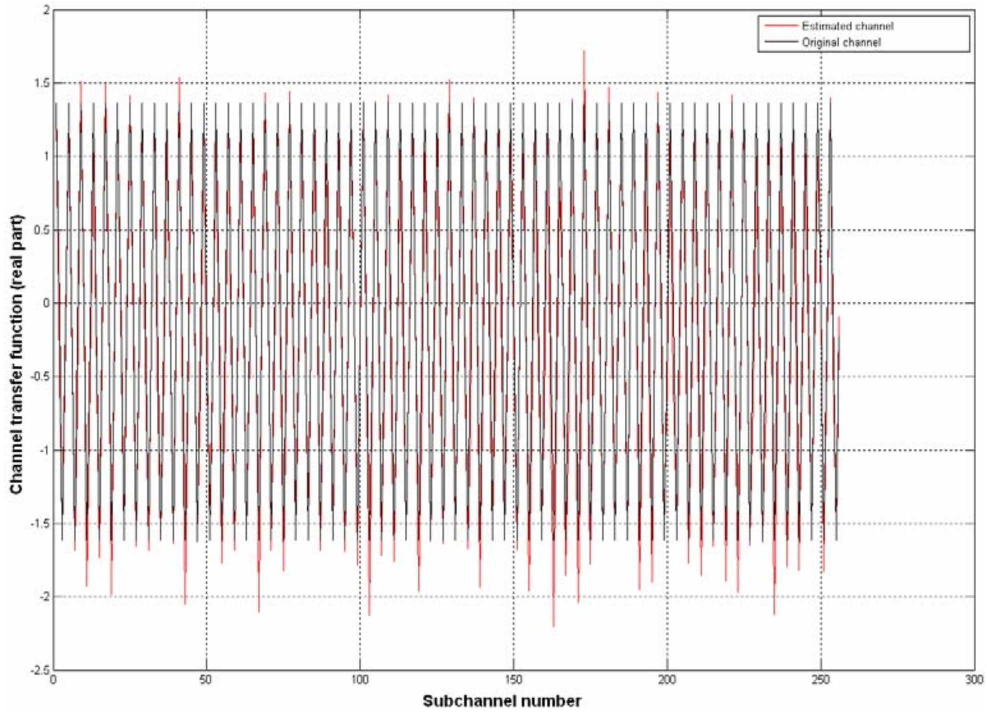

Figure 5.28 Real part of estimated (LMS result) and original channel transfer functions at 20th symbol versus subchannel number graph (SNR = 18 dB)

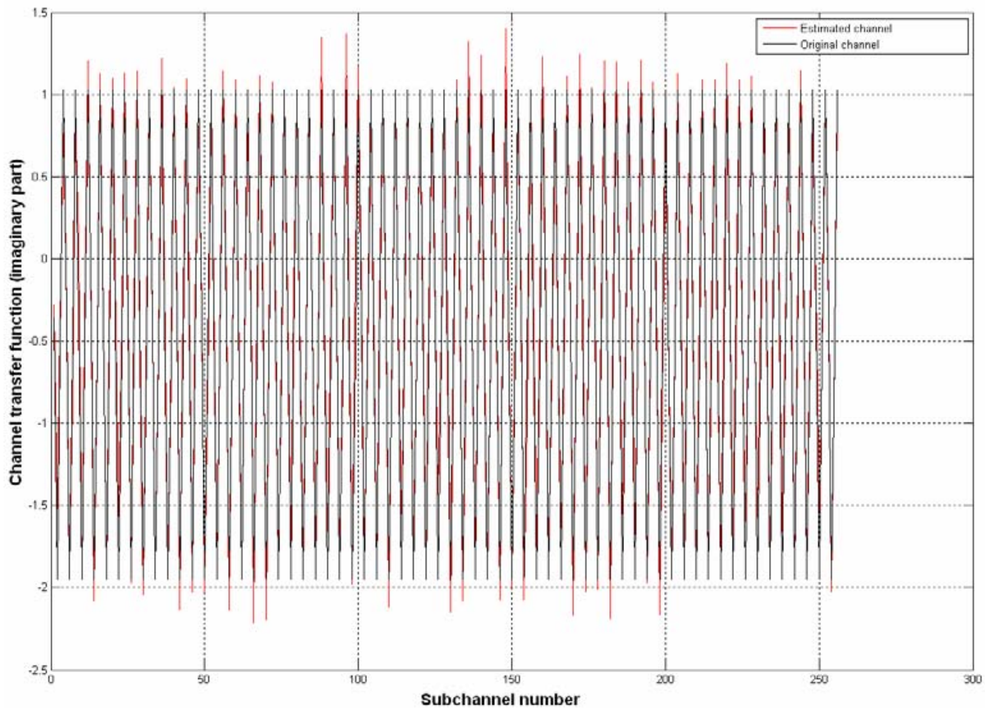

Figure 5.29 Imaginary part of estimated (LMS result) and original channel transfer functions at 20th symbol versus subchannel number graph (SNR = 18 dB)

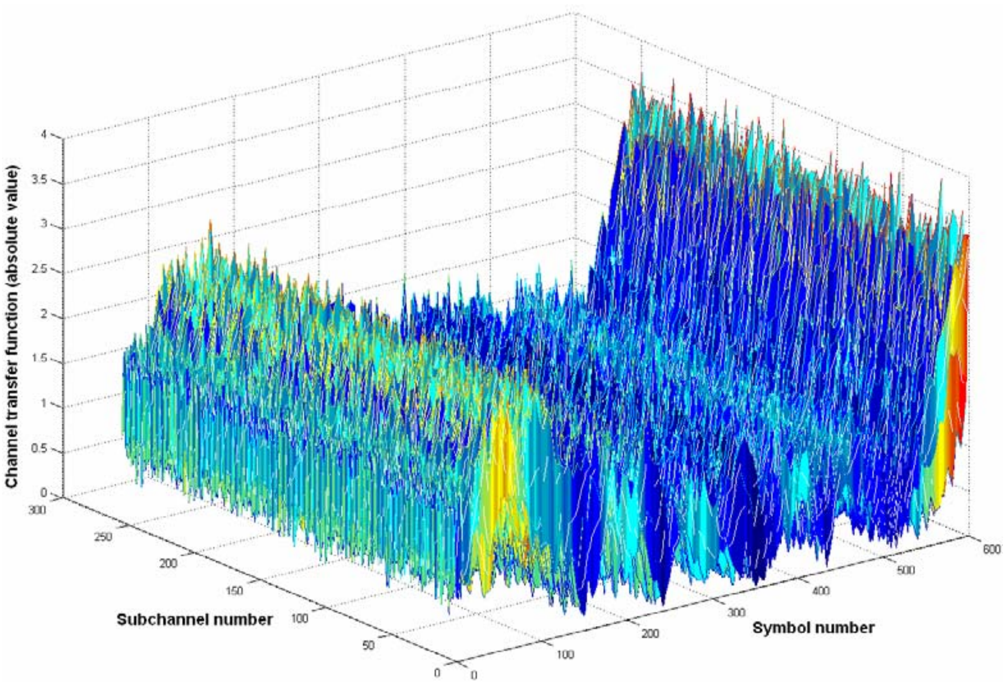

Figure 5.30 Absolute value of the estimated HF channel transfer function (LMS result) over whole frequency time grid (SNR=18 dB)

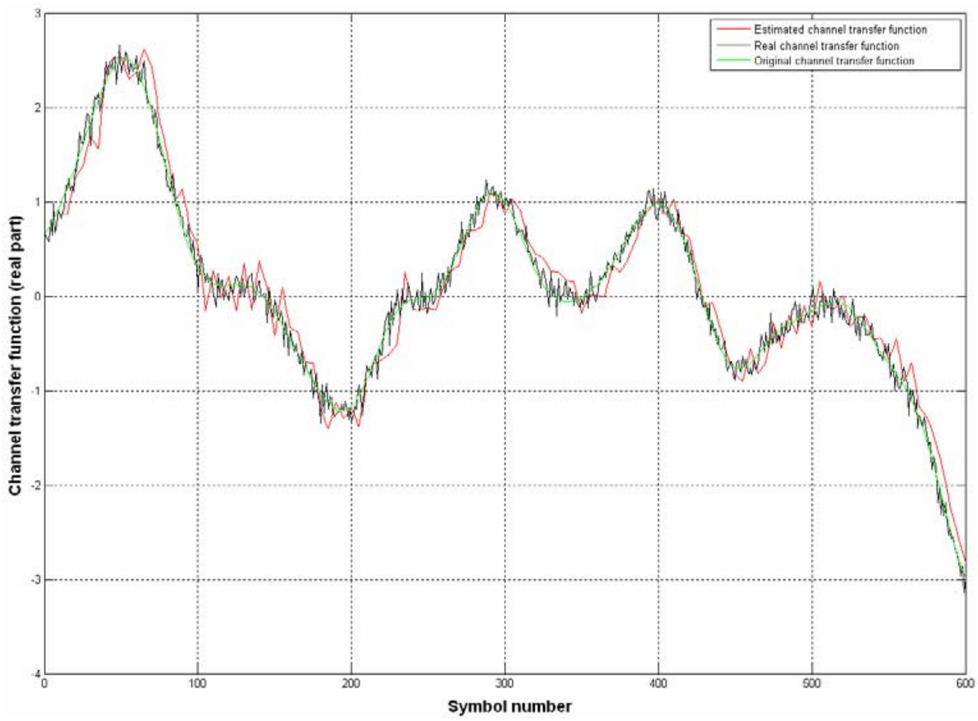

Figure 5.31 Real part of estimated (adaptive LMS result), real and original channel transfer functions at 1st subchannel versus symbol number graph (SNR = 18 dB)

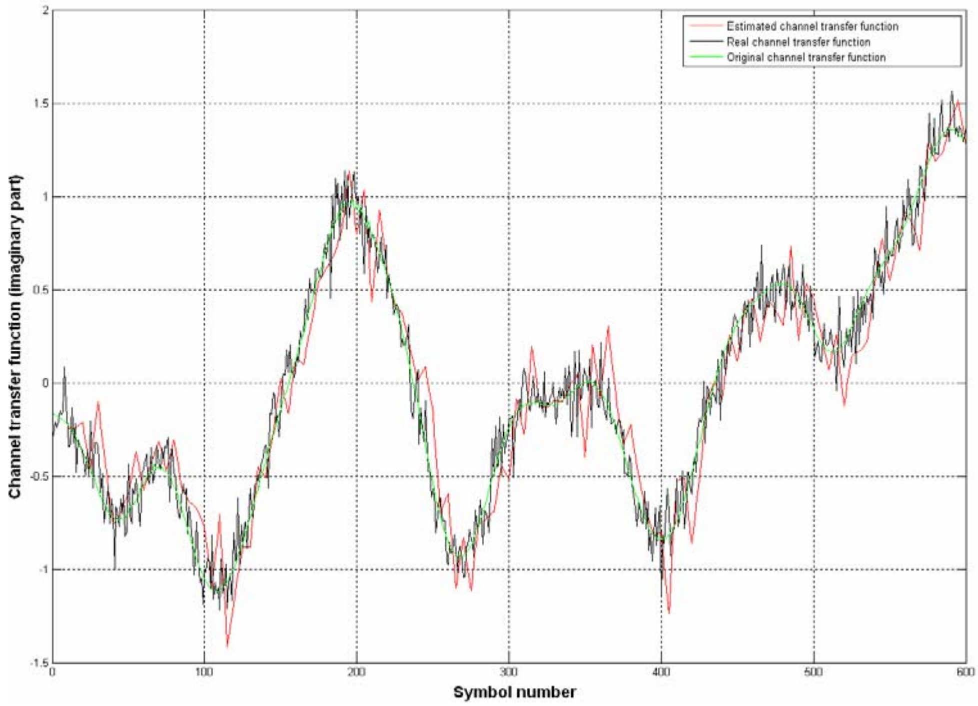

Figure 5.32 Imaginary part of estimated (adaptive LMS result), real and original channel transfer functions at 1st subchannel versus symbol number graph (SNR = 18 dB)

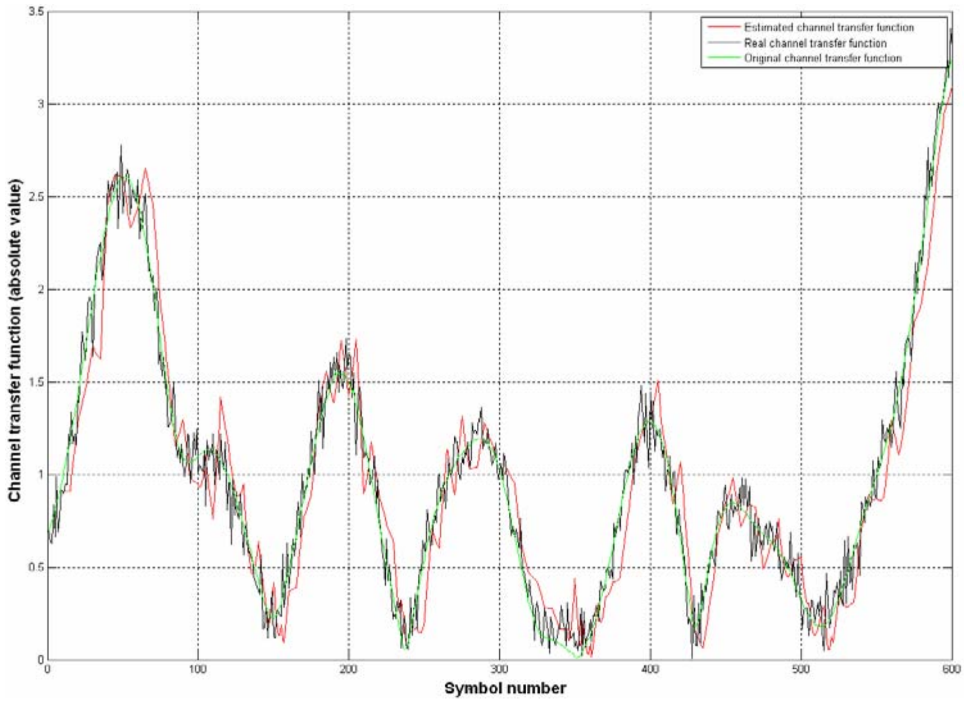

Figure 5.33 Absolute value of estimated (adaptive LMS result), real and original channel transfer functions at 1st subchannel versus symbol number graph (SNR = 18 dB)

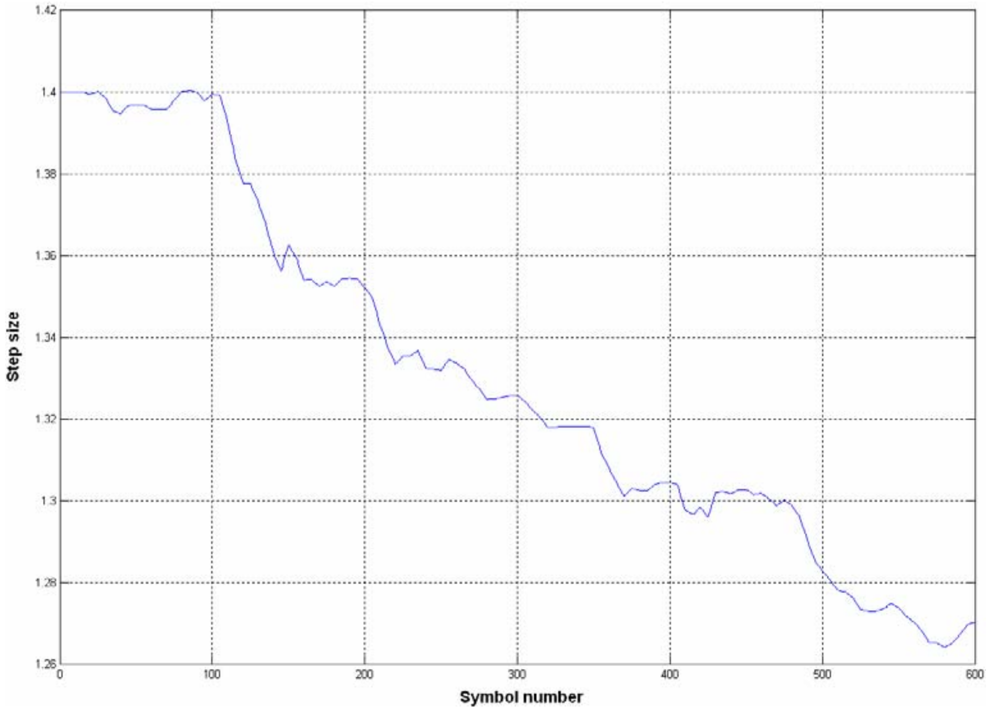

Figure 5.34 Step size (adaptive LMS result) at 1st subchannel versus symbol number graph (SNR = 18 dB)

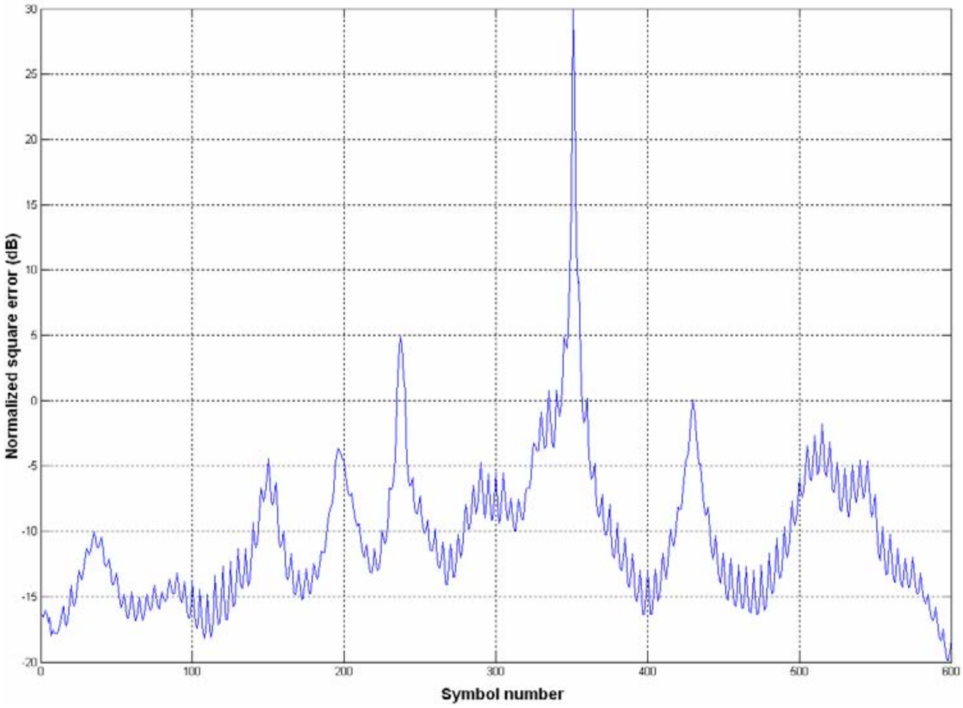

Figure 5.35 Normalized square error averaged over all subchannels (adaptive LMS result) versus symbol number graph (SNR = 18 dB)

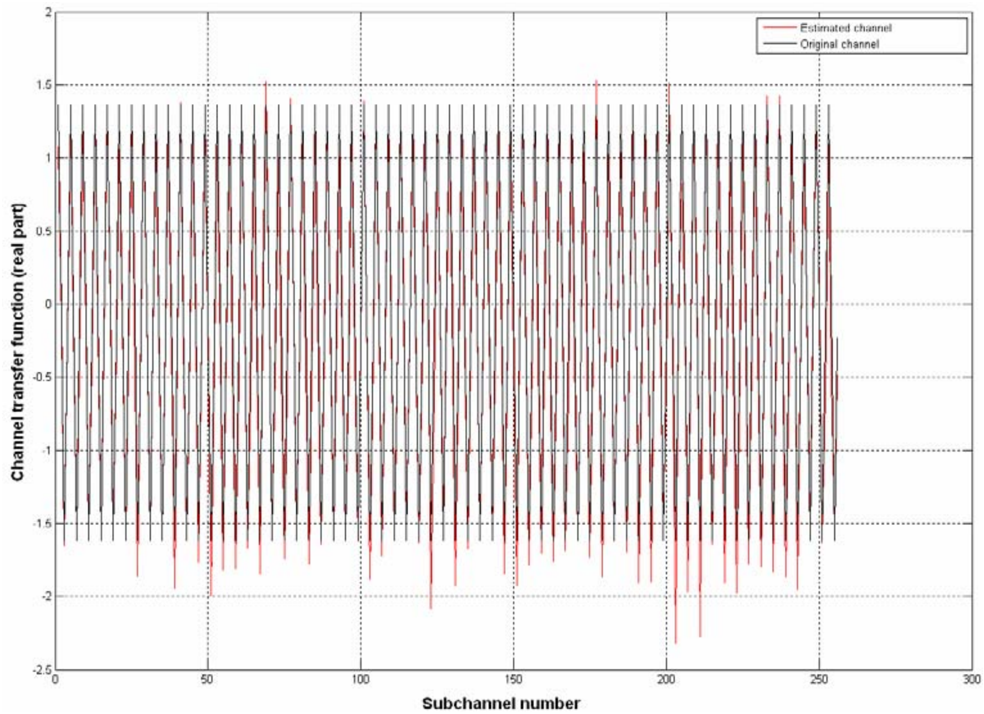

Figure 5.36 Real part of estimated (adaptive LMS result) and original channel transfer functions at 20th symbol versus subchannel number graph (SNR = 18 dB)

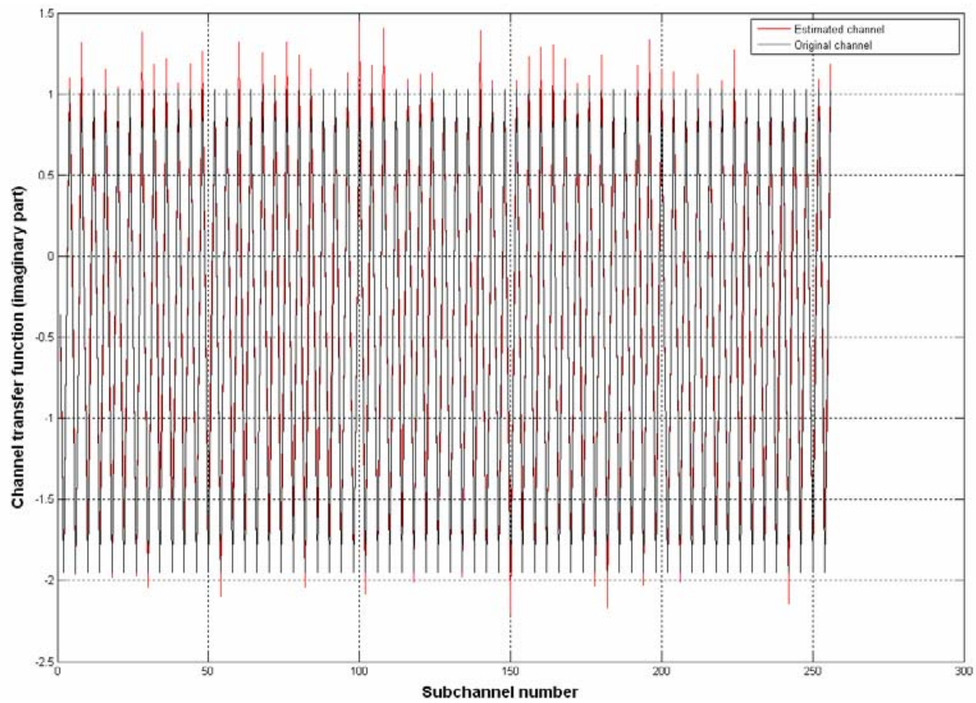

Figure 5.37 Imaginary part of estimated (adaptive LMS result) and original channel transfer functions at 20th symbol versus subchannel number graph (SNR = 18 dB)

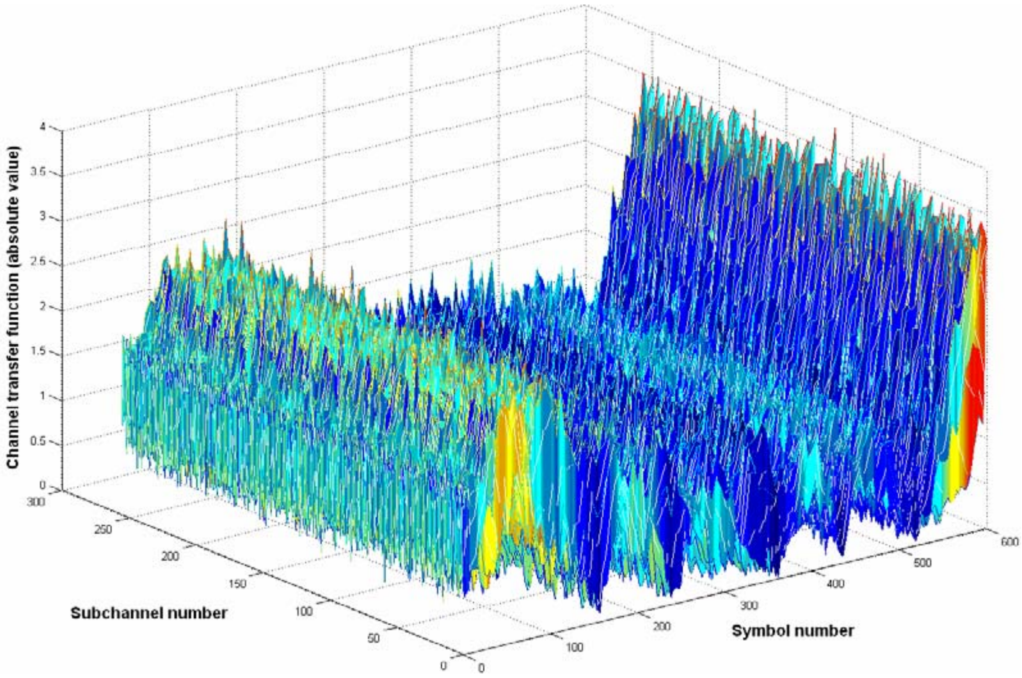

Figure 5.38 Absolute value of the estimated HF channel transfer function (adaptive LMS result) over whole frequency time grid (SNR=18 dB)

For LMS and adaptive LMS methods, there is an apparent delay in tracking (see Figures 5.24-5.26 and Figures 5.31-5.33), which does not exist for LS and LMMSE cases and it is longer compared to the RLS and Kalman filter cases as will be shown in the following figures. This is because the convergence durations of the LMS and adaptive LMS methods are longer compared to that of the others [39]. This explains why LMS and adaptive LMS methods have the worst performance as observed in the SER vs. SNR and the NMSE vs. SNR graphs (see Figure 5.4-5.7).

It can also be observed that adaptive scheme increases the performance (see Figures 5.24-5.38). If the step size decreases, methods become more robust against noise but the delay in tracking increases. On the other hand, if the step size increases, methods become more susceptable against noise but the delay in tracking decreases. For this reason, for nonadaptive LMS case, the step size must be selected carefully. Since adaptive LMS has variable step size which depends on the tracked data, the performance of the adaptive scheme is naturally higher.

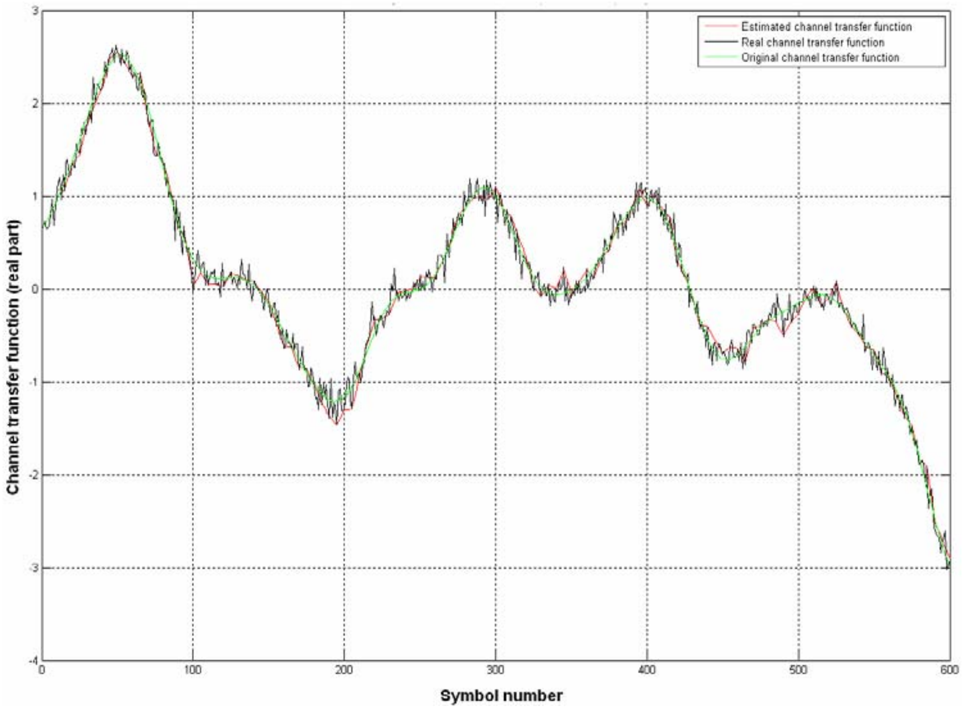

Figure 5.39 Real part of estimated (RLS result), real and original channel transfer functions at 1st subchannel versus symbol number graph (SNR = 18 dB)

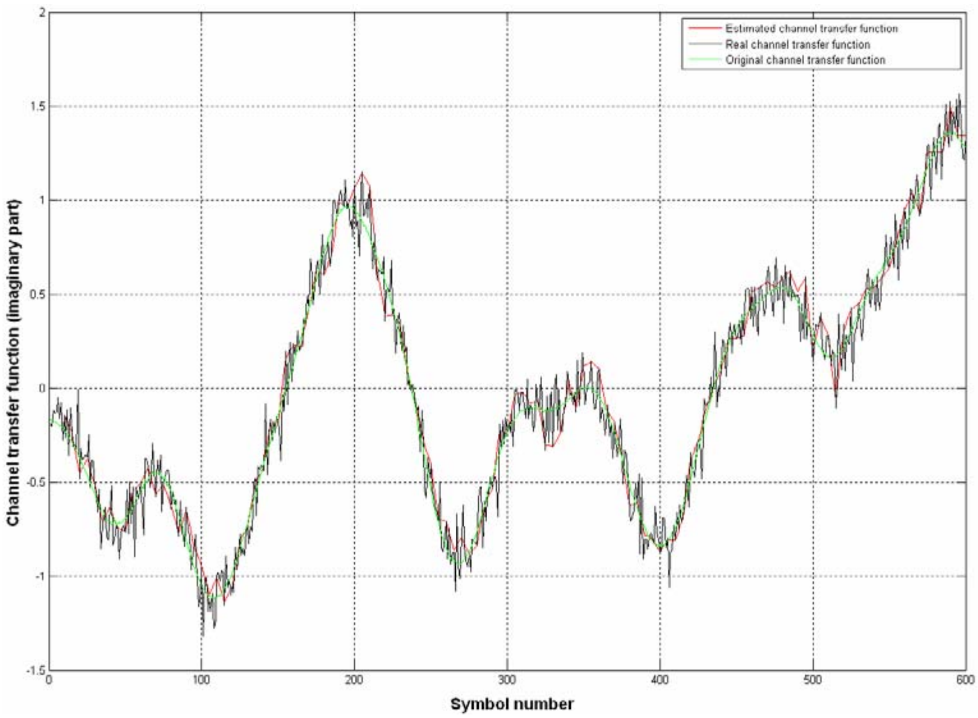

Figure 5.40 Imaginary part of estimated (RLS result), real and original channel transfer functions at 1st subchannel versus symbol number graph (SNR = 18 dB)

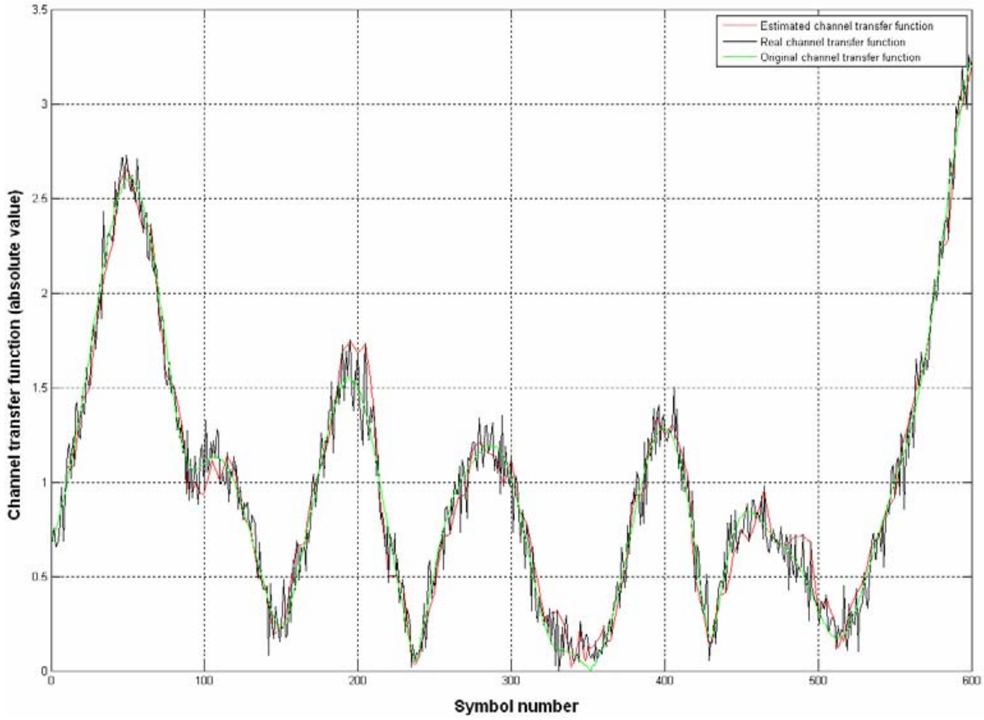

Figure 5.41 Absolute value of estimated (RLS result), real and original channel transfer functions at 1st subchannel versus symbol number graph (SNR = 18 dB)

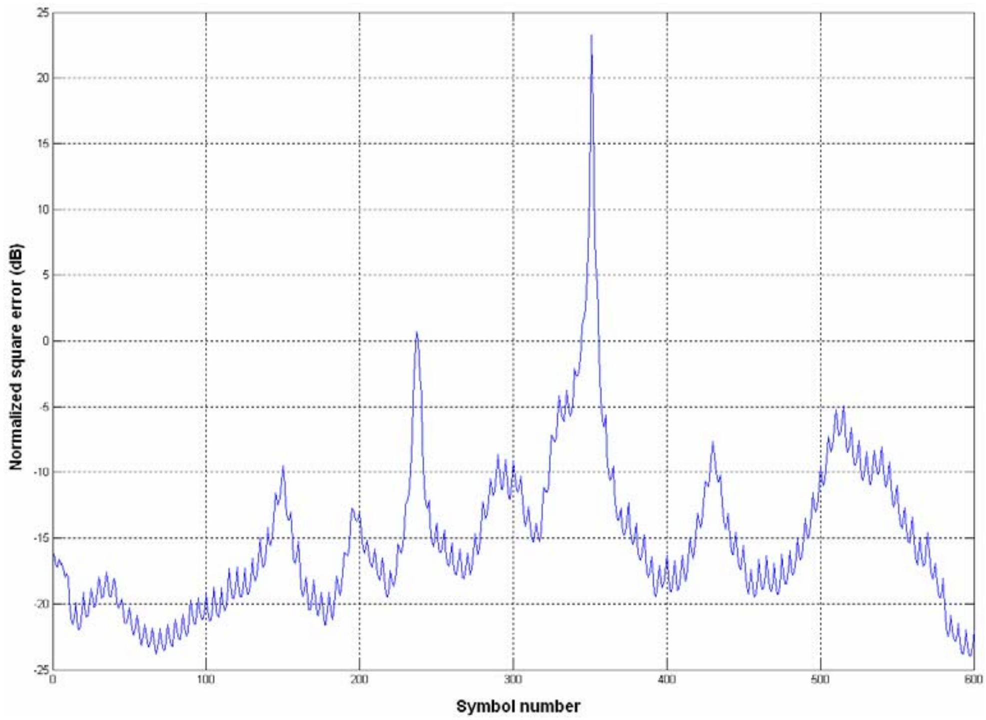

Figure 5.42 Normalized square error averaged over all subchannels (RLS result) versus symbol number graph (SNR = 18 dB)

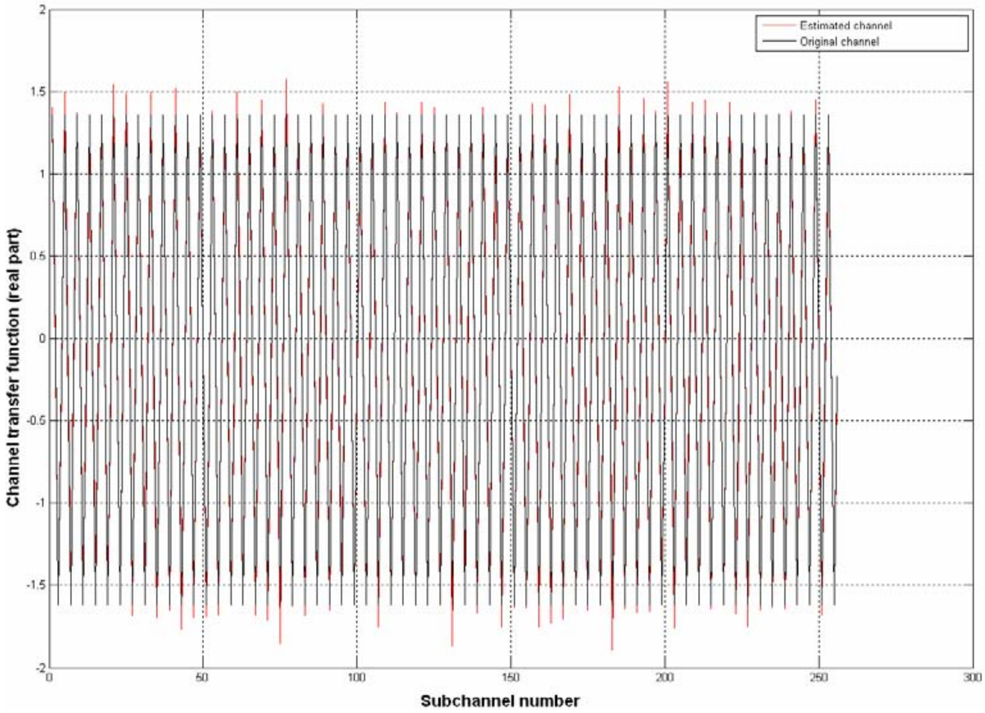

Figure 5.43 Real part of estimated (RLS result) and original channel transfer functions at 20th symbol versus subchannel number graph (SNR = 18 dB)

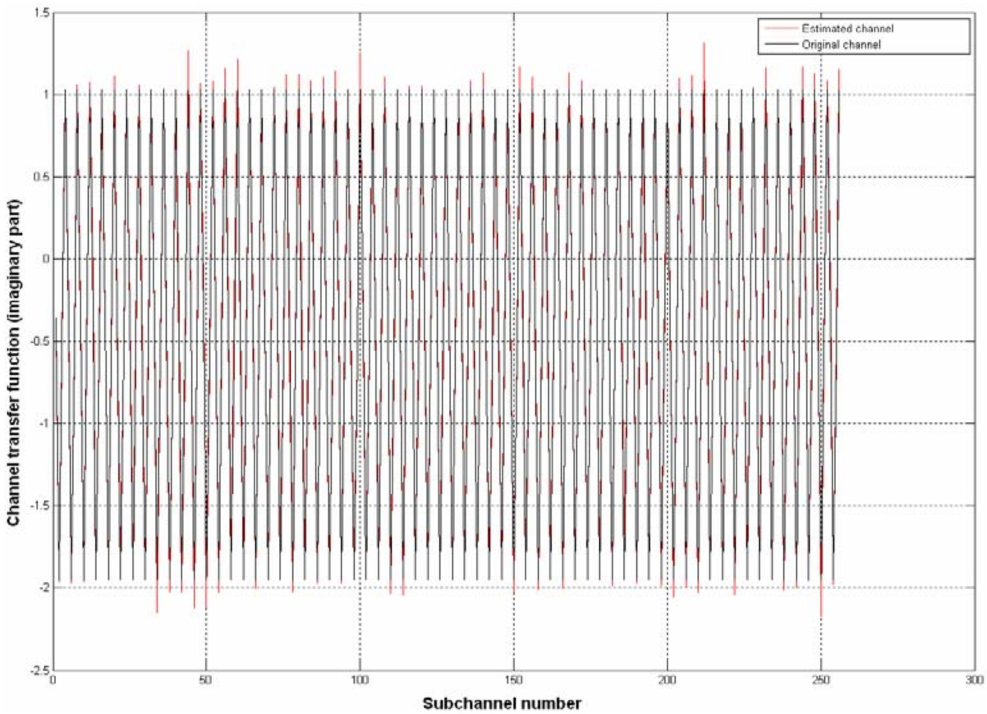

Figure 5.44 Imaginary part of estimated (RLS result) and original channel transfer functions at 20th symbol versus subchannel number graph (SNR = 18 dB)

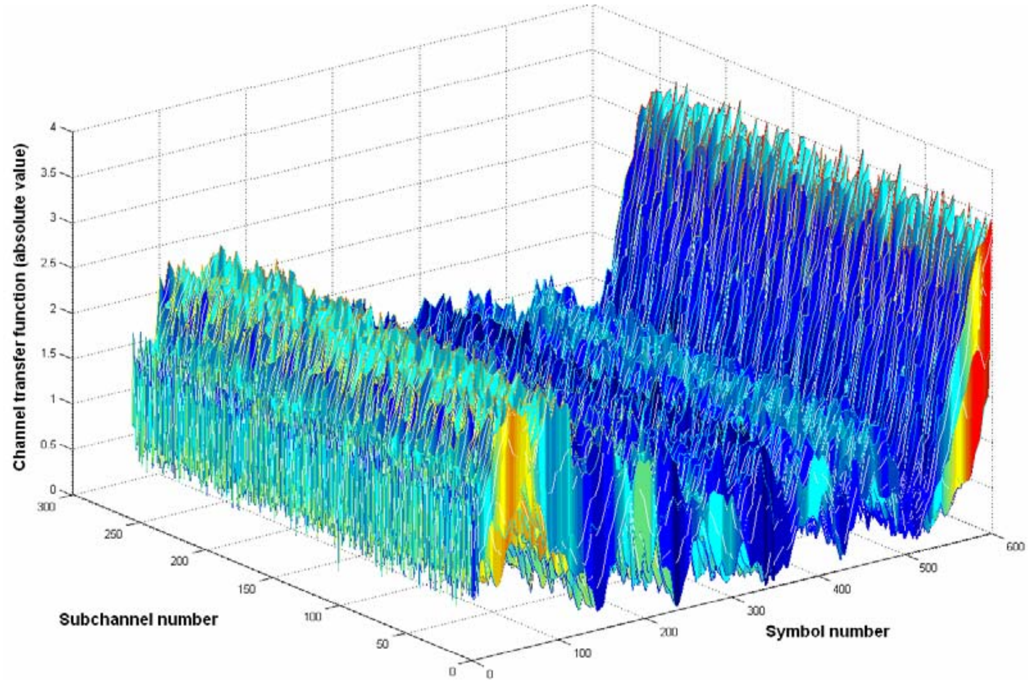

Figure 5.45 Absolute value of the estimated HF channel transfer function (RLS result) over whole frequency time grid (SNR=18 dB)

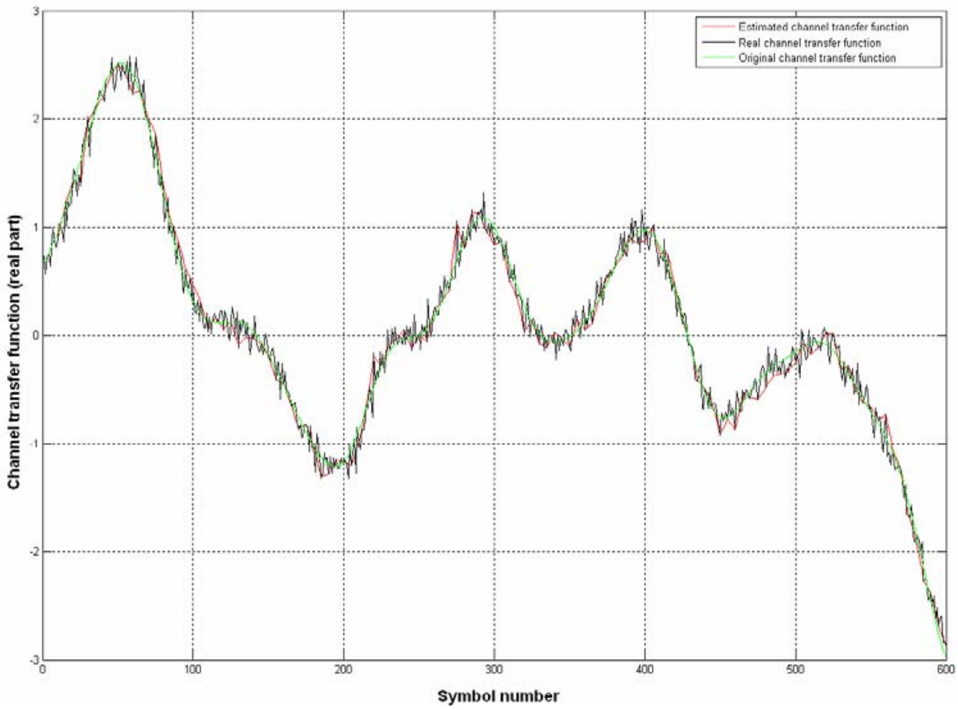

Figure 5.46 Real part of estimated (adaptive RLS result), real and original channel transfer functions at 1st subchannel versus symbol number graph (SNR = 18 dB)

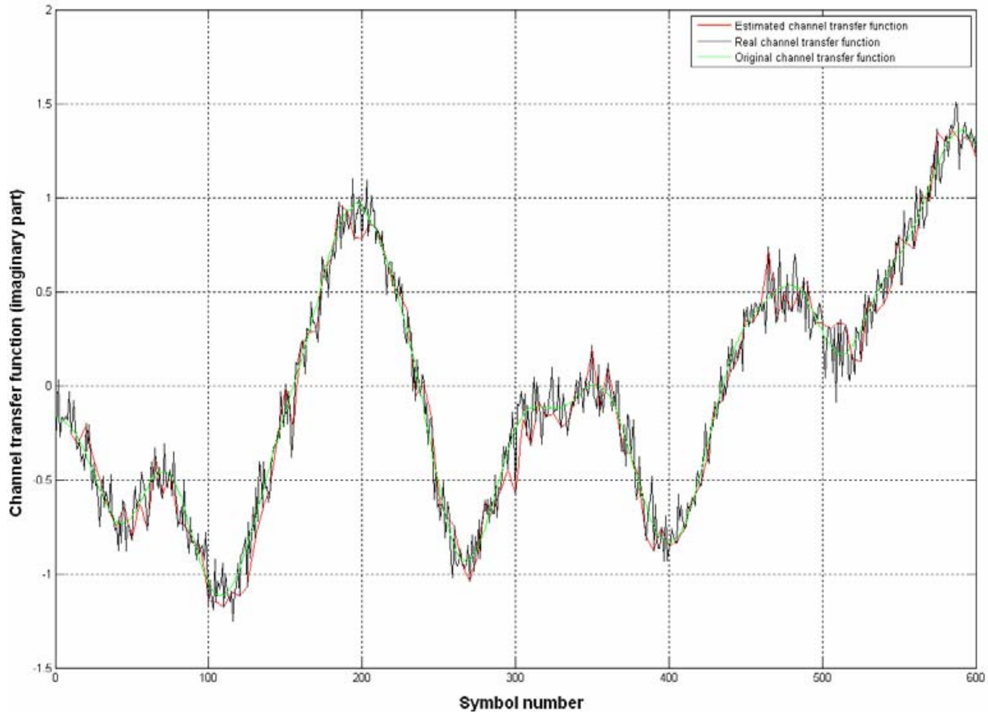

Figure 5.47 Imaginary part of estimated (adaptive RLS result), real and original channel transfer functions at 1st subchannel versus symbol number graph (SNR=18 dB)

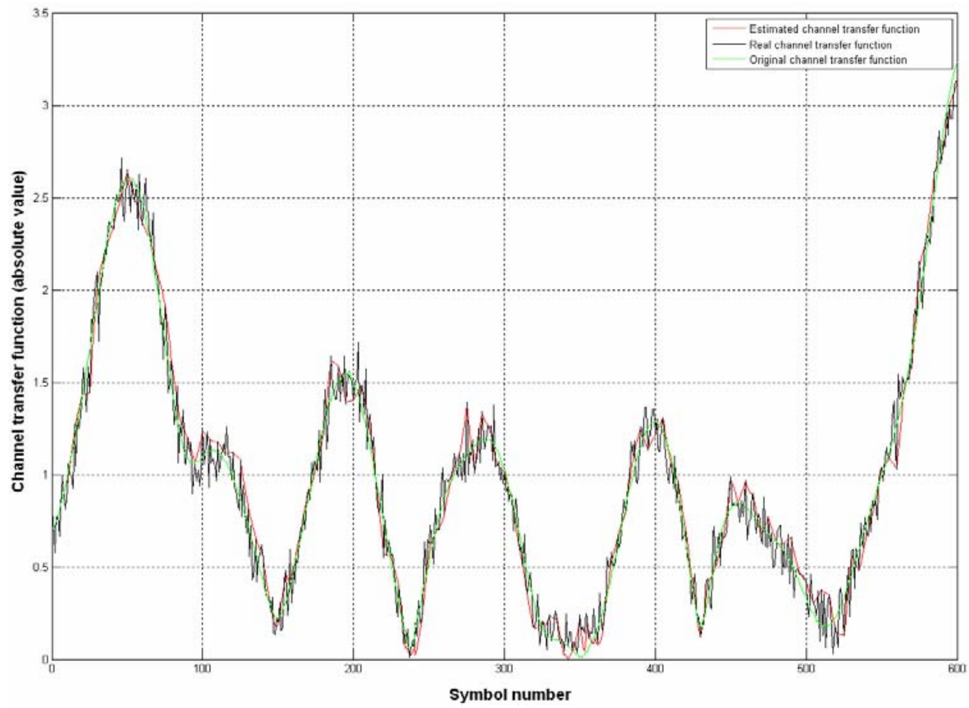

Figure 5.48 Absolute value of estimated (adaptive RLS result), real and original channel transfer functions at 1st subchannel versus symbol number graph (SNR = 18 dB)

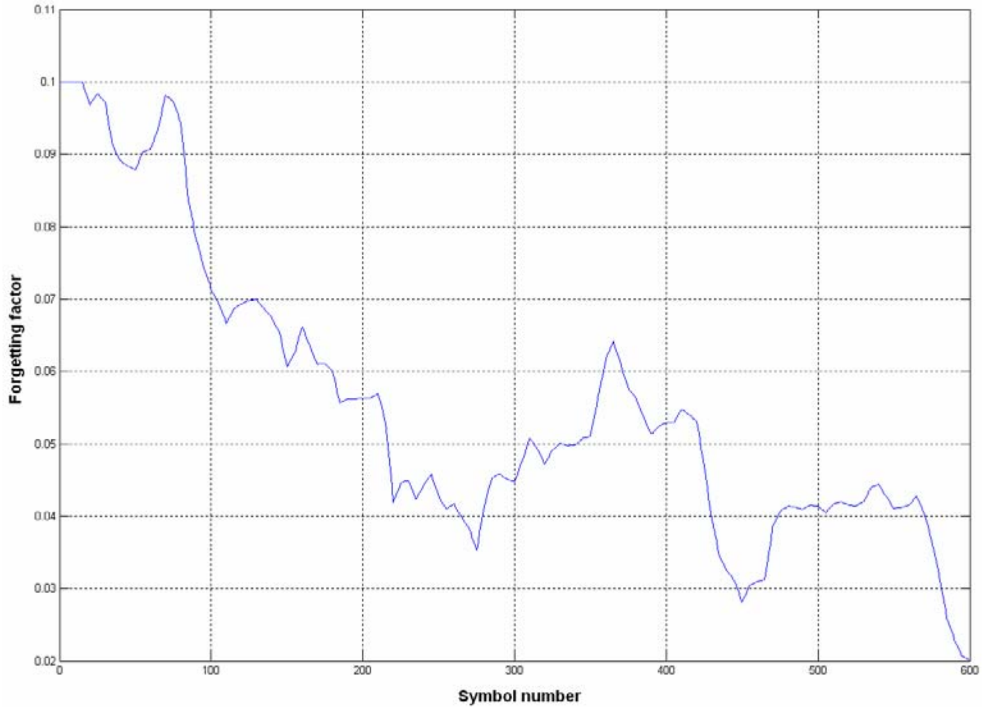

Figure 5.49 Forgetting factor (adaptive RLS result) at 1st subchannel versus symbol number graph (SNR = 18 dB)

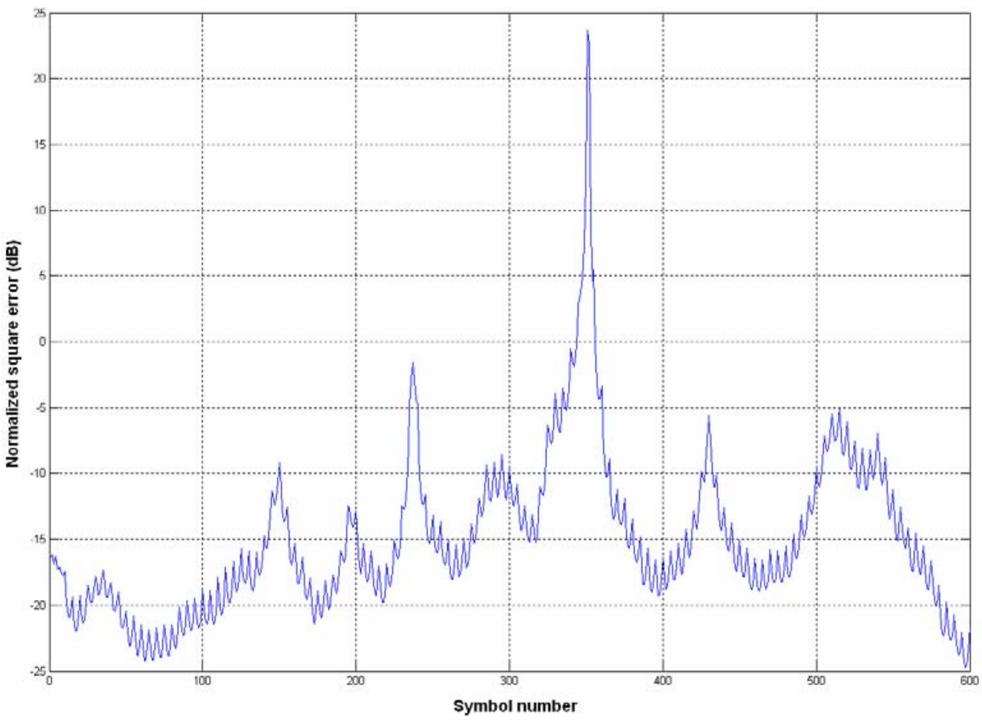

Figure 5.50 Normalized square error averaged over all subchannels (adaptive RLS result) versus symbol number graph (SNR = 18 dB)

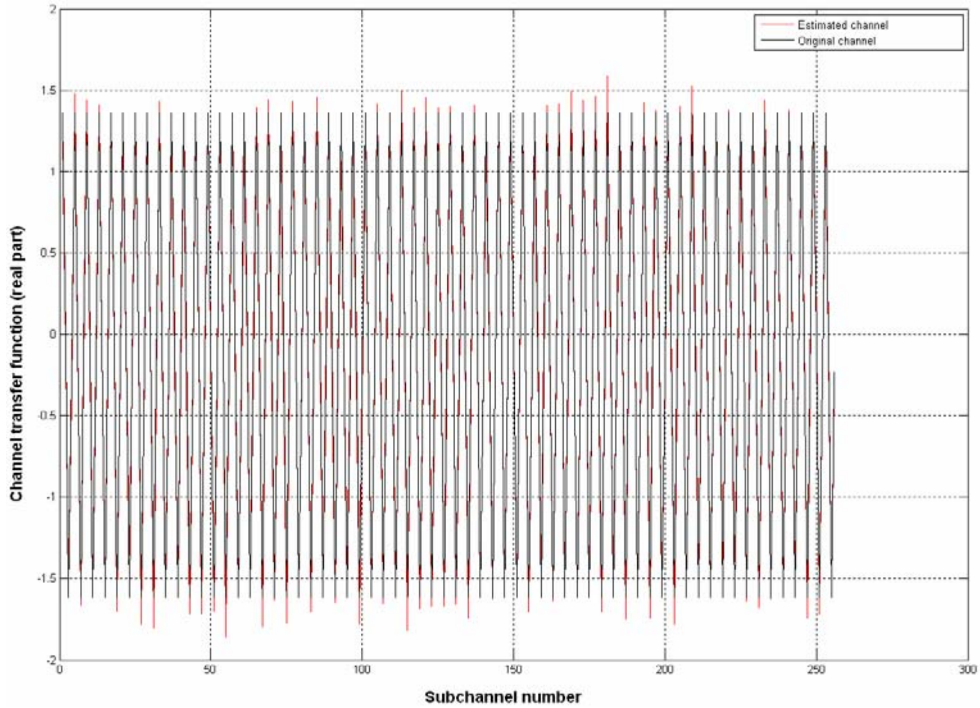

Figure 5.51 Real part of estimated (adaptive RLS result) and original channel transfer functions at 20th symbol versus subchannel number graph (SNR = 18 dB)

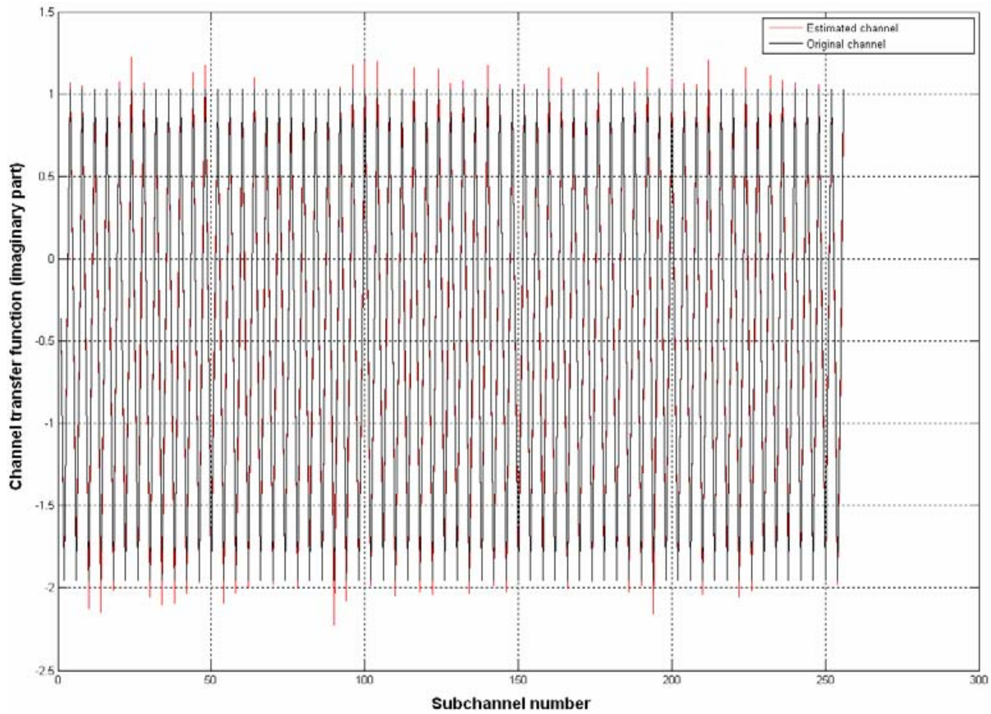

Figure 5.52 Imaginary part of estimated (adaptive RLS result) and original channel transfer functions at 20th symbol versus subchannel number graph (SNR = 18 dB)

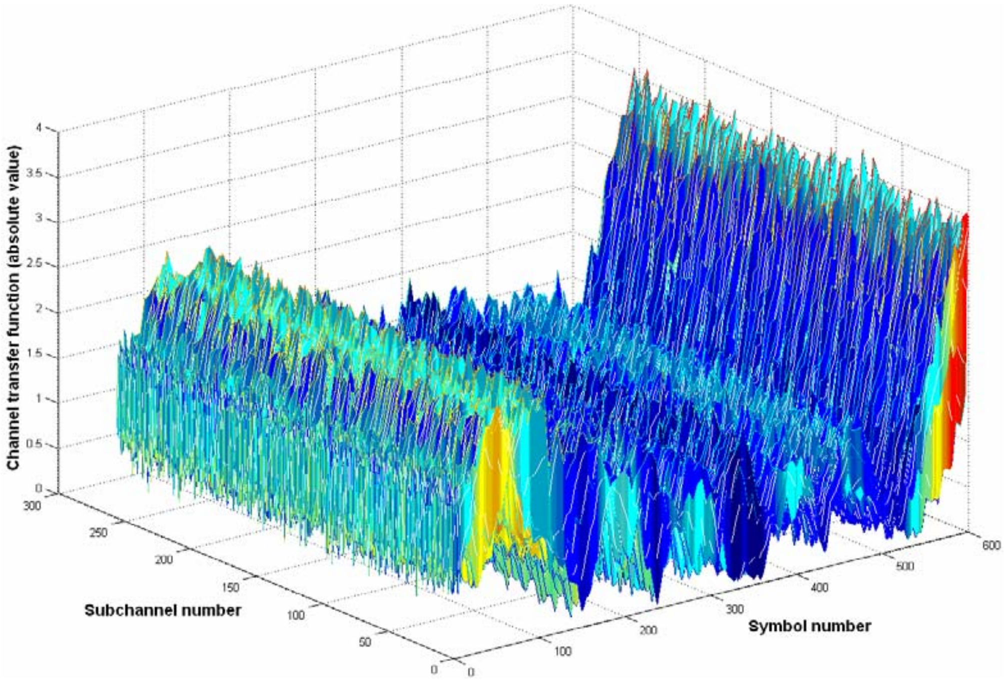

Figure 5.53 Absolute value of the estimated HF channel transfer function (adaptive RLS result) over whole frequency time grid (SNR=18 dB)

For RLS and adaptive RLS methods, the delay in tracking is almost eliminated and performance increases. This is an expected result, because the conversion duration is less than that of the LMS and the adaptive LMS methods [39].

As in the case of LMS methods, for RLS methods, it can be observed that adaptive scheme increases the performance. As the forgetting factor decreases, filtering performance increases and the methods become more robust against noise. However, filtering introduces delay and as the the forgetting factor is decreased more, the delay in tracking increases. Naturally, it reduces the performance. On the other hand, if the forgetting factor increases, the RLS method can respond rapid to changes in the input data. This decreases the delay in tracking. However, at this time this method becomes more susceptable to noise. Hence for nonadaptive RLS, the forgetting factor should be selected carefully. Since adaptive RLS algorithm has variable forgetting factor which depends on the tracked data, the performance of the adaptive scheme is naturally higher.

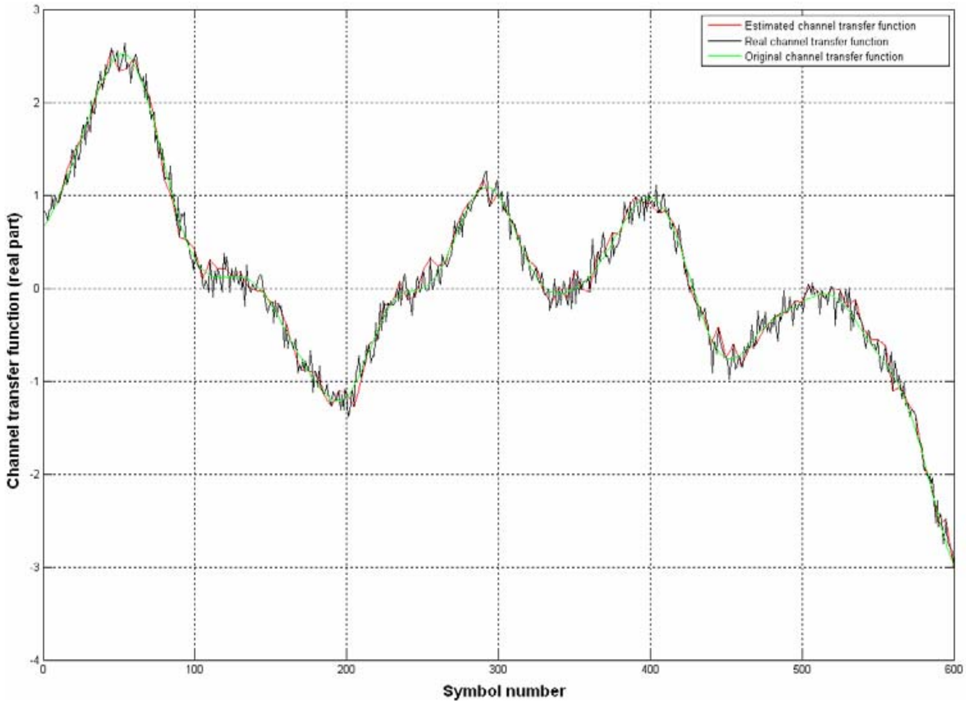

Figure 5.54 Real part of estimated (Kalman CP result), real and original channel transfer functions at 1st subchannel versus symbol number graph (SNR = 18 dB)

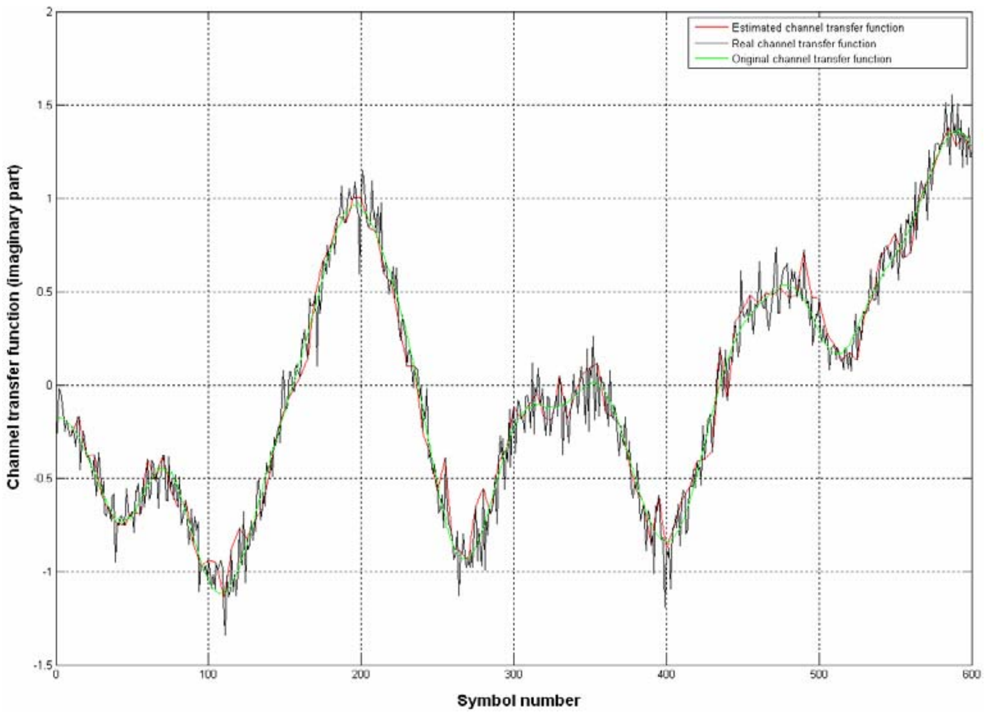

Figure 5.55 Imaginary part of estimated (Kalman CP result), real and original channel transfer functions at 1st subchannel versus symbol number graph (SNR = 18 dB)

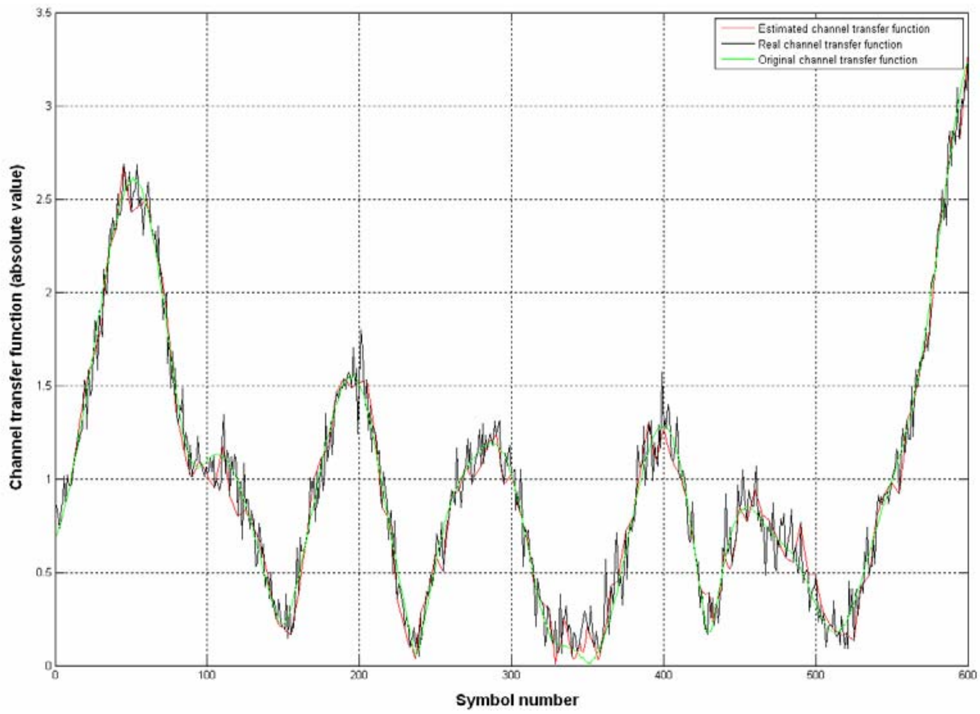

Figure 5.56 Absolute value of estimated (Kalman CP result), real and original channel transfer functions at 1st subchannel versus symbol number graph (SNR = 18 dB)

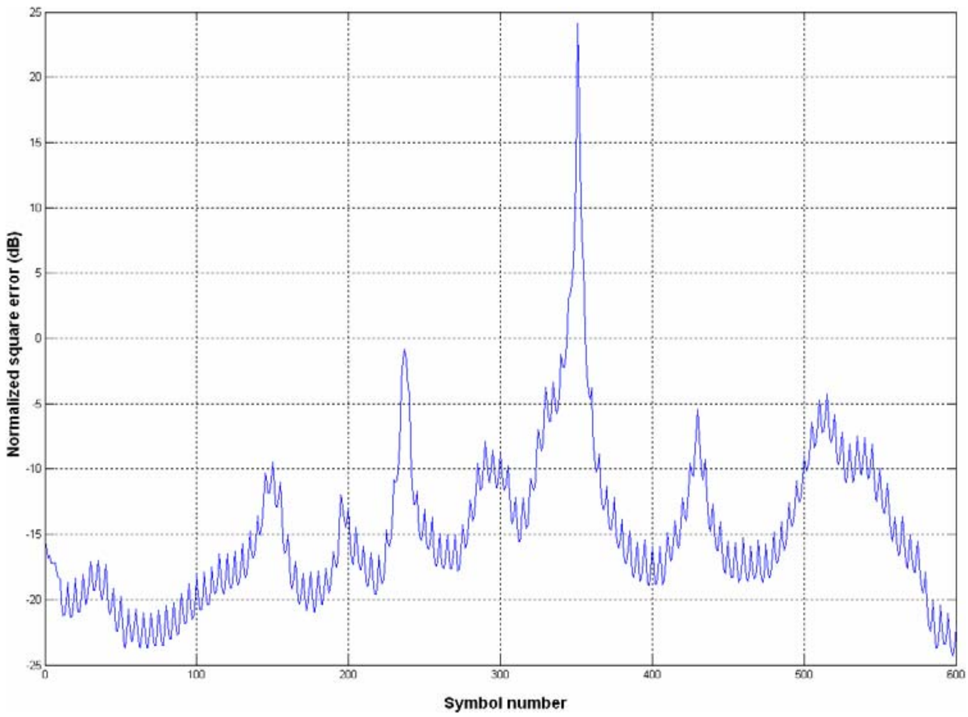

Figure 5.57 Normalized square error averaged over all subchannels (Kalman CP result) versus symbol number graph (SNR = 18 dB)

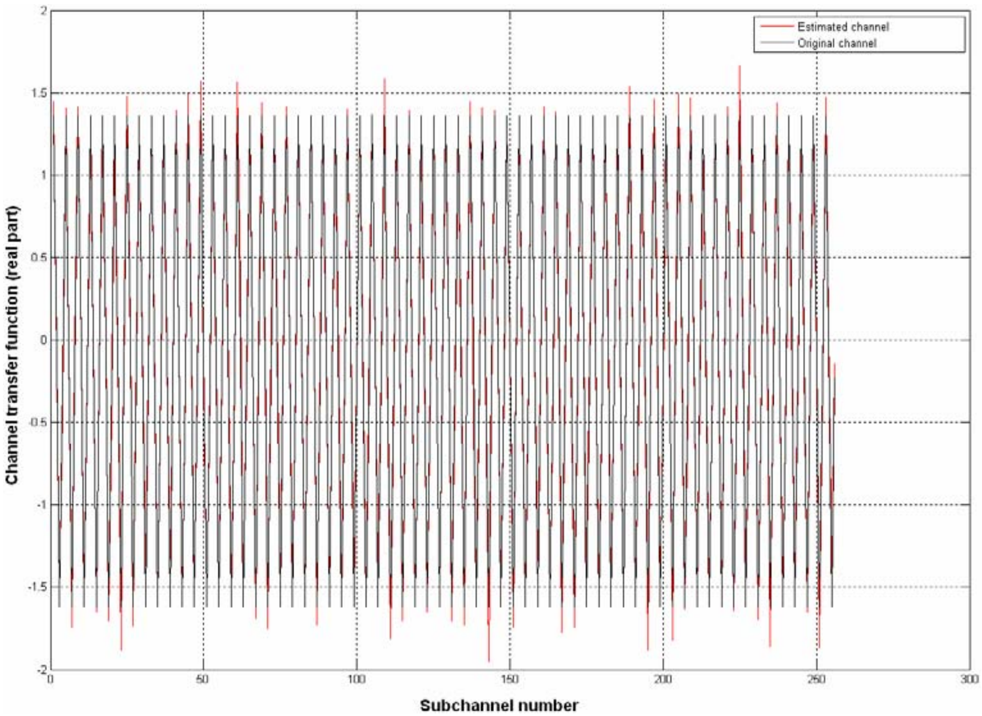

Figure 5.58 Real part of estimated (Kalman CP result) and original channel transfer functions at 20th symbol versus subchannel number graph (SNR = 18 dB)

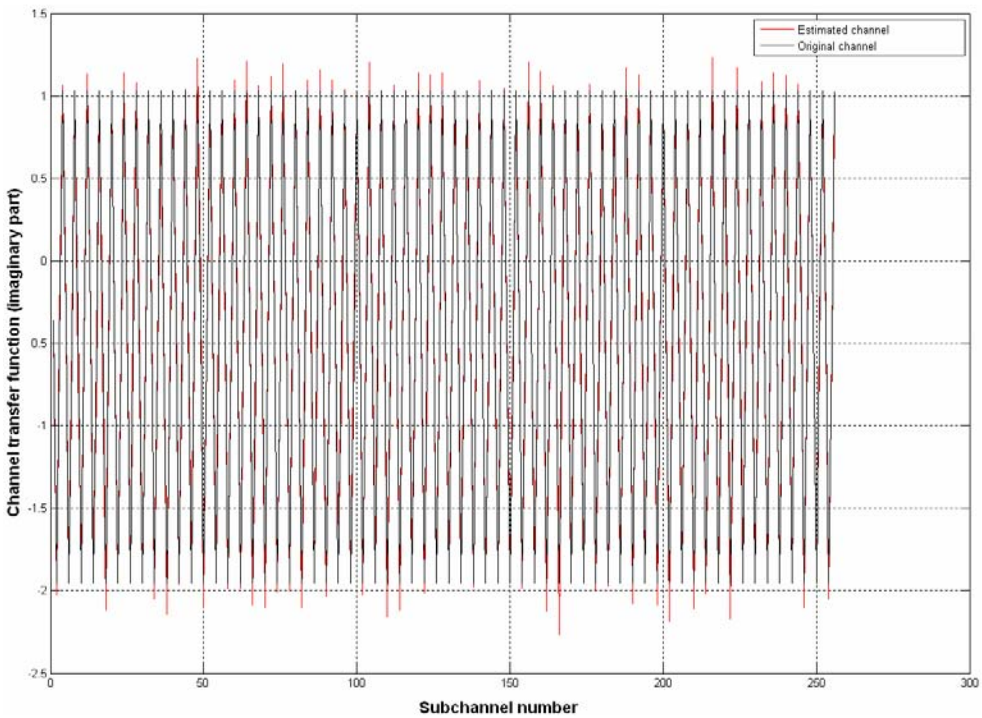

Figure 5.59 Imaginary part of estimated (Kalman CP result) and original channel transfer functions at 20th symbol versus subchannel number graph (SNR = 18 dB)

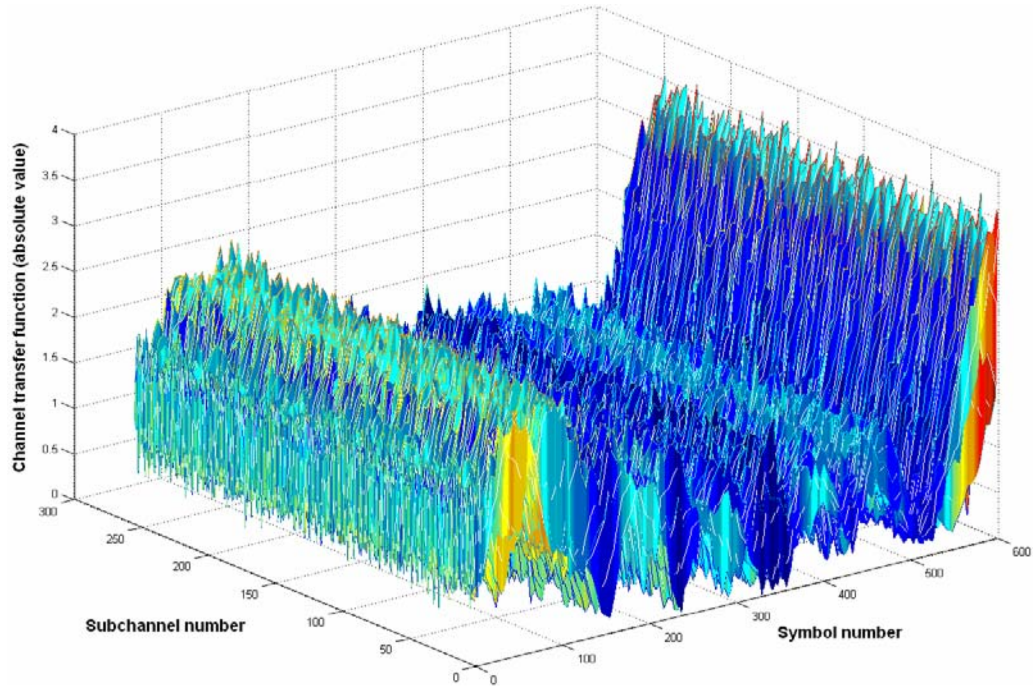

Figure 5.60 Absolute value of the estimated HF channel transfer function (Kalman CP result) over whole frequency time grid (SNR=18 dB)

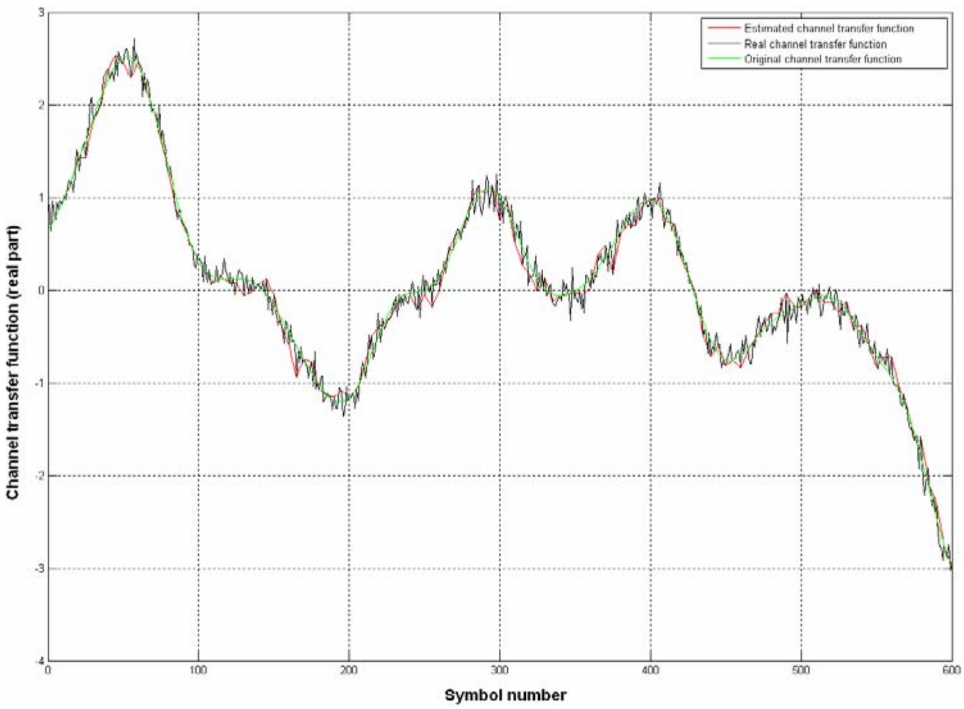

Figure 5.61 Real part of estimated (Kalman CV result), real and original channel transfer functions at 1st subchannel versus symbol number graph (SNR = 18 dB)

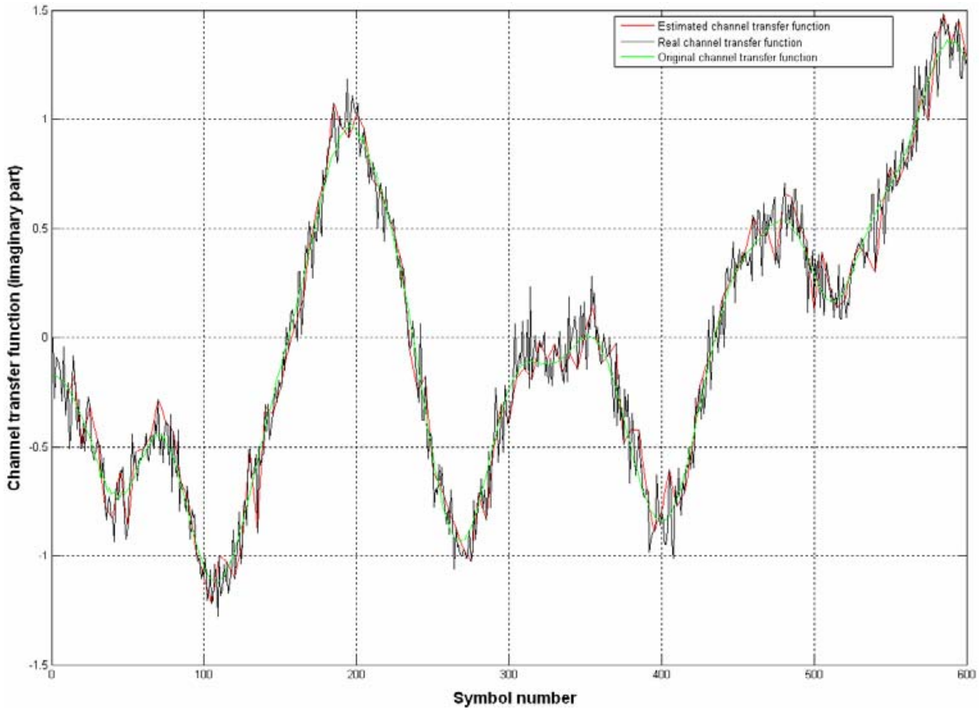

Figure 5.62 Imaginary part of estimated (Kalman CV result), real and original channel transfer functions at 1st subchannel versus symbol number graph (SNR = 18 dB)

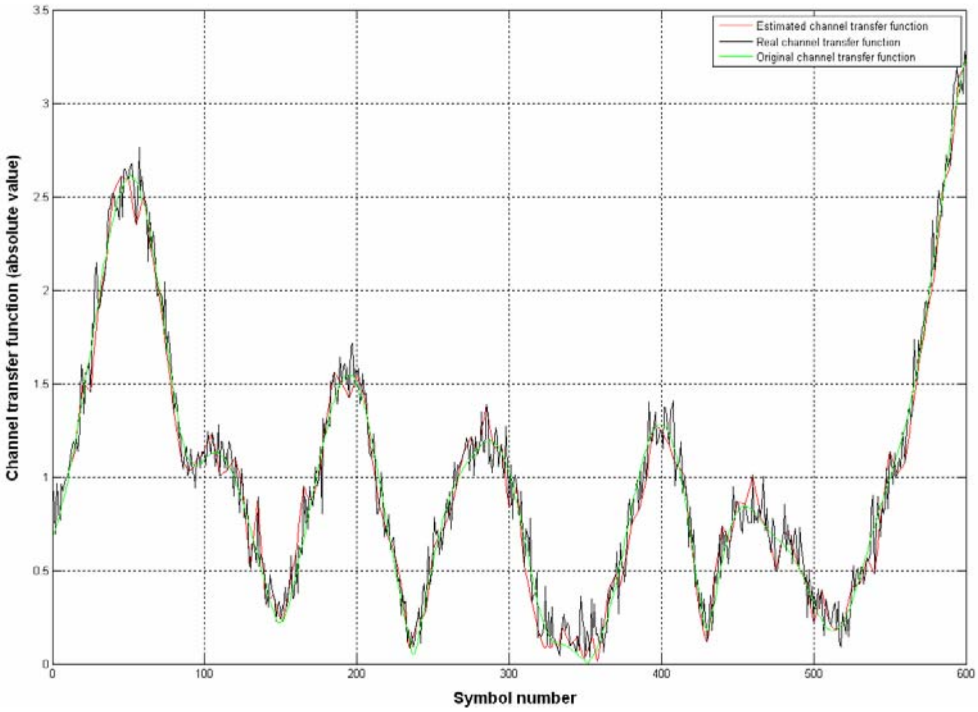

Figure 5.63 Absolute value of estimated (Kalman CV result), real and original channel transfer functions at 1st subchannel versus symbol number graph (SNR = 18 dB)

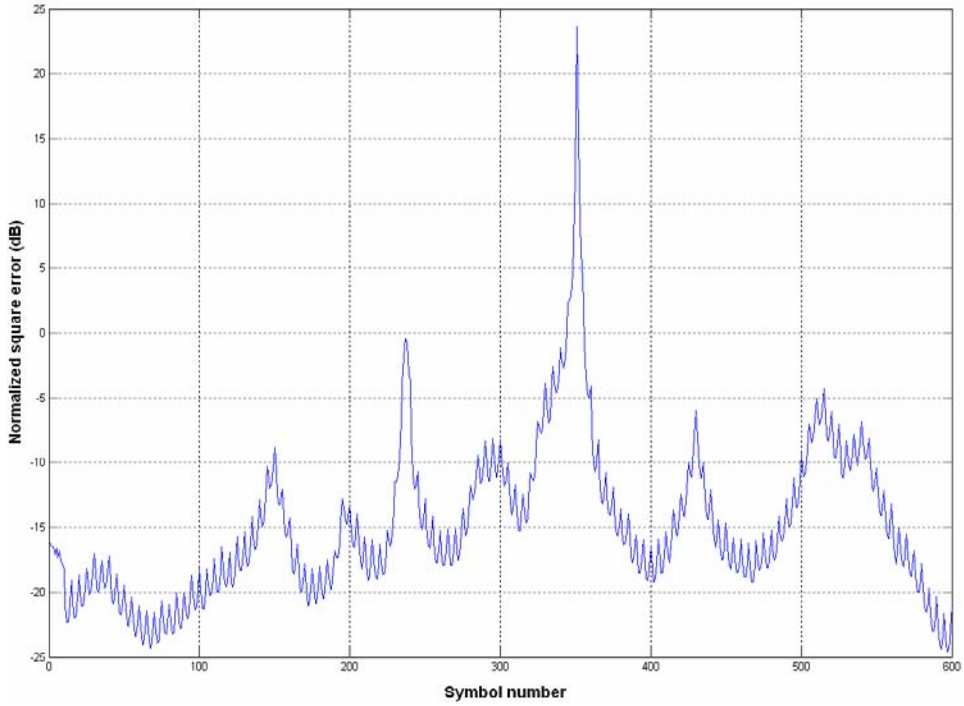

Figure 5.64 Normalized square error averaged over all subchannels (Kalman CV result) versus symbol number graph (SNR = 18 dB)

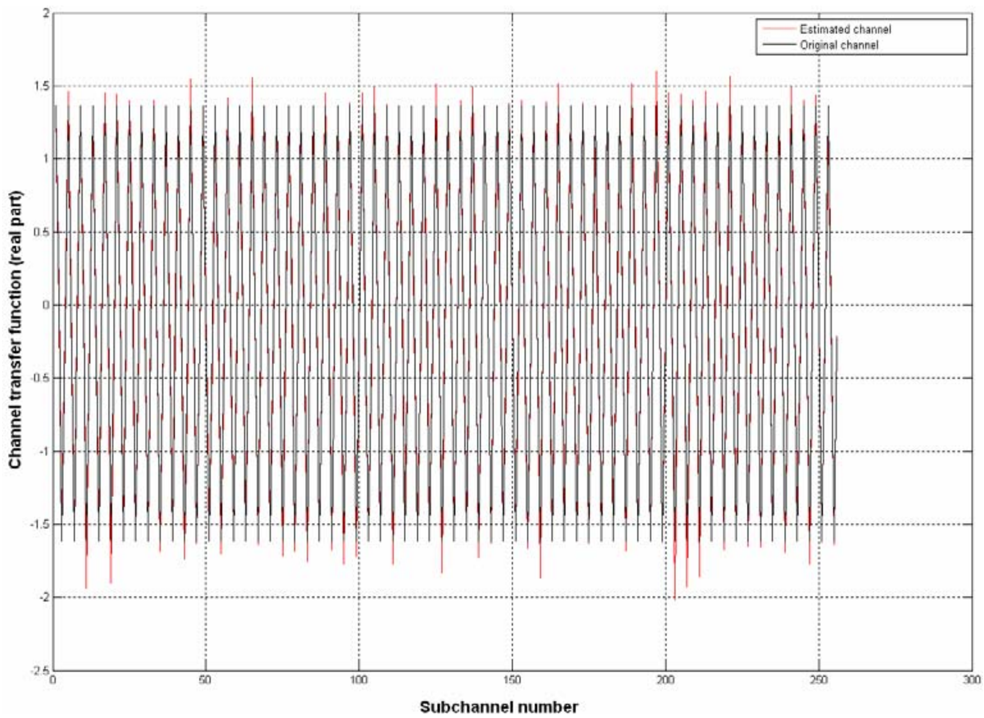

Figure 5.65 Real part of estimated (Kalman CV result) and original channel transfer functions at 20th symbol versus subchannel number graph (SNR = 18 dB)

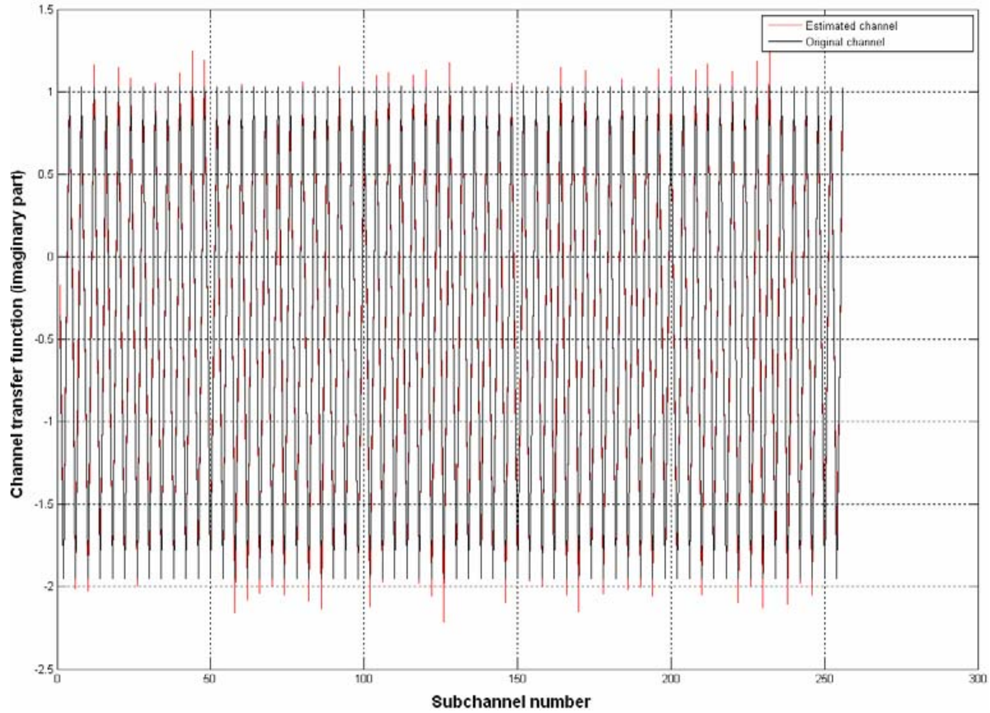

Figure 5.66 Imaginary part of estimated (Kalman CV result) and original channel transfer functions at 20th symbol versus subchannel number graph (SNR = 18 dB)

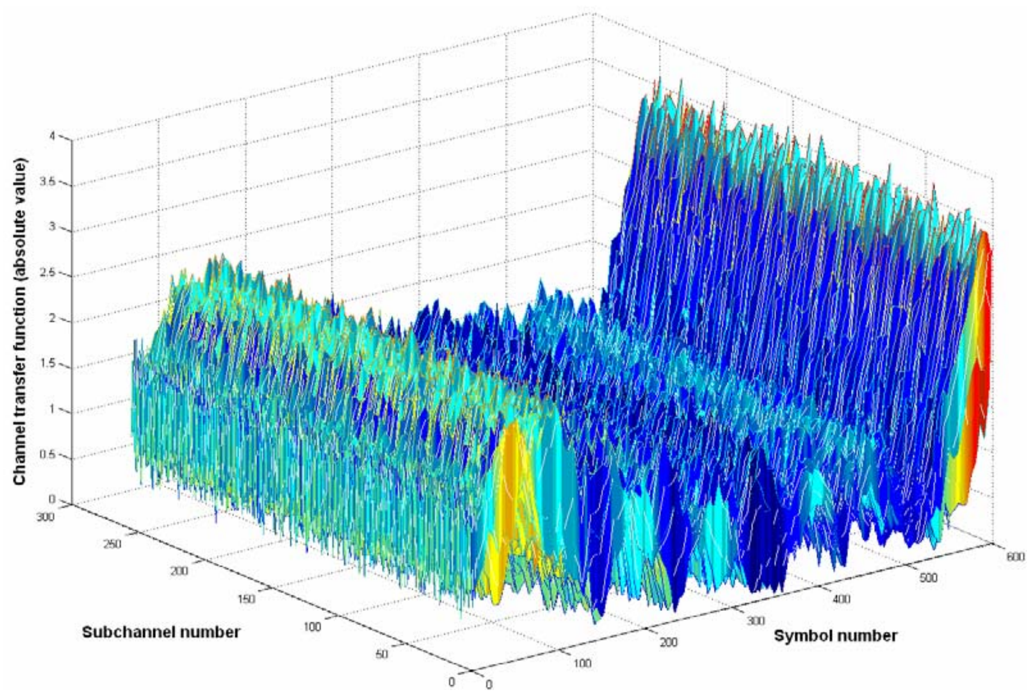

Figure 5.67 Absolute value of the estimated HF channel transfer function (Kalman CV result) over whole frequency time grid (SNR=18 dB)

When the results shown in Figures 5.54-5.67 are investigated, it can be observed that the constant position model based Kalman filter and the constant velocity model based Kalman filter track the data without any apparent delay and without any unexpected result.

CHAPTER 6

CONCLUSIONS

In this work some channel estimation and tracking methods are compared. These methods are least squares (LS) channel estimation method, linear minimum mean square error (LMMSE) channel estimation method, least mean squares (LMS) channel tracking method, recursive least squares (RLS) channel tracking method, and Kalman filter channel tracking method. For LMS and RLS methods, some adaptive structures are also investigated. Moreover, for Kalman filter method, two types of Kalman filter are employed. These are constant position model based Kalman filter and constant velocity model based Kalman filter. These methods are implemented on an OFDM system working over high frequency (HF) channel.

It should be noted that, in this work the aim is not constructing a complex OFDM system and making the performance of the system reach its peak. Instead, the aim is constructing a simple OFDM system and investigating only the estimation and tracking performances of the above methods in this system.

The simulations were performed using the CCIR poor HF channel. When the simulation results are investigated, it is observed that the performance of the LMS and adaptive LMS have the worst performance. This is because the convergence duration is longer compared to that of other tracking methods and delay in tracking causes reduction in the performance. The best performance is obtained by the constant velocity model based Kalman filter and adaptive RLS methods. They are followed by RLS, constant position model based Kalman filter, LMMSE, and LS methods. But, as SNR becomes lower than nearly 4 dB, LMMSE channel estimation method becomes the best method. Adaptive LMS and RLS algorithms give better performance compared to the nonadaptive LMS and RLS algorithms.

In the simulations, the process and noise covariance matrices of the Kalman filters, giving the lowest NMSE, are found at the SNR value of 18 dB by trial and error. For other SNR values, the same covariance matrices are used. If for each SNR the covariance matrices giving the lowest NMSE were found, the performance of the Kalman filters might become better. This issue can be investigated as a future work.

In the tracking of the HF channel frequency response over time with the Kalman filter channel tracking algorithm, constant position model and constant velocity model were used. A measurement model specific for HF channel can be investigated as a future work.

During estimating/tracking the channel, when deep fades occur, the performance drops rapidly. For this reason, coding should be used in order to compensate the performance loss at deep fades [6].

One final note is that since the channel transfer function is periodic in frequency domain as given in equation (5.4), although in this work the channel is estimated and tracked over each subchannels separately, the data from other subchannels can be used in order to increase the performance.

REFERENCES

[1] Ching-Nunh Yang, *OFDM Advantages and Disadvantages*, http://sna.csie.ndhu.edu.tw/~cnyang/MCCDMA/sld021.htm, 10 Oct. 2001.

[2] Ahmad R. S. BAHAI, Burton R. Saltzberg, *Multi-Carrier Digital Communications- Theory and Applications of OFDM*, Springer; 2 edition, 7 Oct. 2004.

[3] Mustafa Fikret Ottekin, *Analysis and Performance Evaluation of Multicarrier Modulation Systems*, M.S. thesis, METU July 1992.

[4] Bahadır CANPOLAT, *Performance Analysis of Adaptive Loading OFDM under Rayleigh Fading with Diversity Combining*, Ph.D. thesis, METU September 2001.

[5] Adil Kürşat ERGÜT, *Time Synchronization in OFDM*, M.S. thesis, METU December 2002.

[6] Y.H. Kim, I. Song, H.G. Kim, T. Chang, and H.M. Kim, *Performance Analysis of a Coded OFDM System in Time Varying Multipath Rayleigh Fading Channels*, IEEE Trans. on Veh. Technol, vol. 54, no. 1, Jan. 2005.

[7] Hüseyin ANIKTAR, *A Study on Subcarrier Synchronization in OFDM Systems*, M.S. thesis, METU September 2002.

[8] Clarc C. Watterson, John R. Juroshek, and William D. Bensema, *Experimental Confirmation of an HF Channel Model*, IEEE Transactions on Communication Technology, vol. com–18, no. 6, December 1970.

[9] Philip A. Bello, *Characterization of Randomly Time Variant Linear Channels*, IEEE Trans. on Communication Systems, vol. CS–11, pp. 360–393, December 1963.

[10] Robert S. Kennedy, *Fading Dispersive Communication Channels*, Wiley-Interscience, New York 1969.

[11] J. G. Proakis, *Digital Communications*, 3rd ed., Mc-Graw Hill: New York, 1995.

[12] Phillip A. Bello, *A Troposcatter Channel Model*, IEEE Transactions on Communication Technology, Vol. Com–17, no. 2, April 1969.

[13] John M. Goodman, *HF Communications, Science and Technology*, Van Nostrand Reinhold publication,1992.

[14] John F. Mastrangelo, John J. Lemmon, Lewis E. Vogler, James A. Hoffmeyer, Lauren E. Pratt, and Christopher J. Behm, *A New Wideband High Frequency Channel Simulation System*, IEEE Transactions on Communications, Vol. 45, No. 1, January 1997.

[15] J.E.M. Nilsson and T.C. Giles, *Wideband Multi-Carrier Transmission for Military HF Communication*, Proc. IEEE Military Communications Conference (MILCOM 97), Monterey, California, USA, CD ROM, 2-5 November 1997.

[16] V. E. Gherm, N. N. Zernov, H. J. Strangeways and M. Darnell, *Scattering functions for wideband HF channels*, HF Radio Systems and Techniques, Conference Publication No. 474 IEE 2000.

[17] A. F. Kurpiers, *Improved Channel Estimation and Demodulation for OFDM on HF Ionospheric Channels*, HF Radio Systems and Technologies, Conference Publication No. 474, IEE 2000.

[18] Ye Li, Leonard J. Cimini Jr., Nelson R. Sollenberger, *Robust Channel Estimation for OFDM Systems with Rapid Dispersive Fading Channels*, IEEE Transactions on Communications, vol. 46, no. 7, July 1998 pp. 902-915.

[19] Osvaldo Simeone, Yeheskel Bar-Ness, Umberto Spagnolini, *Pilot-Based Channel Estimation for OFDM Systems by Tracking the Delay-Subspace*, IEEE Transactions on Wireless Communications, vol. 3, no. 1, January 2004 pp. 315-325.

[20] S. Colieri, M. Ergen, A. Puri, A. Bahai, *A Study of Channel Estimation in OFDM Systems,* Vehicular Technology Conference, 2002. Proceedings. VTC 2002-Fall. 2002 IEEE 56th Vol. 2, Page(s):894 - 898, 24-28 September 2002.

[21] Baoguo Yang, K. B. Letaief, Roger S. Cheng, Zhigang Cao, *Robust and Improved Channel Estimation for OFDM Systems in Frequency Selective Fading Channels*, GLOBECOM 1999-IEEE Global Telecommunications Conference, no. 1, pp. 2499-2503, December 1999.

[22] J. J. Van de Beek, O. Edfors, M. Sandell, S. K. Wilson, P. O. Borjesson, *On Channel Estimation in OFDM Systems*, Proc. VTC'95,pp. 815-819, July 1995.

[23] Seung Young Park, Chung Gu Kang, *Performance of Pilot Assisted Channel Estimation for OFDM Systems under Time-varying Multipath Rayleigh Fading with Frequency Offset Compensation*, Vehicular Technology Conference Proceedings, 2000. VTC 2000-Spring Tokyo. 2000 IEEE 51st Volume 2, 15-18 May 2000 Page(s):1245 – 1249.

[24] Ove Edfors, Magnus Sandell, Jan-Jaap van de Beek, Sarah Kate Wilson, Per Ola Börjesson, *OFDM Channel Estimation by Singular Value Decomposition*, IEEE Transactions on Communications, vol. 46, no. 7, July 1998 pp. 931-939.

[25] W. Lee and J. Zhu, *Channel Estimation for High-Speed Packet-Based OFDM Communication Systems*, Proc. of IEEE Int'l Symp. on Wireless Personal Multimedia Communications (WPMC) '02, Honolulu, Hawaii, pp. 1293-1298, October 27-30, 2002.

[26] M. Ito, S. Suyama, K. Fukawa, H. Suzuki, *An OFDM Receiver with Decision-directed Channel Estimation for the Scattered Pilot Scheme in Fast Fading Environments*, Vehicular Technology Conference, 2003. VTC 2003-Spring. The 57th IEEE Semiannual Volume 1, 22-25 April 2003, Page(s):368-372.

[27] Ye Li, *Pilot Symbol Assisted Channel Estimation for OFDM in Wireless Systems*, IEEE Transactions on Vehicular Technology, Vol. 49, No.4, July 2000.

[28] Won-Gyu Song, Jong-Tae Lim, *Pilot Symbol Aided Channel Estimation for OFDM with Fast Fading Channels*, Broadcasting, IEEE Transactions, Volume 49, Issue 4, December 2003 Page(s):398 – 402.

[29] Haiyun Tang, Kam Y. Lau, Robert W. Brodersen, *Interpolation-Based Maximum Llikelihood Channel Estimation Using OFDM Pilot Symbols*, GLOBECOM 2002 - IEEE Global Telecommunications Conference, vol. 21, no. 1, November 2002 pp. 1870-1874.

[30] F. Tufvesson, T. Maseng, *Pilot Assisted Channel Estimation for OFDM in Mobile Cellular Systems*, Broadcasting, IEEE Transactions, Volume 49, Issue 4, December 2003 Page(s):398-402.

[31] Y. Xue, X. Zhu, *Wireless Channel Tracking Based on Self-Tuning Second-Order LMS Algorithm*, IEE Proc. Commun, Vol. 150, No. 2, April 2003.

[32] Dieter Schafhuber, Markus Rupp, Gerald Matz, Franz Hlawatsch, *Adaptive Identification and Tracking of Doubly Selective Fading Channels for Wireless MIMO-OFDM Systems*, Signal Processing Advances in Wireless Communications, 2003. SPAWC 2003. 4th IEEE Workshop, 15-18 June 2003, Page(s):417-421.

[33] Qassim Nasir and Faisal Ali Shah, *Predictive LMS for Mobile Channel Tracking*, Journal of Applied Sciences 5(2): 337-340, 2005.

[34] Christos Komninakis, Christina Fragouli, Ali H. Sayed, Richard D. Wesel, *Multi-Input Multi-Output Fading Channel Tracking and Equalization Using Kalman Estimation*, IEEE Transactions on Signal Processing, Vol. 50, No. 5, May 2002.

[35] Voicu Filimon, Werner Kozek, Werner Kreuzer, Gernot Kubin, *LMS and RLS Tracking Analysis for WSSUS Channels*, Acoustics, Speech, and Signal Processing, 1993. ICASSP-93., 1993 IEEE International Conference, Volume 3, 27-30 April 1993 Page(s): 348-351 .

[36] Zheng Yuanjin, *A Novel Channel Estimation and Tracking Method for Wireless OFDM System Based on Pilots and Kalman Filtering*, Circuits and Systems, 2003. ISCAS '03. Proceedings of the 2003 International Symposium, Volume 2, 25-28 May 2003 Page(s):II-17-II-20.

[37] Dieter Schafhuber, Gerald Matz, Franz Hlawatsch, *Kalman Tracking of Time-Varying Channels in Wireless MIMO-OFDM Systems*, Signals, Systems and Computers, 2003. Conference Record of the Thirty-Seventh Asilomar Conference, Volume 2, 9-12 November 2003 Page(s):1261-1265.

[38] Min Dong, Lang Tong, Brian M. Sadler, *Optimal Pilot Placement for Channel Tracking in OFDM*, MILCOM 2002. Proceedings, Volume 1, 7-10 October 2002 Page(s):602-606.

[39] S. Haykin, *Adaptive Filter Theory*, 3rd ed. Englewood Cliffs, NJ: Prentice -Hall, 1996.

[40] Marc C. Necker, Gordon L. Stüber, *Totally Blind Channel Estimation for OFDM over Fast Varying Mobile Channels*, ICC 2002-IEEE International Conference on Communications, vol. 25, no. 1, April 2002 pp. 421-425.

[41] Yan Wang, Chi-Ying Tsui, R.S. Cheng, Wai Ho Mow, *Threshold Channel Estimation for OFDM in Wireless Systems*, Vehicular Technology Conference, 2003. VTC 2003-Spring. The 57th IEEE Semiannual Volume 3, 22-25 April 2003 Page(s):1586-1589.

[42] L. Mazet, V. Buzenac-Settineri, M. de Courville, P. Duhamel, *An EM-based Semi-blind Channel Estimation Algorithm Designed for OFDM Systems*, Signals, Systems and Computers, 2002. Conference Record of the Thirty-Sixth Asilomar Conference, Vol. 2, Page 1642-1646, November 2002.

[43] Chengyang Li, Sumit Roy, *Subspace-Based Blind Channel Estimation for OFDM by Exploiting Virtual Carriers*, IEEE Transactions on Wireless Communications, vol. 2, no. 1, January 2003, pp. 141-150.

[44] Bertrand Muquet, Marc de Courville, Pierre Duhamel, *Subspace-based Blind and Semi-blind Channel Estimation for OFDM System*, IEEE Transactions on Signal Processing, Vol. 50, No. 7, July 2002.

[45] Wei Bai, Chen He, Ling-ge Jiang, Hong-wen Zhu, *Blind Channel Estimation in MIMO-OFDM Systems*, GLOBECOM 2002-IEEE Global Telecommunications Conference, vol. 21, no. 1, November 2002, pp. 325-329.

[46] Y. Lin, H. Wang, and B. Chen, *Blind Identification of the Wireless OFDM Channel Using Receiver Diversity*, Proceedings of the 6th International Conference on Signal Processing (ICSP'2002), Beijing, China, August, 2002.

[47] Wookwon Lee, *On Channel Estimation for OFDM Systems in Multipath Environments with Relatively Large Delay Spread*, Vehicular Technology Conference, 2003. VTC 2003-Spring. The 57th IEEE Semiannual, Volume 2, 22-25 April 2003 Page(s):1303-1307.

[48] A. P. Clark, S. Harihan, *Adaptive Channel Estimator for an HF Radio Link,* IEEE Transactions on Communications, Vol. 37, No. 9, September 1989.

[49] Frank M. Hsu, *Square Root Kalman Filtering for High Speed Data Received over Fading Dispersive HF Channels,* IEEE Transactions on Information Theory, Vol. 28, No. 5, September 1982.

[50] Joseph M. Perl, David Kagan, *Real Time HF Channel Parameter Estimation,* IEEE Transactions on Communications, Vol. 34, No. 1, January 1986.

[51] Yaakov Bar-Shalom, X. Rong Li, Thiagalingam Kirubarajan, *Estimation with Applications to Tracking and Navigation*, Wiley-Interscience Publication, 2001

[52] W. N. Furman and J. W. Nieto, *Understanding HF Channel Simulator Requirements in Order to Reduce HF Modem Performance Measurement Variability*, Nordic HF conference August 14-16 2001, HF-01.

[53]CCIR Recommendation 520-1. Use of High Frequency Ionospheric Channel Simulators.

APPENDIX A

HIGH FREQUENCY (HF) CHANNEL DESIGN

The steps for HF channel design are given as below [52]:

1- The channel is modelled by tap delay line model as shown in Figure A.1.

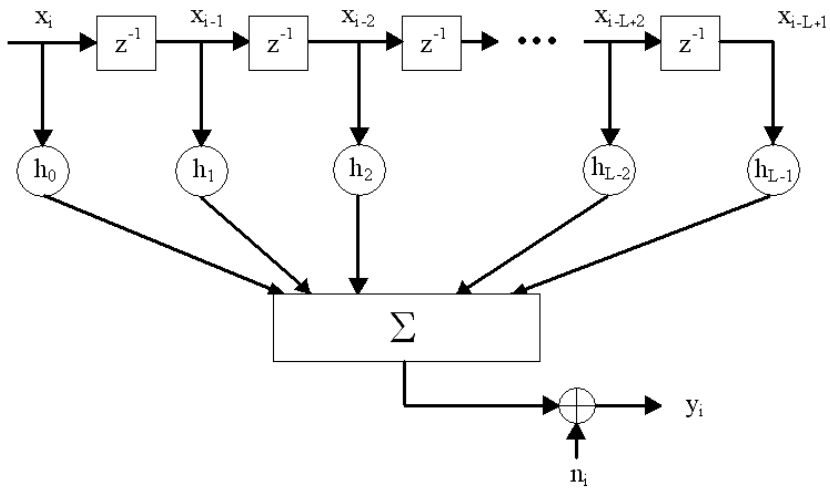

Figure A.1 Tap delay line model

2- Fading taps (for tap delay line) are obtained by filtering complex white Gaussian noise samples.

3- Filters used for fading process have a Gaussian shaped power spectrum (frequency domain) with Doppler spread of power spectrum equal to twice the standard deviation. Equation (A.1) is used to compute the filter taps based on the sampling rate of the channel simulator. The length of the filter is set to at least the length where the computed tap is 0.001 smaller than the maximum tap. The filter is symmetrical about maximum tap (tap for time 0).

$$f_j(t) = \sqrt{2}e^{-\pi^2 t^2 d_j^2}, \quad -\infty < t < \infty \tag{A.1}$$

In equation (A.1), d_j is the desired Doppler spread. This equation is obtained by computing the inverse Fourier transform of the Gaussian shaped amplitude equation

$$\left|H_j(t)\right|^2 = \frac{e^{-f^2/d_j^2}}{\sqrt{\pi d_j^2/2}}, \quad -\infty < t < \infty \tag{A.2}$$

4- Fading taps are computed 40 times faster than the desired fade rate (recommendation by [52]). The update rate is based on the Doppler spread in order to minimize the number of taps required to sample the impulse response.

5- Fading taps are interpolated to symbol rate of the waveform (nearly 10^7 samples a second) to avoid introducing large discontinuities in the output of the simulator.

6- Additive white Gaussian noise (AWGN) was used as noise source.

In the simulations, Watterson HF channel model is used based on the International Radio Consultative Committee (CCIR) Poor HF channel. In this channel, there are two paths. Each path has 1 Hz Doppler spread (d_j) and the channel delay is 2.0 ms and one has zero delay.

Together with the CCIR Poor HF channel, CCIR Moderate HF channel and CCIR Good HF channel parameters are shown in Table A.1.

Table A.1 CCIR HF channel parameters [53]

	Delay	Doppler Spread
Poor	2 ms	1 Hz
Moderate	1 ms	0.5 Hz
Good	0.5 ms	0.1 Hz

APPENDIX B

MAXIMUM A POSTERIORI (MAP) SIGNAL DETECTION

In the maximum a posteriori probability (MAP) signal detection criterion, the signal maximizing the a posteriori probability is selected [11]. A posteriori probability is defined as P(signal a_m was tranmitted| y_m) which is abbreviated as $P(a_m| y_m)$. According to the Bayes' rule, the posterior probability can be expressed as follows:

$$P(a_m \mid y_m) = \frac{p(y_m \mid a_m)P(a_m)}{p(y_m)} \tag{B.1}$$

Here, $p(y_m| a_m)$ is the conditional probability density function (pdf) of the observed signal given a_m, $P(a_m)$ is the a priori probability that a_m was tranmitted and $p(y_m)$ is the pdf of y_m. $p(y_m)$ can be written as follows:

$$p(y_m) = \sum_m p(y_m \mid a_m)P(a_m) \tag{B.2}$$

From equations (B.1) and (B.2), it can be observed that the computation of the posterior probability $P(a_m| y_m)$ requires the knowledge of the a priori probability $P(a_m)$ and the conditional pdf $p(y_m| a_m)$.

Some simplification occurs in the MAP criterion when a_m take values with equal probabilities. That is, if $0 \leq a_m \leq N-1$, then, in equation (B.1) $P(a_m)=1/N$. Furthermore, in this case the denominator in equation (B.1) does not depend on which signal is transmitted. Hence, the decision rule based on finding the signal that maximizes $P(a_m|y_m)$ is equivalent to finding the signal that maximizes $p(y_m|a_m)$.

In the case of an AWGN, natural logarithm of $p(y_m | a_m)$ is given by the following expression:

$$\ln p(y_m | a_m) = -\frac{1}{2} N \ln(2\pi\sigma^2) - \frac{1}{2\sigma^2}(y_m - a_m)^2 \tag{B.3}$$

Since natural logarithm is a monotonic function, the maximum of $\ln p(y_m | a_m)$ over a_m is equivalent to finding the signal a_m that minimizes the Euclidean distance, which is given as follows.

$$D(y_m, a_m) = \|y_m - a_m\|^2 \tag{B.4}$$

$D(y_m, a_m)$ is the distance metric. Hence, it can be said that for the AWGN, the decision rule based on MAP criterion with equal probabilities reduces to finding the signals a_m that are closest in distance to the received signal y_m.

APPENDIX C

DERIVATION OF THE LEAST SQUARES (LS) ESTIMATION METHOD

In LS estimation, the cost function given in (C.1) should be minimized with respect to $\overline{H}_n$ [51].

$$C = \left\| \overline{a}_n \overline{H}_n - \overline{y}_n \right\|^2 = \left(\overline{a}_n \overline{H}_n - \overline{y}_n \right)^H \left(\overline{a}_n \overline{H}_n - \overline{y}_n \right) \qquad \text{(C.1)}$$

Hence, the estimated channel can be found by the following expression:

$$\hat{\overline{H}}_n = \min_{\overline{H}_n} \left\| \overline{a}_n \overline{H}_n - \overline{y}_n \right\|^2 \qquad \text{(C.2)}$$

Let $\overline{H}_n = \overline{R}_n + j\overline{I}_n = \begin{bmatrix} R_{0,n} + jI_{0,n} \\ R_{1,n} + jI_{1,n} \\ \vdots \\ R_{N-1,n} + jI_{N-1,n} \end{bmatrix}$, where $\overline{R}_n$ and $\overline{I}_n$ are the real and imaginary parts of $\overline{H}_n$, respectively.

Now, let us find the gradient of C with respect to $\overline{H}_n$ in order to find $\overline{H}_n$ giving smallest C. For this purpose, the gradient operator given in (C.3) is used.

$$\nabla_H = \begin{bmatrix} \frac{\partial}{\partial R_0} + j\frac{\partial}{\partial I_0} \\ \frac{\partial}{\partial R_1} + j\frac{\partial}{\partial I_1} \\ \vdots \\ \frac{\partial}{\partial R_{N-1}} + j\frac{\partial}{\partial I_{N-1}} \end{bmatrix} \qquad \text{(C.3)}$$

$$
\begin{aligned}
\nabla_{H_n} C &= \nabla_{H_n}\left((\bar{a}_n \bar{H}_n - \bar{y}_n)^H (\bar{a}_n \bar{H}_n - \bar{y}_n)\right) \\
&= \nabla_H \left(\bar{H}_n^H \bar{a}_n^H \bar{a}_n \bar{H}_n - \bar{H}_n^H \bar{a}_n^H \hat{a}_n - \bar{y}_n^H \bar{a}_n \bar{H}_n + \bar{y}_n^H \bar{y}_n\right) \\
&= \bar{a}_n^H \bar{a}_n \bar{H}_n + j\left(j\bar{a}_n^H \bar{a}_n \bar{H}_n\right) + \bar{a}_n^H \bar{a}_n \bar{H}_n + j\left(-j\bar{a}_n^H \bar{a}_n \bar{H}_n\right) \\
&\quad - \bar{a}_n^H \bar{y}_n - j(j\bar{a}_n^H \bar{y}_n) - \bar{a}_n^H \bar{y}_n - j(-j\bar{a}_n^H \bar{y}_n) \\
&= 2\bar{a}_n^H \bar{a}_n \bar{H}_n - 2\bar{a}_n^H \bar{y}_n \\
&= 0
\end{aligned}
\tag{C.4}
$$

Then

$$
\bar{a}_n^H \bar{a}_n \bar{H}_n = \bar{a}_n^H \bar{y}_n \tag{C.5}
$$

As a result, the estimation is obtained as follows:

$$
\hat{\bar{H}}_n = \left[\left(\bar{a}_n^H \bar{a}_n\right)^{-1} \bar{a}_n^H\right] \bar{y}_n \tag{C.6}
$$

APPENDIX D

DERIVATION OF RECURSIVE LEAST SQUARES (RLS) METHOD

In RLS method, the aim is to find $H_{k,n}$ using

$$H_{k,n} = \Phi_{k,n}^{-1} Z_{k,n} \tag{D.1}$$

by obtaining $\Phi_{k,n}^{-1}$. In section 4.2.3.2, the recursive expressions of $Z_{k,n}$ and $\Phi_{k,n}$ are obtained as follows:

$$Z_{k,n} = \sum_{i=0}^{n} \lambda^{n-i} d_{k,i} a_{k,i}^{*} = \lambda . \sum_{i=0}^{n-1} \lambda^{n-1-i} d_{k,i} a_{k,i}^{*} + d_{k,n} a_{k,n}^{*} = \lambda Z_{k,n-1} + d_{k,n} a_{k,n}^{*} \tag{D.2}$$

$$\Phi_{k,n} = \sum_{i=1}^{n} \lambda^{n-i} a_{k,i} a_{k,i}^{*} = \lambda \sum_{i=1}^{n-1} \lambda^{n-1-i} a_{k,i} a_{k,i}^{*} + a_{k,n} a_{k,n}^{*} = \lambda \Phi_{k,n-1} + a_{k,n} a_{k,n}^{*} \tag{D.3}$$

Since, the data to be estimated $H_{k,n}$ is one dimensional, $H_{k,n}$, $Z_{k,n}$ and $\Phi_{k,n}$ are scalars. But the data to be estimated can be a matrix. In this case, $H_{k,n}$, $Z_{k,n}$ and $\Phi_{k,n}$ will be matrices. In order to find $\Phi_{k,n}^{-1}$, $H_{k,n}$, $Z_{k,n}$ and $\Phi_{k,n}$ can be assumed to be matrices and the following matrix inversion lemma can be used. Naturally, the matrix equations are also valid for scalars.

Matrix inversion lemma [39]: Let $\overline{A}$ and $\overline{B}$ denote two positive definite M-by-M matrices related by the following equation.

$$\overline{A} = \overline{B}^{-1} + \overline{C}\,\overline{D}^{-1}\overline{C}^{H} \tag{D.4}$$

where D is another positive definite N-by-M matrix, and C is an M-by-N matrix. According to the matrix inversion lemma, the inverse of $\overline{A}$ can be expressed as follows:

$$\overline{A}^{-1} = \overline{B} - \overline{B}\,\overline{C}(\overline{D} + \overline{C}^{H}\overline{B}\,\overline{C})^{-1}\overline{C}^{H}\overline{B} \tag{D.5}$$

Now, with the assumption that $\Phi_{k,n}$ is positive definite and therefore nonsingular, the matrix inversion lemma can be used as follows:

$$\Phi_{k,n} = \lambda\Phi_{k,n-1} + a_{k,n}a^{*}_{k,n} = \overline{B}^{-1} + \overline{C}\,\overline{D}^{-1}\overline{C}^{H} \tag{D.6}$$

where $\overline{B}^{-1} = \lambda.\Phi_{k,n-1}$, $\overline{C} = a_{k,n}$ and $\overline{D} = 1$ are scalars. Hence,

$$\Phi^{-1}_{k,n} = \lambda^{-1}\Phi^{-1}_{k,n-1} - \frac{\lambda^{-2}\Phi^{-1}_{k,n-1}a_{k,n}a^{*}_{k,n}\Phi^{-1}_{k,n-1}}{1 + \lambda^{-1}a^{*}_{k,n}\Phi^{-1}_{k,n-1}a_{k,n}} \tag{D.7}$$

For convenience, let (D.8) denote the gain.

$$k_{n} = \frac{\lambda^{-1}\Phi^{-1}_{k,n-1}a_{k,n}}{1 + \lambda^{-1}a^{*}_{k,n}\Phi^{-1}_{k,n-1}a_{k,n}} \tag{D.8}$$

Then, (D.7) can be written as follow:

$$\Phi^{-1}_{k,n} = \lambda^{-1}\Phi^{-1}_{k,n-1} - \lambda^{-1}k_{n}a^{*}_{k,n}\Phi^{-1}_{k,n-1} \tag{D.9}$$

By rearranging (D.8), the following relation is obtained:

$$k_{n}\left(1 + \lambda^{-1}a^{*}_{k,n}\Phi^{-1}_{k,n-1}a_{k,n}\right) = \lambda^{-1}\Phi^{-1}_{k,n-1}a_{k,n} \tag{D.10}$$

Then

$$
\begin{aligned}
k_n &= \lambda^{-1}\Phi_{k,n-1}^{-1}a_{k,n} - k_n\left(\lambda^{-1}a_{k,n}^{*}\Phi_{k,n-1}^{-1}a_{k,n}\right) \\
&= \left(\lambda^{-1}\Phi_{k,n-1}^{-1} - k_n\left(\lambda^{-1}a_{k,n}^{*}\Phi_{k,n-1}^{-1}\right)\right)a_{k,n} \\
&= \Phi_{k,n}^{-1}a_{k,n}
\end{aligned} \tag{D.11}
$$

$$
\begin{aligned}
H_{k,n} &= \Phi_{k,n}^{-1}Z_{k,n} \\
&= \Phi_{k,n}^{-1}\left(\lambda Z_{k,n-1} + d_{k,n}a_{k,n}^{*}\right) \\
&= \lambda\Phi_{k,n}^{-1}Z_{k,n-1} + \Phi_{k,n}^{-1}d_{k,n}a_{k,n}^{*} \\
&= \lambda\left(\lambda^{-1}\Phi_{k,n-1}^{-1} - \lambda^{-1}k_n a_{k,n}^{*}\Phi_{k,n-1}^{-1}\right)Z_{k,n-1} + \Phi_{k,n}^{-1}d_{k,n}a_{k,n}^{*} \\
&= \Phi_{k,n-1}^{-1}Z_{k,n-1} - k_n a_{k,n}^{*}\Phi_{k,n-1}^{-1}Z_{k,n-1} + \Phi_{k,n}^{-1}d_{k,n}a_{k,n}^{*} \\
&= H_{k,n-1} - k_n a_{k,n}^{*}H_{k,n-1} + \Phi_{k,n}^{-1}d_{k,n}a_{k,n}^{*} \\
&= H_{k,n-1} + k_n\left(d_{k,n}\frac{a_{k,n}^{*}}{a_{k,n}} - a_{k,n}^{*}H_{k,n-1}\right)
\end{aligned} \tag{D.12}
$$

As a result

$$
H_{k,n} = H_{k,n-1} + k_n\left(d_{k,n}\frac{a_{k,n}^{*}}{a_{k,n}} - a_{k,n}^{*}H_{k,n-1}\right) \tag{D.13}
$$